Evaluation of TiO_2 as a Pt-Catalyst Support in a Direct Ethanol Fuel Cell

Ashley Rebecca Gordon

Thesis submitted to the faculty of the Virginia Polytechnic Institute and State University in partial fulfillment of the requirements for the degree of

Master of Science
In
Mechanical Engineering

Michael W. Ellis
David A. Dillard
Doug J. Nelson

March 12, 2012
Blacksburg, Virginia

Keywords: ethanol oxidation, electrochemical analysis, cyclic voltammetry, potentiostatic hold, polarization curves, OCV, power density

Evaluation of TiO_2 as a Pt-Catalyst Support in a Direct Ethanol Fuel Cell

Ashley Rebecca Gordon

Abstract

Direct ethanol fuel cells are of interest due to the high energy density, ease of distribution and handling, and low toxicity of ethanol. Difficulties lie in finding a catalyst that can completely oxidize ethanol and resist poisoning by intermediate reaction species. Degradation of the catalyst layer over time is also an issue that needs to be addressed. In this work, niobium doped-titanium dioxide (Nb-TiO_2) is investigated as a platinum (Pt) support due to its increased resistance to corrosion compared to the common catalyst support, carbon. It has also been seen in the literature that TiO_2 is able to adsorb OH and assist in freeing Pt sites by further oxidizing CO_{ad} to CO_2 and thereby increasing the catalytic activity of catalysts toward ethanol oxidation. The TiO_2 support is mixed with carbon, forming Nb-TiO_2-C, in order to increase the conductivity throughout the support. The electrochemical activity and direct ethanol fuel cell (DEFC) performance of this novel catalyst is investigated and compared to that of two common catalysts, carbon supported Pt (Pt/C) and carbon supported platinum-tin (PtSn/C). While the conductivity of the Pt/Nb-TiO_2-C electrodes was low compared to that of the carbon supported electrodes, the overall catalytic activity and performance of the TiO_2 supported catalyst was comparable to that of the Pt/C catalyst based on the electrochemically active surface area.

Dedicated to my loving and supportive family, without whom I would not have made it this far.

Thank you Charlie, Sandra, and Chase.

Acknowledgements

I would like to begin by thanking Dr. Michael Ellis for providing me with the opportunity to work in the Sustainable Energy Lab at Virginia Tech. His teaching, patience, support, and encouragement were key to my success as a graduate student. What I learned while working for Dr. Ellis will carry with me even after I graduate. The knowledge I have gained applies to all aspects of life and not just to my engineering education. Many thanks for your time and lessons.

Dr. Junbo Hou also deserves a very special thanks for all of the assistance and knowledge he provided me. I appreciate the time he took to teach me new testing methods and troubleshoot with me when things did not go as planned.

Thank you to my committee members, Dr. Dillard and Dr. Nelson, for volunteering their time to review my thesis and attend my defense. I learned a lot from both professors through their classes and discussions over my research. I also appreciate the encouragement Dr. Dillard provided while I was applying to the graduate program at Virginia Tech and the opportunity I was given by Dr. Dillard and Dr. Ellis to get involved in a fuel cell research project.

To my fellow graduate students in the Sustainable Energy Lab (past and present), thanks for all of your help and encouragement. My experience at Virginia Tech would not have been the same without you guys. Your friendship, jokes, advice, and assistance made the lab more than just a place to do research.

Last, but not least, thanks to my extended family, friends, and roommate for all of their support. Whether or not they were interested in the experiments or topics I was discussing, they were there to listen to my struggles, as well as my successes, and I greatly appreciate that!

Table of Contents

List of Figures

List of Tables

1. INTRODUCTION

Alternative energy technology is the focus of a wide range of current research efforts. New forms of cleaner, renewable energy conversion techniques are being investigated with the hope that one day the world will be powered completely by renewable energy. While existing forms of energy resources and energy conversion systems are able to meet today's energy needs, the world-wide energy demand is increasing at an astonishing rate and the resources that fuel the majority of current power production methods are limited. Many forms of present-day energy conversion are also harmful to the environment due to the gases that are released into the atmosphere and the habitats that are disrupted for resource removal. While it may be impossible to produce power without any harmful effects to the environment when looking at the complete life cycle of a power plant or device, it is realistic to convert energy via methods that are less damaging.

Fuel cells are one form of alternative energy technology that is desirable because they directly convert chemical energy to electrical energy with a high theoretical efficiency (83% for a hydrogen fuel cell operating at 25°C). Fuel cells are also advantageous because they release less, if any, harmful emissions during operation and, in some cases, the fuel used to power fuel cells can be considered renewable. There are many different types of fuel cells that are powered by various fuels and that can be used for stationary or transportation purposes.

Polymer electrolyte membrane (PEM) fuel cells have been the focus of much fuel cell research, especially for use in automotives because of their high power density and their low-temperature operating range. While hydrogen-fueled PEM fuel cells have been studied extensively, the difficulties of hydrogen production, transportation to fueling stations, and on-board hydrogen storage in personal vehicles has led researchers to look elsewhere for fuel possibilities. Alcohols are a promising candidate because they have a high energy density (energy per unit volume) and they exist in liquid form at room temperature, which allows for easier handling, transportation, and storage. Among the alcohol group, methanol has received some attention, but because ethanol is less toxic and has a slightly higher mass energy density, ethanol is also being considered. Another advantage of ethanol is that it can be produced from biomass, so in many cases it is deemed renewable and carbon neutral.

Figure 1-1 illustrates the components of a typical laboratory scale PEM fuel cell. The anode side of a fuel cell is where oxidation occurs and electrons are released. The electrons then flow through a circuit to the cathode side and oxygen reduction takes place. The center of a PEM fuel cell is the MEA (membrane electrode assembly). This assembly involves a polymer electrolyte membrane, which conducts protons but not electrons, with a catalyst layer on either side. The catalyst layer is usually different on the anode and cathode sides since different reactions are occurring at each location. Outside the catalyst layer is the gas diffusion layer (GDL), which as its name suggests,

helps to diffuse the reactants so that the flow is equally distributed onto the catalyst layer. The GDL also assists in conducting electrons and removing any products, such as water, that could block the flow of reactants. One or more gaskets between the MEA and graphite flow plates help to ensure a good seal. The graphite plates contain flow channels that also contribute to even distribution of the reactants and water dispersion/removal. The last pieces of the fuel cell are the current collectors and end plates. The end plates are bolted together so that all of the components are touching, forming continuous channels for the reactants, electrons, and protons to flow through.

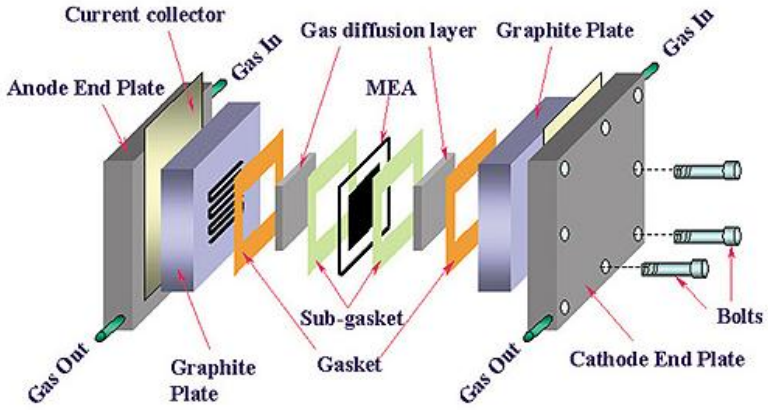

Figure 1-1. PEM fuel cell components [1] (Reprinted with permission from Europa Science Ltd © 2003).

In a direct ethanol fuel cell (DEFC), ethanol (C_2H_5OH) is oxidized at the anode with the potential to release twelve electrons. For all twelve electrons to be released,

the carbon-carbon (C-C) bond must be broken so that ethanol is oxidized completely. The waste products formed at the anode, carbon dioxide (CO_2) and water (H_2O), exit the cell. Hydrogen protons are conducted through the membrane while electrons are forced to flow through an external circuit to the cathode, where the protons and electrons combine with oxygen (O_2) to produce more water. This process is illustrated in Figure 1-2.

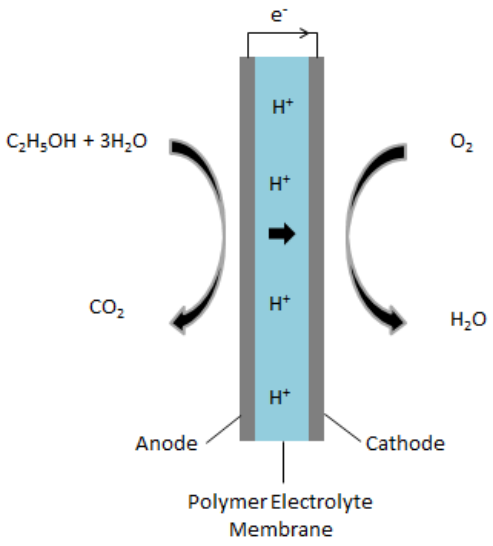

Figure 1-2. Ethanol PEM fuel cell.

Various research efforts on the fuel cell components mentioned above are continuously leading to improvements in the overall efficiency and performance of the fuel cell. While many of the research contributions apply to both hydrogen and ethanol

fuel cells, the catalyst required to fully oxidize ethanol is not the same as that which has been optimized for the oxidation of hydrogen. Carbon supported platinum (Pt/C) has led to good performance in a hydrogen fueled cell but does not produce the same results in an ethanol fuel cell. Because of its success in hydrogen fuel cells, Pt/C has been the starting point for catalyst research for ethanol fuel cells. The poor performance demonstrated with a Pt/C anode catalyst in ethanol fuel cells implies that the complete oxidation of ethanol is not occurring and the C-C bond is remaining intact. For ethanol fuel cells to become a feasible, cost effective form of energy conversion, ethanol must be completely oxidized so that all twelve electrons can participate in electricity production.

An effective catalyst for ethanol fuel cells is one that can break the C-C bond, freeing all twelve electrons and leading to the formation of CO_2. Ideally, the catalyst would be effective even at room conditions, though PEM fuel cells are usually operated at elevated temperatures (60 - 90°C) to increase the chemical reaction kinetics and efficiency of the fuel cell. While catalyst performance would improve at higher temperatures, the maximum temperature of a PEM fuel cell is restricted by the temperature range that the various components can withstand, with the membrane usually acting as the limiting factor. Another very important characteristic of a catalyst is durability. Both the active metal (e.g. platinum) and the supporting material (e.g. carbon) should be resistant to degradation. For the catalyst, degradation can occur by

poisoning due to the adsorption of intermediate species from the ethanol reaction (like CO) which block the surface of platinum, thereby decreasing the active area of the catalyst. In addition, as the fuel cell experiences voltage cycling, the carbon support can be degraded, allowing consolidation or sintering of the Pt particles, thus leading to loss of active area.

This study investigates the effect of a catalyst with a non-carbon support on the ethanol oxidation reaction and ethanol fuel cell performance. In this case, platinum is supported by niobium doped titanium dioxide with 10% carbon black (Pt/Nb-TiO_2-C) added to improve electrical conductivity through the catalyst layer. The goals of this work are to establish the feasibility of TiO_2 as a catalyst support, characterize the ethanol oxidation reaction on Pt supported by TiO_2, examine the influence of the support on poisoning of the catalyst layer, and to compare the performance of a TiO_2 supported catalyst to common carbon supported catalysts. Electrochemical tests are used to identify reaction characteristics on thin film electrodes and a direct ethanol fuel cell is used to compare the performance of various membrane electrode assemblies.

2. LITERATURE REVIEW

2.1. Introduction

Fuel cells are of great interest because they convert chemical energy directly into electricity. Liquid alcohol fuel cells have many advantages over pure hydrogen fed fuel cells including easier fuel storage and handling, easier fuel distribution to fueling stations, and an existing liquid fueling infrastructure [2-10]. Much research has been aimed toward direct methanol fuel cells since methanol has good kinetics of oxidation compared to other alcohols at low temperatures and is known to oxidize completely to CO_2, meaning the maximum transfer of electrons is occurring [6]. The toxicity of methanol and its high crossover rate in fuel cells have led researchers to investigate other, safer, alcohols, such as ethanol [2-4, 6-9, 11-13]. Ethanol has a slightly higher mass energy density (8 kWh/kg) compared to methanol (6 kWh/kg) [2, 6, 8, 12-15] and is noted to have an energy density close to that of gasoline (ethanol: 21 MJ/L, gasoline: 31 MJ/L) [5, 12]. Since ethanol can be derived from biomass, it can also be considered a renewable and carbon neutral resource [2, 4-8, 10-13, 16].

2.2. Ethanol Oxidation

The complete oxidation of ethanol (CH_3CH_2OH), which leads to the transfer of 12 electrons in a direct ethanol fuel cell (DEFC), involves the breaking of a C-C bond and

the further oxidation of CO to CO_2, but in many cases ethanol is only partially oxidized, leading to the formation of unwanted by-products, mainly acetaldehyde and acetic acid [2, 12, 13, 16, 17]. These products result in the transfer of only 2 or 4 electrons, respectively, decreasing the performance and efficiency of a direct ethanol fuel cell. Equations (2.1-2.3) show ethanol oxidation reactions for the formation of acetaldehyde, acetic acid, and CO_2 in an acid electrolyte. It is important to choose a catalyst and operating conditions that will favor the complete oxidation of ethanol to CO_2. It is difficult to state which conditions work best, since the effects of operating conditions are interdependent, as well as dependent on the catalyst and membrane chosen. A variety or research efforts are underway with the goal of identifying a DEFC system that will lead to the rapid and complete electrochemical oxidation of ethanol.

$$\boldsymbol{CH_3CH_2OH \rightarrow CH_3CHO + 2H^+ + 2e^-} \qquad \textit{(2.1)}$$

$$\boldsymbol{CH_3CH_2OH + H_2O \rightarrow CH_3COOH + 4H^+ + 4e^-} \qquad \textit{(2.2)}$$

$$\boldsymbol{CH_3CH_2OH + 3H_2O \rightarrow 2CO_2 + 12H^+ + 12e^-} \qquad \textit{(E° = 0.085 V)} \qquad \textit{(2.3)}$$

In addition to acid media, ethanol can also be electrochemically oxidized in alkaline media which presents advantages for the chemical kinetics but presents

challenges in the area of membrane development. The lower potential onset of ethanol oxidation and higher peak current densities seen in voltammetry tests in alkaline versus acid media, as well as a decrease in overpotential in polarization experiments in alkaline media fuel cells versus acid media fuel cells, imply that both the ethanol oxidation reaction (EOR) and the oxygen reduction reaction (ORR) exhibit faster kinetics in alkaline media [4, 10, 18, 19]. In addition to faster kinetics, some studies suggest that the C-C bond is actually easier to break in alkaline media, leading to more complete ethanol oxidation [2, 4, 10, 18]. In contrast, Yu *et al.*'s review [20] investigated ethanol oxidation on palladium, gold, and platinum-ruthenium catalysts and found that C-C bond breaking and CO_2 formation were not observed in an alkaline fuel cell.

It has been shown though, that the use of anion exchange membranes (AEMs) in DEFCs has led to a better fuel cell performance than in DEFCs using an aqueous alkaline electrolyte [20]. For this reason, DEFCs using AEMs continue to be investigated and results have shown improved open circuit voltages (OCV) and higher maximum power density (decrease in both anode and cathode overpotential) in comparison with traditional cation exchange membranes (CEMs) at the same operating conditions [4, 18, 21]. In the alkaline environment (AEM), the EOR can also be catalyzed using non-precious metal catalyst, such as Ag and Ni, which are less expensive than the Pt-containing catalysts used in acid (DEM) direct ethanol fuel cells [2, 4, 19]. The performance of an alkaline DEFC with a non-Pt catalyst flowing 3.0 M

ethanol and 7.0 M KOH at 2.0 mL/min with pure oxygen was shown to be comparable, if not better, than other alcohol-fed fuel cells with an OCV of 0.9 V and a maximum power density of 60 mW/cm^2 at 40°C [4]. Decreased fuel crossover has also been observed in AEM-DEFCs due to the direction of OH^- transport through the fuel cell (cathode to anode), opposite to that in CEM-DEFCs [20].

When comparing the products formed at similar current densities (~ 30 mA/cm^2) and at room conditions using an AEM versus a CEM, a larger portion of acetic acid (90%) was produced with the AEM-DEFC, while equal amounts of acetic acid and acetaldehyde were formed using a CEM-DEFC [21]. The increase in formation of acetic acid means an increase in electron transfer (4 e^- versus 2 e^- for acetaldehyde), and therefore an increase in performance with the AEM-DEFC at room conditions and low current density. However, the oxidation is still incomplete (93% of the products formed at room temperature are either acetaldehyde or acetic acid [21]) and acetic acid is a terminal product, which is very difficult to oxidize further.

While AEM-DEFC systems appear promising, the materials used for the electrolytic membrane remain at a very early stage of development. By comparison, more progress has been made in the development of CEM materials, which were first introduced in the mid-1960s [4, 10, 22]. CEMs, such as Nafion® are stable in strong bases and show good chemical stability up to 125°C [22]. The currently available AEMs

suffer not only from high cost, poor chemical stability, and poor thermal stability but also exhibit an ionic conductivity that is much lower, about an order of magnitude, than that of Nafion® membranes [10, 20]. The formation of carbonate (from CO_2 in the air or product stream) and its substitution into the AEM can further decrease the ionic conductivity of an AEM-DEFC, as well as block porous electrodes [4, 19-21]. This particular effect can possibly be mitigated by supplying the ethanol feed with KOH solution which seems to avoid the decrease in AEM ionic conductivity by replacing carbonate with OH^- in an AEM [21].

Novel ideas for DEFC membranes are being investigated in order to achieve higher operating temperatures, which result in increased reaction kinetics and increased fuel cell performance. For example, acid-doped polybenzimidazole (PBI) membranes allow operation at high temperatures (~ 170°C) with good thermal stability and mechanical properties, low cost, high proton conductivity (with phosphoric acid doping), and low electro-osmotic drag coefficient (meaning the movement of protons across the membrane is not dependent on membrane hydration) [7, 19, 23]. Wang *et al.* [7] conducted experiments using a phosphoric acid-doped PBI membrane in a DEFC and found the average percent yield of CO_2 (based on all oxidized products measured) over a temperature range of 150°C – 190°C to be 39.7 ± 8.5 % on a Pt/C catalysts and 32.1 ± 6.1 % on a PtRu/C catalyst (both having a 4 mg/cm^2 Pt loading) when flowing a 5 molar ratio of H_2O/C_2H_5OH solution and air.

While acid-doped PBI membranes appear promising, more research is needed to determine the optimal phosphoric acid doping along with the water:ethanol ratio in order to produce the maximum DEFC performance and CO_2 yield. It is important for the acid-doped PBI membrane DEFCs to be at least comparable in performance and durability to Nafion® membrane DEFCs to justify the additional challenges associated with high temperature operation. An *et al*. [10] tested a CEM-DEFC consisting of an alkaline supported ethanol anode, a Na^+-form Nafion® N117 membrane, and an acid supported hydrogen peroxide cathode, as shown in Figure 2-1. In this work, the theoretical voltage of a DEFC was calculated when hydrogen peroxide was utilized as the oxidant in both an AEM-DEFC and a CEM-DEFC. The AEM-DEFC theoretical cathode potential increased with the use of hydrogen peroxide (as compared to that when oxygen was used) from 0.4 V to 0.87 V and the CEM-DEFC theoretical cathode potential increased from 1.23 V to 1.78 V. The calculated theoretical anode potentials were 0.09 V for the CEM-DEFC and -0.74 V for the AEM-DEFC. In order to have the highest theoretical cell voltage, an alkaline supported ethanol anode, which would normally be employed in an AEM-DEFC, was combined with an acid supported hydrogen peroxide cathode, which would be found in a CEM-DEFC, giving a theoretical cell voltage of 2.52 V, which is much higher than that of other DEFCs. Experimentally, an OCV of 1.60 V was measured, along with a peak power density of 240 mW/cm^2, at 60°C (flowing 3 M ethanol with 5 M sodium hydroxide at 2 mL/min at the anode and 4 M

hydrogen peroxide with 1 M sulfuric acid at 2 mL/min at the cathode), which is lower than the theoretical value, but higher than results for other DEFC experiments.

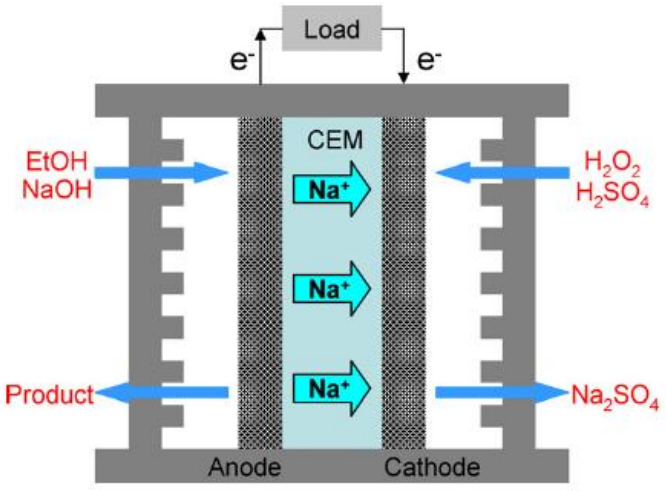

Figure 2-1. CEM-DEFC with an alkaline anode and acid cathode [10] (Reprinted with permission from Elsevier © 2011).

While progress continues with AEM materials and higher temperature CEM materials, current low temperature (<100°C) CEM materials offer advantages of low cost, good durability relative to AEM materials, and good compatibility with the high moisture content reactant stream required for the complete oxidation of CO_2 (i.e. Eq. 3). Thus, in this work, we focus on the use of low temperature CEM materials and analyze the applicability of novel catalyst/support systems that may provide reasonable current density and relatively complete oxidation in a system built around a traditional CEM material.

2.3. Ethanol Oxidation in Acid Environment

Electro-oxidation on platinum in acid media has been discussed by Lai *et al.* [2]. They identify two parallel pathways which can occur:

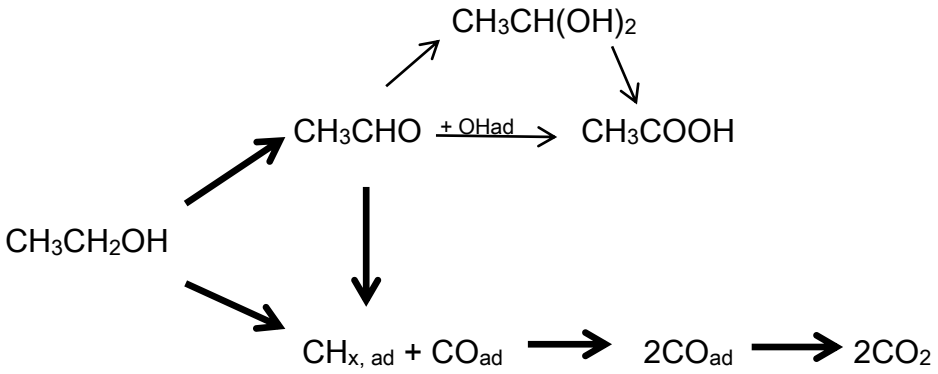

In the top pathway, the C-C bond remains intact and ethanol is oxidized to acetaldehyde. The acetaldehyde can then convert to acetic acid (which remains as a final product) either by reacting with adsorbed OH (OH_{ad}) or via hydration and the formation of germinal dial ($CH_3CH(OH)_2$) [2, 24] . The C-C bond can be broken in both acetaldehyde (top pathway) or in ethanol (bottom pathway), yielding CH_{ad} and CO_{ad}. According to Lai *et al.* [2], CH_{ad} is converted to CO_{ad} (between 0.10 and 0.45 V vs RHE) and further oxidized to CO_2 (between 0.45 and 0.70 V vs RHE). While the bottom pathway shows the double bond breaking in ethanol in order to form the adsorbed

intermediates, it is believed by Lai *et al.* [2] and Willsau and Heitbaum [25] that the double bond is more easily broken in acetaldehyde.

There appears to be a general agreement that ethanol and acetaldehyde form an adsorbed intermediate before further oxidation to CO_2 during ethanol oxidation on platinum in an acidic electrolyte, though it remains unclear precisely what this intermediate is. Colmati *et al.* [11], in agreement with Lai *et al.* [2], used Fourier transform infrared experiments on stepped platinum electrodes and concluded that the C-C bond can be broken at potentials as low as 0.1 V vs RHE. Many authors have shown that the ethanol oxidation peak around 0.65 – 0.75 V vs RHE in the forward voltammetry scan is at least partly due to further oxidation of the adsorbed intermediate to CO_2 [2, 11, 17, 25]. Oxidation of CO_{ad} to CO_2 has been reported, at room temperature, to begin at low potentials, 0.4 V vs RHE in 0.1 M ethanol [17] and ~0.2 V vs RHE in 0.5 M ethanol Lai *et al.* [2]. The further oxidation of adsorbed CO to CO_2 likely involves a Langmuir-Hinshelwood (LH) mechanism [11, 15]:

$$\boldsymbol{CO_{ad} + OH_{ad} \rightarrow CO_2 + H^+ + e^-} \qquad (2.4)$$

This mechanism shows that CO_2 formation is based on both adsorbed CO and adsorbed OH, which is most likely from water. The need for both adsorbed species

indicates that the rate of the reaction is dependent on the coverage of the catalyst by the two species and that the CO_{ad}, OH_{ad}, and other adsorbed intermediates are likely competing for active surface sites [15].

Cyclic voltammetry (CV) plots for the oxidation of ethanol in $HClO_4$ or H_2SO_4 on pure Pt or Pt/C have a general shape that has been described by many authors and is depicted in Figure 2-2 [2, 17]. Beginning at 0.05 V vs RHE in a CV conducted at room temperature, oxidation is initially blocked by adsorbed species on Pt (such as CO_{ad} and CH_{ad}, which further oxidizes to CO_{ad} between 0.1 and 0.45 V vs RHE) up to about 0.4 V vs RHE. The increase in current density that begins around 0.4 V vs RHE is due to the further oxidation of the CO_{ad} to CO_2 (which peaks around 0.6 V vs RHE) and to the incomplete oxidation of ethanol to acetaldehyde and acetic acid (which peaks ~0.85 V vs RHE). After this peak, the surface of the Pt is blocked by Pt oxide formation and OH_{ad}, leading to a drop in the current density. Further oxidation of acetaldehyde to acetic acid can be seen beginning around 1.0 V vs RHE and continuing until the sweep is reversed. At the start of the reverse sweep, the Pt surface is blocked by oxides, which are reduced at potentials less than ~0.8 V vs RHE. The only oxidation peak seen on the reverse sweep is ~ 0.75 V vs RHE and, at room temperature, is due solely to incomplete ethanol oxidation. An increase in the peak current densities indicates increased catalytic activity, due to either an increase in overall ethanol conversion (meaning an increase in the percent of ethanol oxidized) and/or more complete ethanol

oxidation (e.g. an increase in the percent of CO_2 formation). An earlier onset of oxidation (indicated by a negative potential shift on the forward scan and a positive potential shift on the reverse scan) implies that the catalyst active sites are becoming available sooner (after being blocked by intermediate species) for oxidation. A negative shift in the potential at which the current density peaks occur in the CV suggests that the anode overpotential in a fuel cell would be less, leading to an overall increase in cell voltage.

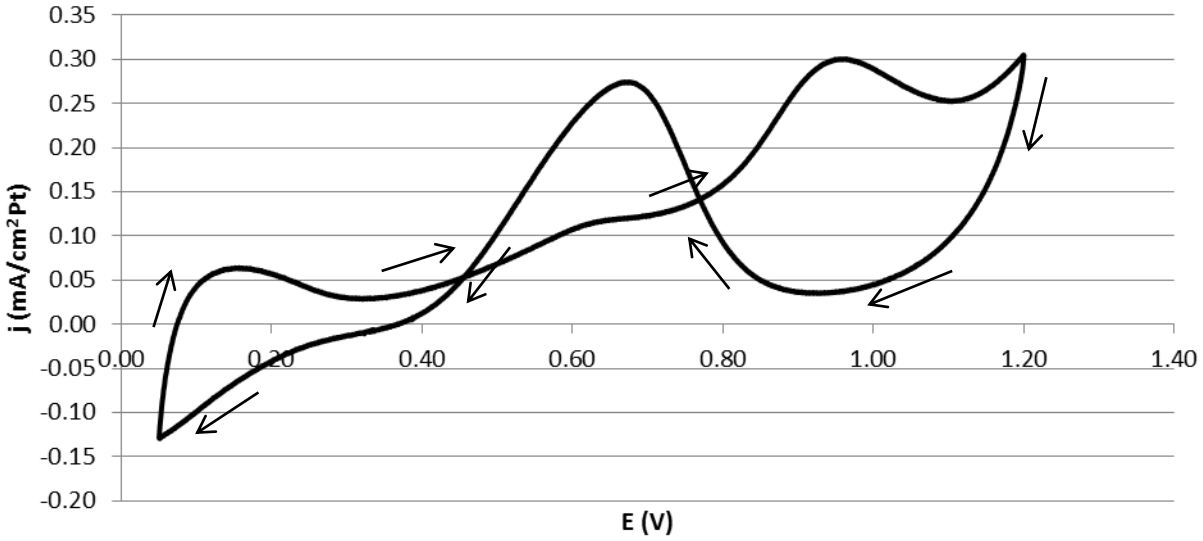

Figure 2-2. CV on a Pt/C electrode in 0.1 M ethanol solution with 0.1 M H_2SO_4.

In order to evaluate the oxidation of ethanol on various catalysts, researchers look not only at the current and power densities produced, but also at the formation of ethanol oxidation products (CO_2, acetaldehyde, and acetic acid) in electrochemical and fuel cell tests. The results of product analysis are varied and are presented in multiple formats. The (percent) yield of a product refers to the moles (or concentration) of the particular product compared to the total moles (or concentration) of oxidized products measured. The CO_2 current efficiency is a ratio of the current for ethanol oxidation to CO_2 to the total Faradaic current for ethanol oxidation. The variations in the product yields and the CO_2 current efficiency reported can be due not only to the choice of catalyst, membrane, ethanol concentration, and operating conditions, but also to the technique and setup used to analyze the products.

Various parameters have an effect on the DEFC performance and CO_2 production. An increase in CO_2 production, based on CO_2 current efficiency and concentrations (mol/L) of CO_2 in the anode products, has been seen with a decrease in ethanol concentration, but at the lower concentrations (0.1 M or less) the current density is not high enough to be feasible in a working DEFC [6, 15, 17]. The peak current density in 0.1 M ethanol solution was only 20% of the peak current density seen in 1 M ethanol solution in the same experiment (just under 1 mA/cm^2 versus almost 5 mA/cm^2) [15]. Camara and Iwasita [15] showed that, at room temperature with a carbon supported platinum (Pt/C) electrode, the maximum current density after a 20 minute

hold at 0.5 V vs RHE was 8 μA/cm^2 with 0.5 M ethanol in 0.1 M $HClO_4$ solution. They saw that the current density after the 20 minute hold decreased if the ethanol concentration was raised or lowered. An increase in ethanol concentration led to an increase in electrode poisoning by intermediate species. This maximum current density can also be explained by looking at how the variation in ethanol concentration affects product formation. Camara and Iwasita [15] reported that acetaldehyde was the primary product for ethanol concentrations above 0.2 M and that acetaldehyde production was seen to increase as the ethanol concentration increased from 0.1 M to 0.5 M, at which point the amount of acetaldehyde produced stabilized when using a Pt/C electrode, even as the ethanol concentration was further increased to 1.0 M. They also found that CO_2 formation was low at all concentrations in comparison to acetaldehyde and acetic acid. In a study by Mann *et al.* [5] on a PtSnInO/C catalyst in a DEFC at 130°C using various concentrations of ethanol at the anode and oxygen at the cathode, an increase in ethanol concentration from 0.2 M to 1 M led to an increase in fuel cell performance. While a current density of only 120 – 140 mA/cm^2 at 0.1 V was seen when using the 0.2 M ethanol, a current density close to 350 mA/cm^2 was seen with 1 M ethanol concentration. When they increased the concentration to 6 M, the OCV decreased slightly but the slope of the polarization curve remained the same as that of the polarization curve with 1 M ethanol concentration. This constant slope indicated that the ethanol oxidation reaction kinetics were not affected by the increase in ethanol

concentration from 1 M to 6 M, unlike in the increase from 0.2 M to 1 M ethanol concentration, implying that the reaction kinetics were independent of ethanol concentration at concentrations greater than 1 M, at least on the PtSnInO/C catalyst. The decrease in the OCV, which was also seen with the increase in concentration from 0.2 M to 1 M, was attributed to increased crossover of ethanol through the Nafion® membrane, along with oxygen crossover to the anode side of the cell, where non-electrochemical oxidation of ethanol was found to occur.

Temperature is another variable that has been shown to have a significant effect on the product formation and performance of DEFCs. An increase in temperature leads to faster reaction kinetics and an increase in the C-C bond breaking, which results in increased fuel cell performance and an increase in CO_2 formation (based on CO_2 current efficiency) [6, 17, 26]. Andreadis *et al.* [26] saw a 200% increase in the maximum power density (from about 3 mW/cm^2 to about 9 mW/cm^2) on a PtRu/C catalyst in a DEFC, flowing 1.0 M ethanol at 0.5 mL/min and humidified oxygen at 50 mL/min, as the temperature was increased from 60°C to 90°C. The amount of oxidized products (acetic acid, acetaldehyde, and CO_2), based on both the mole fraction of the oxidized products out of the total moles of products measured by gas chromatography and on the CO_2 current efficiency, increased with an increase in temperature on PtRu/C (60°C - 90°C), PtSnInO/C (90°C - 135°C), and Pt/C (23°C-100°C) catalysts [5, 17, 26]. While the overall percent of ethanol conversion increases, the percent of acetaldehyde

produced was shown to decrease with an increase in temperature on the same PtRu/C and PtSnInO/C catalysts since more complete ethanol oxidation is occurring. Sun *et al.* [17] performed CV's in 0.1 M ethanol on a Pt/C catalyst at temperatures ranging from 23°C to 100°C and reported an increase in the CO_2 current efficiency with an increase in temperature (~45% at 100°C). They also saw a decrease in the potential at the onset of ethanol oxidation and at the peak current density in the forward scan, implying an increase in OH_{ad} and CO_{ad} oxidation. On the negative scan, the authors saw that CO_2 formed only when at a temperature of at least 40°C, with the CO_2 current efficiency only reaching 2.7% at 40°C but increasing to 50% at 100°C. Following the same trends, Ghumman *et al.* [12] saw an increase in CO_2 yield (based on moles of electrons due to CO^2 out of the total moles of electrons measured) from 15% at 80°C to 51-81% at 100°C with a Pt/C catalyst in a fuel cell operating at a constant current of 40 $mAcm^2$ while flowing 0.5 M ethanol at 0.2 mL/min and dry oxygen at 30 mL/min. The CO_2 yield when using PtRu/C was much lower, around 25%, at 100°C in the same setup. They noted that the increased temperature resulted in an ethanol/water vapor fed fuel cell, which has been shown by Ghumman *et al.* [12] and others [16] to lead to a greater yield of CO_2, even at lower temperatures. While the operation of a DEFC under a constant discharge current is more stable at higher temperatures, the temperature range is limited by the membrane used (most often Nafion®) and once temperatures

surpass 100°C, membrane dehydration and damage can occur, which will decrease the fuel cell's performance [12, 26].

Other operating conditions that influence ethanol oxidation rates and CO_2 yield include the reactant flow rates, the cell voltage, and the cell current. Changing the flow rate of the reactants affects the convection in the flow field channel and alters the amount of time the reactants are in the electrochemically active area [6]. It is important to have a high enough flow rate to replenish the reactants as they are consumed for the electrochemical reaction, though it has been seen that the CO_2 production in a fuel cell can decrease if the flow rate is too high. When Rao *et al.* [6] increased the flow rate of the reactants for a 0.1 M ethanol concentration DEFC using a Pt/C anode, the CO_2 current efficiency reached a maximum of ~53 % at 2.5 ml/minute, but then dropped as the flow rate increased. The decrease in CO_2 current efficiency was attributed to a decrease in the time an ethanol molecule spent in the catalyst layer (the electrochemically active area).

Sun *et al.* [17] found that the CO_2 current efficiency decreased on a Pt/C catalyst during at steady-state potentiostatic hold in various ethanol concentration solutions as the cell potential was increased from 0.48 V vs RHE to 0.68 V vs RHE. They state that this trend of a decrease in CO_2 formation with an increase in potential has been seen by others and is due to an increase in Pt coverage by OH_{ad} and surface oxides at higher

potentials, which leaves less sites available for breaking the C-C bond. Using a PtSn/C anode, Rousseau *et al.* [13] increased the current density of a DEFC flowing 2 M ethanol from 24 mA/cm^2 to 40 mA/cm^2 at 80°C and saw an increase in the ethanol crossover rate and a decrease in the percent yield of CO_2 (8% to 4.4%) and acetaldehyde (17.2% to 15.9%), with acetic acid having the largest yield (~75%). During galvanostatic tests on a 4 cm^2 electrode, Andreadis *et al.* [26] saw that while an increase in current density (from 20 mA to 120 mA) on a PtRu/C anode led to an increase in ethanol conversion, the percent yield of CO_2 decreased while that of acetaldehyde increased [26]. Though the percent yield of CO_2 is lower than that of acetaldehyde and acetic acid on a number of electrocatalysts, it is clear that the catalyst itself has a large impact on the performance of and products produced by a DEFC.

2.4. Acid Electrolyte Catalysts

Many different electrocatalysts have been employed in DEFCs. While an ideal catalyst (i.e. one that accomplishes rapid and complete oxidation of ethanol to CO_2) has not yet been identified, much has been learned about what is required of the catalyst in a DEFC and discoveries are continually made about how various catalyst systems affect the ethanol oxidation reaction and overall fuel cell performance. Finding metals that can improve the ethanol oxidation reaction and are also stable in acid medium over

long periods of time is challenging [3]. Platinum-based catalysts are common in hydrogen fuel cells using acidic media, so platinum has been the starting point for finding an ideal catalyst for use in a DEFC [2, 16]. Unfortunately, the dissociative adsorption of organic molecules, such as ethanol, leads to poisoning of the Pt catalyst [3, 27-29]. Lamy *et al.* [3] propose that a bi-metallic catalyst can be used to improve ethanol oxidation, but in order to completely oxidize ethanol to CO_2 at low potentials, a third metal might be necessary. A tri-metallic catalyst could increase the activation of H_2O and catalyst coverage of OH_{ad} at low potentials, allowing CO_{ad} to be further oxidized at lower potentials. Both bi- and tri-metallic catalysts are less affected by adsorbed species and more active for ethanol oxidation than pure Pt/C catalysts [13, 29].

The OCV of a DEFC, flowing 1 M ethanol at 1 mL/min at the anode with excess oxygen supplied at the cathode, was less than 0.4 V at 120°C on a Pt/C catalyst with a Pt loading of ~0.6 mg/cm^2 [5] and ~0.55 V at 90°C with a Pt loading of 2.0 mg/cm^2 [9]. Platinum has been paired with ruthenium (Ru) and tin (Sn) and supported on carbon (PtRu/C and PtSn/C) in hopes of increasing the performance of a DEFC. While both have been reported as promising electrocatalysts [9, 12-14], many issues remain and other catalysts continue to be explored. The addition of Ru to Pt/C increased the OCV (which relates to a decrease in catalyst poisoning) in the 120°C, 1 M ethanol/oxygen DEFC mentioned previously to ~0.5 V with a 0.6 mg/cm^2 Pt loading and to 0.67 V with

a 1.3 mg/cm^2 Pt loading in the 90°C cell, but these values are only about half of the theoretical potential for ethanol oxidation (1.145 V) [5, 9, 13]. The increased performance seen by the PtRu/C catalyst (which implies the catalyst is more active for ethanol oxidation) is an improvement over Pt/C as far as current and power density are concerned, but it has not been shown to improve the CO_2 current efficiency [12-14, 26]. In fact, high amounts of Ru appear to lower the rate of C-C bond breakage [6, 13]. Andreadis *et al.* [26] have also demonstrated that it was difficult to break the C-C bond over a PtRu/C catalyst and have reported a maximum CO_2 percent yield (based on the ratio of the moles of CO_2 formed compared to the total moles of product) of 0.5%, which occurred at 90°C and 40 mA. In relation to catalyst poisoning, both Ru and Sn are beneficial in that they provide sites for OH_{ad}, which in turn will oxidize CO_{ad} to CO_2 on nearby Pt sites, freeing Pt active sites for further ethanol oxidation [29-31]. It is known though that CO adsorption occurs on both Pt and Ru surfaces, thereby blocking sites for OH adsorption, which is necessary for the complete oxidation of ethanol, while Sn, on the other hand, does not adsorb CO [9, 28, 30]. Gasteiger *et al.* [28] found that when Sn is paired with Pt (Pt:Sn atomic ratio of 3:1), there is a decrease in the onset potential of CO oxidation, implying a decrease in CO poisoning on the Pt surface. In a rotating disk electrode experiment with CO saturated 0.5 M H_2SO_4 at 62°C, the authors found that CO oxidation began as low as 0.25 V vs RHE on the PtSn surface, which is 0.5 V lower than the onset potential seen on Pt and 0.15 V lower than that on pure Ru. Lamy

et al. [3] also found that that addition of Sn to Pt/C significantly decreased the poisoning effect by CO_{ad}.

When Sn is added to a Pt/C catalyst, ethanol oxidation has been reported to begin at lower electrode potentials, as stated above, and to produce higher peak current densities in CVs, as well as lead to a higher peak power density and OCV relative to Pt/C and PtRu/C catalysts [3, 5, 9, 13, 28, 30, 31]. While the catalytic activity toward ethanol oxidation is increased with the addition of Sn to a Pt/C catalyst, the C-C bond breaking is actually inhibited, leading to a decrease in CO_2 production [3, 13, 31]. The formation of acetaldehyde is also decreased though an increase in acetic acid occurs [13]. OCVs in the region of 0.7 V - 0.8 V vs RHE in DEFCs flowing aqueous ethanol solutions and oxygen at various temperatures have been reported with the addition of Sn to the Pt/C catalyst [3, 5, 9, 13, 30, 32]. The Pt to Sn atomic ratio has an effect on the ethanol oxidation activity and fuel cell performance [30]. Zhou *et al.* [30] investigated the effects of the ratio of Sn to Pt and saw that while the addition of Sn increases the sites available for OH_{ad}, too much Sn can decrease the number of active sites available on Pt, as well as decrease the conductivity in the catalyst, leading to a decrease in fuel cell performance. They found an optimal Pt:Sn atomic ratio (in terms of fuel cell performance) to be 3:2 at 60°C but 2:1 at higher temperatures (75°C and 90°C). The procedure by which the PtSn/C catalyst is prepared can also affect the EOR on the catalyst. It has been reported that when Sn forms SnO_2, better results are seen in

ethanol electrochemical and fuel cell experiments due to the ability of the tin-oxide to provide oxygen species to further oxidize CO_{ad} and other, similar intermediate species [5, 9, 30, 32]. Jiang *et al.* [32] found that when SnO_2 formed, the current density at 0.4 V vs SCE during a CV in 0.5 M H_2SO_4 at 50 mV/s at room temperature was 1.788 mA/cm^2 as compared to 0.547 mA/cm^2, which was seen when Sn did not form SnO_2. In a DEFC with a Nafion® membrane at 90°C flowing 1.0 M ethanol at 1.0 mL/min and un-humidified oxygen at a pressure of 0.2 MPa, the same authors found the OCV of the SnO_2-forming catalyst to be 0.819 V vs SCE with a peak power density of 79.5 mW/cm^2 compared to 0.7 V vs SCE and 47.0 mW/cm^2 for the PtSn/C catalyst which did not contain SnO_2 particles. Some authors conclude that a combination of alloyed PtSn and SnO_x in the PtSn/C catalyst is necessary for optimal performance [31, 32].

In addition to PtSn, other bi-metallic catalysts have been explored but the results have shown decreased DEFC performance and less complete ethanol oxidation. For example, at 90°C PtRu/C, PtPd/C, and PtW/C catalysts (metal atomic ratio of 1:1 for all three catalysts) demonstrated both lower OCVs and power densities compared to PtSn/C (1:1 atomic ratio) in a DEFC operated at 90°C with a Nafion®-115 membrane flowing 1.0 M ethanol at 1.0 mL/min and un-humidified oxygen at 120 mL/min at a pressure of 0.2 MPa [30]. These bi-metallic catalysts were shown by Zhou *et al.* [30] to have peak current densities on the forward, 10 mV/s sweep of a CV at room temperature in a solution of 1.0 M ethanol and 0.5 M H_2SO_4 at lower potentials than

Pt/C. However, the peak current density of the forward scan for these other bimetallic catalysts was still lower than for PtSn/C (56.2 mA/cm^2 at 0.710 V vs SCE). The PtSn/C current density was double that of all the other catalysts, with the exception of PtW/C, which had a peak current density of 49.4 mA/cm^2 at 0.755 V vs SCE. Li *et al.* [29] investigated the pairing of Pt with Pb and Ru, to form PtPb/C and PtRuPb/C catalysts (not alloyed), on ethanol oxidation and compared the results to those they produced with Pt/C and PtSn/C catalysts on a glassy carbon electrode, all prepared in similar manners with a catalyst loading of 0.11 mg/cm^2. At low potentials (below 0.3 V vs SHE) during a linear voltammogram in 1 M ethanol solution with 0.1 M H_2SO_4, the PtSn/C (4:1 atomic ratio of Pt to Sn) electrode resulted in the highest current densities, followed closely by the PtRuPb/C (1:1:0.3 atomic ratio) electrode. At higher potentials (0.5 V – 0.9 V vs SHE), the PtPb/C (4:1 atomic ratio) electrode outperformed the other electrodes, showing the highest catalytic activity by far (2-4 times higher current densities) in the 1 M ethanol solution. The early onset of oxidation witnessed on the Pb-containing electrodes, indicates that Pb, like Sn, helps to oxidize reaction intermediates and free Pt sites. Potentiostatic tests at 0.5 V and 0.6 V in 1 M ethanol solution also resulted in a Pb-containing catalyst achieving the best performance over other catalysts tested.

Zhou *et al.* [9] explored the use of tri-metallic catalysts. An increase in performance over a PtRu/C (1:1 atomic ratio) catalyst with a 1.3 mg/cm^2 Pt loading was

seen with the addition of W or Mo to PtRu/C (1:1:1 atomic ratio) but the tri-metallic catalysts fell short of the performance of a PtSn /C (1:1 atomic ratio) catalyst at the same conditions (90°C with 1 M ethanol). Results of the addition of Ru to PtSn/C are unclear though. While Rousseau *et al.* [13] saw an improved performance with PtSnRu/C (86:10:4 atomic ratio), in regards to OCV and power density, over Pt_9Sn_1/C and Pt/C catalysts with a Pt loading of 3 mg/cm^2 and 2 M ethanol solution at 80°C, Zhou *et al.* [9] found that even though the PtSnRu/C (1:1:1 atomic ratio) catalyst resulted in an improved performance over PtRu/C (1:1 atomic ratio), the PtSn/C (1:1 atomic ratio) still had the top performance with a 1.3 mg/cm^2 loading at 90°C. It was noted that the addition of Ru to the PtSn/C catalyst improved the conductivity of the catalyst but also decreased the lattice parameters, which may be the reason for the decrease in performance [9]. Mann *et al.* [5] experimented with PtSnInO and found that a polarization curve of a DEFC at 130°C, flowing 1 M ethanol at 1 mL/min and un-humidified oxygen at 100 mL/min, produced current densities about 40% higher when using the PtSnInO/C catalyst than when using the PtSnO/C catalyst that was also tested. They also saw a decrease in the mole fraction of acetaldehyde and an increase in the mole fraction of acetic acid produced with PtSnInO/C compared with PtSnO/C at 130°C, which demonstrates that PtSnInO/C leads to higher oxidized products than PtSnO/C.

Other, non-platinum based, catalysts have been studied in both acid and alkaline environments. Even in alkaline media, gold does a poor job of breaking the C-C bond [2]. On the other hand, Pd-(Ni-Zn)/C outperforms other known anode electrocatalysts for ethanol oxidation in alkaline media [33]. When compared to Pd/C in alkaline media, Pd-(Ni-Zn)/C had a higher power output, producing 170 mW/cm^2 at 80°C [33]. Along with catalyst composition, the catalyst loading and thickness are also important. More complete ethanol oxidation (higher CO_2 current efficiency) is seen with an increase in platinum loading, with a plateau beginning to form around 8 mg/cm^2 for a 40% Pt/C catalyst in an acid media DEFC at 90°C using 0.1 M ethanol concentration and differential electrochemical mass spectrometry [6]. Increasing the catalyst loading increases the electrochemically active surface area, while increasing the catalyst layer thickness increases the residence time of the reactants, both of which encourage more complete oxidation of ethanol [6].

As seen by the descriptions of catalysts mentioned above, most common catalysts are supported by carbon (for example, Vulcan XC72) because carbon has high electron conductivity and high surface area, but the carbon support can corrode in a working fuel cell, thereby degrading the catalyst layer and decreasing the fuel cell's performance [34]. It has been reported that carbon oxidation on this Vulcan carbon support occurs at 65°C at potentials greater than 0.8 V vs RHE [35, 36]. When a fuel cell is used in an automotive application, the potential of the cell spikes to above 1.2 V

vs RHE when the vehicle is starting up or shutting down, which greatly affects the durability of the carbon supported catalyst [37]. Titanium dioxide (TiO_2) appears to be a potential substitute for carbon since it has shown better resistance to corrosion and is commercially available at a low cost [34]. The addition of TiO_2 to catalysts for both hydrogen and methanol PEM fuel cells has resulted in an increase in fuel cell performance and, in some cases, an increase in the electrochemically active surface area of the catalyst layer [38-40]. Kim *et al.* [38] added TiO_2 supported Au to a PtRu/C electrode and reported an increase in CO oxidation, possibly due to an increase in sites available for adsorption of OH provided by the TiO_2 (similar to the effect seen by the addition of Sn to a Pt/C electrode) [39]. One downside of TiO_2 is that it is a semiconductor and therefore, for it to be used in a fuel cell catalyst application, the electronic conductivity must be improved [34]. Niobium (Nb)-doped TiO_2 has been suggested to have increased conductivity over undoped TiO_2 due to the decrease in the band gap of TiO_2 by the Nb [34, 41].

In this work, the electrochemical activity and fuel cell performance of a Nb-doped TiO_2 supported Pt catalyst (Pt/Nb-TiO_2) is examined. While Pt/C catalysts have not produced the best results for ethanol oxidation, Pt is the starting point for the majority of catalysts used for ethanol oxidation in acid media. The electrochemical activity and performance of the Pt/Nb-TiO_2 catalyst is compared to two common DEFC catalysts, Pt/C and PtSn/C, in order to see how the change in catalyst support affects the

electrode active area, catalytic activity, ethanol oxidation reaction, and fuel cell performance. The reported performances of Pt/C and PtSn/C catalysts, along with a few other common DEFC catalysts, are summarized in Table 2-1. An increase in OH_{ad} sites due to the addition of TiO_2 could lead to catalytic activity and DEFC performances similar to that of a PtSn/C catalyst. If the catalytic activity is at least comparable to that seen on a Pt/C catalyst, the novel catalyst could increase the lifetime of a DEFC without compromising the fuel cell performance.

Table 2-1. Summary of common acid media DEFC catalysts.

Catalyst	Atomic Ratio	Anode Loading	Anode Conditions	Cathode Conditions	Cell Temp (°C)	Peak Power (mW/cm^2 MEA)	Reference
Pt/C	-	1.5 mg Pt/cm^2	0.1 M Ethanol	-	110	8	Lamy *et al.* [3]
	-	1.3 mg Pt/cm^2	1 M Ethanol	O_2	90	11	Zhou *et al.* [9, 30]
	-	2.0 mg Pt/cm^2	2 M Ethanol (14.7 psig)	O_2 (44.1 psig)	80	5	Rousseau *et al.* [13]
PtPd/C	1:1	1.3 mg Pt/cm^2	1 M Ethanol	O_2	90	12	Zhou *et al.* [9, 30]
PtW/C	1:1	1.3 mg Pt/cm^2	1 M Ethanol	O_2	90	16	Zhou *et al.* [9, 30]
PtRu/C	4:1	1.5 mg metal/cm^2	0.1 M Ethanol	-	110	12	Lamy *et al.* [3]
	1:1	1.3 mg Pt/cm^2	1 M Ethanol	O_2 (un-humidified)	90	29	Zhou *et al.* [9, 30]
	-	2.0 mg Pt/cm^2	1 M Ethanol	O_2 (humidified)	60	4	Andreadis *et al.* [26]
	-	2.0 mg Pt/cm^2	1 M Ethanol	O_2 (humidified)	70	6	Andreadis *et al.* [26]
	-	2.0 mg Pt/cm^2	1 M Ethanol	O_2 (humidified)	80	8	Andreadis *et al.* [26]
	-	2.0 mg Pt/cm^2	1 M Ethanol	O_2 (humidified)	90	10	Andreadis *et al.* [26]
	1:1	1.3 mg Pt/cm^2	1 M Ethanol	O_2 (29.4 psig)	90	30	Song *et al.* [14]
PtSn/C	9:1	1.5 mg metal/cm^2	0.1 M Ethanol	-	50	6	Lamy *et al.* [3]
	9:1	1.5 mg metal/cm^2	0.1 M Ethanol	-	70	13	Lamy *et al.* [3]
	9:1	1.5 mg metal/cm^2	0.1 M Ethanol	-	90	20	Lamy *et al.* [3]
	9:1	1.5 mg metal/cm^2	0.1 M Ethanol	-	100	23	Lamy *et al.* [3]
	9:1	1.5 mg metal/cm^2	0.1 M Ethanol	-	110	23	Lamy *et al.* [3]
	4:1	1.5 mg metal/cm^2	0.1 M Ethanol	-	110	26	Lamy *et al.* [3]
	1:1	1.3 mg Pt/cm^2	1 M Ethanol	O_2	90	52	Zhou *et al.* [9, 30]
	2:1	1.3 mg Pt/cm^2	1 M Ethanol	O_2 (29.4 psig)	90	48	Song *et al.* [14]
	2:1	1.3 mg Pt/cm^2	1 M Ethanol	O_2 (29.4 psig)	90	60	Song *et al.* [14]
	3:1	1.5 mg Pt/cm^2	1 M Ethanol	O_2 (29.4 psig)	90	47	Jiang *et al.* [32]
	3:1	1.5 mg Pt/cm^2	1 M Ethanol	O_2 (29.4 psig)	90	80	Jiang *et al.* [32]
	100:20	1.0 mg Pt/cm^2	1 M Ethanol (14.7 psig)	O_2 (14.7 psig)	30	5	Vigier *et al.* [24]
	100:20	1.0 mg Pt/cm^2	1 M Ethanol (14.7 psig)	O_2 (14.7 psig)	50	11	Vigier *et al.* [24]
	100:20	1.0 mg Pt/cm^2	1 M Ethanol (14.7 psig)	O_2 (14.7 psig)	70	25	Vigier *et al.* [24]

Catalyst	Atomic Ratio	Anode Loading	Anode Conditions	Cathode Conditions	Cell Temp (°C)	Peak Power (mW/cm^2 MEA)	Reference
PtSn/C	100:20	1.0 mg Pt/cm^2	1 M Ethanol (14.7 psig)	O_2 (14.7 psig)	90	35	Vigier *et al.* [24]
	100:20	1.0 mg Pt/cm^2	1 M Ethanol (14.7 psig)	O_2 (14.7 psig)	110	45	Vigier *et al.* [24]
	-	2.0 mg Pt/cm^2	2 M Ethanol (14.7 psig)	O_2 (44.1 psig)	80	5	Rousseau *et al.* [13]
PtSnRu /C	1:1:1	1.3 mg Pt/cm^2	1 M Ethanol	O_2	90	38	Zhou *et al.* [9, 30]
	86:10:1	2.0 mg Pt/cm^2	2 M Ethanol (14.7 psig)	O_2 (44.1 psig)	80	50	Rousseau *et al.* [13]

Notes:

A "-" indicates the information for the field was not applicable or not given.

3. EXPERIMENTAL PROCEDURES

One of the first steps in evaluating a supported catalyst for an electrochemical reaction, such as that in a DEFC, is to gain a basic understanding of the nature of the reaction taking place on the catalyst surface. Cyclic voltammetry (CV) is a useful and simple technique for understanding the mechanisms involved in electrochemical reactions. In cyclic voltammetry, the potential of a working electrode (measured with respect to a reference electrode) is cycled at a specified rate while the current at the working electrode is measured. In a CV experiment, the current is not only a function of potential, but also of time since the potential varies with time. As the potential varies over a particular range, oxidation and reduction reactions occur at the working electrode/electrolyte interface, yielding characteristic peaks in the measured current. The cyclic voltammogram of a redox reaction is influenced by the mass transfer processes that supply reactants to or remove products from the reaction sites [42]. As the potential increases, the rate of the oxidation reaction (and hence the oxidative current) will increase until the concentration of the reacting species is depleted. At this point, the reaction rate reaches a peak and the current begins to decrease. The CV behavior of a particular reaction is influenced by the supported catalyst on the working electrode, the electrolyte concentration, the potential scan rate, and the fluid motion in the vicinity of the catalyst layer. Manipulation of these parameters, while observing the

effect on CV behavior, can provide insight into the reaction mechanisms that are occurring on the catalyst surface.

Cyclic voltammograms can be recorded while the working electrode is stationary or while the electrode is rotating. Rotating disk electrode (RDE) tests can reduce mass transfer effects, which are seen in stationary electrode tests. In an RDE test, an increase in the rotation causes an increase in the flux of the electrolyte solution (reactant) to the electrode surface, as well as an increase in the rate at which product is removed from the electrode surface, therefore reducing the diffusion limitations that occur in stationary and low speed rotating electrode experiments [43]. If the rotation rate is sufficiently high, current peaks in a rotating disk electrode test will be due to kinetic limitations rather than depletions of the reacting species concentration (diffusion effects) at the electrode surface [44]. From a combination of stationary and RDE tests, one can estimate the electrochemically active surface area of an electrode, along with the limiting current and the number of electrons transferred during the particular reaction under investigation.

In contrast to CV experiments, potentiostatic experiments are conducted by maintaining the working electrode at a constant potential and measuring the resulting current over time. Potentiostatic experiments are particularly useful for observing the poisoning of the working electrode by intermediate species. If the imposed potential

leads to an electrochemical reaction, an initial increase in current will be measured. However, over time the electrode may be covered by intermediate species, which prevent the complete reaction from occurring and cause the current to decrease. The current will also decrease as the concentration of the reactant is depleted near the electrode. Both of these effects, diffusion limits and poisoning, can affect the rate at which the current decreases over time. Proper choice of experimental parameters can often cause these phenomena to occur over different time scales, allowing them to be analyzed separately. The electrochemical tests conducted in this work include stationary disk CV tests (SDCV) to assess catalyst surface area and catalytic activity, as well as stationary disk potentiostatic (SDPS) tests to assess catalyst layer poisoning. Procedures associated with these experiments are discussed in the first section of this chapter and include three basic steps: supported catalyst solution preparation, electrode preparation, and electrochemical measurements.

While electrochemical tests on thin film electrodes can provide fundamental insights into the behavior of a particular supported catalyst, the goal of this research is to demonstrate whether the novel catalyst system tested here can improve the performance of direct ethanol fuel cells. The performance of the catalyst system as implemented in a DEFC can be evaluated by measuring polarization curves, which show how the voltage and current are related for a fuel cell device. For an ethanol fuel cell, the theoretical open circuit voltage (OCV) is 1.145 V, but irreversible losses (i.e.

fuel crossover and/or internal shorts) result in an actual voltage that is lower than 1.145 V. The OCV is a measurement of the cell voltage before any current is supplied to the external load. In a fuel cell test, the OCV will be the highest voltage the cell can achieve and as current to the external load increases, the cell voltage will drop. Figure 3-1 depicts the general shape of a fuel cell polarization curve and identifies the most significant losses for each of three regions of current production. *Activation losses* relate to the electrochemical reaction that is occurring in the fuel cell, *ohmic losses* are associated with the conduction of ions across the fuel cell electrolyte and electrons through the fuel cell device, and *mass transport losses* correlate to the flow of the reactants and products through the cell.

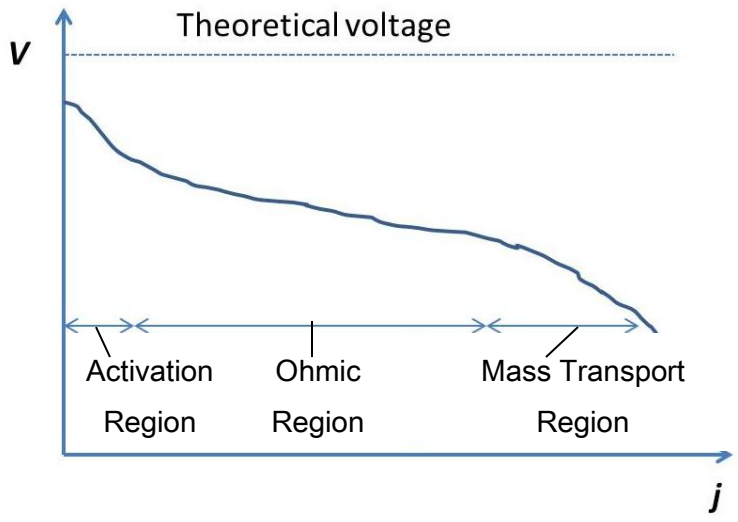

Figure 3-1. General polarization curve for a fuel cell.

Since the current produced by a fuel cell is proportional to the active area of the fuel cell, the voltage is typically plotted versus current density (A/cm^2) instead of current (A). This allows polarization curves to be compared regardless of the fuel cell active area. On a polarization curve, the voltage is related to the efficiency of the fuel cell while the current density is related to the rate of fuel consumption. A power density curve can be produced from a polarization curve by multiplying each voltage value by its corresponding current density value ($P = VI$). When evaluating the performance of a catalyst system within a fuel cell, it is important to consider both the power density and fuel cell efficiency.

Comparing polarization and power density curves among fuel cells incorporating different catalyst systems enables not only the power density and fuel cell efficiency to be compared, but also allows the significance of the various irreversible losses to be assessed. The experiments conducted in this research look at the effect of catalyst support on the performance of an ethanol fuel cell at both room temperature and 60°C. Procedures associated with these experiments are discussed in the final two sections of this chapter and include two basic steps: membrane-electrode-assembly (MEA) fabrication and performance evaluation.

3.1. Thin Film Catalyst Solution Preparation

The catalyst solutions were prepared so that each contained 1.2 mg Pt. Commercial supported catalysts were used for the Pt/C solution (De Nora North America, Inc. E-TEK Division 29.3% Pt on Vulcan XC-72) and the PtSn/C solution (E-TEK Division 40% HP Pt:Sn alloy, 3:1 atomic ratio, on Vulcan XC-72). A niobium-doped titanium dioxide supported Pt catalyst (Pt/Nb-TiO_2) was prepared in-house by Hou [45]. Anatase particles were formed by precipitation from homogeneous solution using titainium(IV) isopropoxide as precursor in aqueous solution (water:titianium mole ratio of 200) that was acidified with nitric acid to pH 1. A white suspension formed instantaneously when the titanium(IV) isopropoxide was added to the aqueous solution. Next, $NbCl_5$ was added drop-wise to the suspension in order to give a Nb:TiO_2 ratio of 5:95 based on weight. The suspension was then peptized at 85°C to disperse the aggregates into smaller (< 20 nm) particles. Evaporation of water and 2-propanol during hydrolysis resulted in condensation of a light blue, translucent colloid that remained stable for several weeks. The gel-like colloid was ground into a powder after it was vacuum dried for 10 hours at 100°C. Afterward, the powder was placed in an alumina crucible and heated for 4 hours at 450°C to form anatase phase and make the particles grow. Impregnation was used to form the Pt/Nb-TiO_2. The Nb-TiO_2 particles were dispersed in IPA and ultrasonicated for 30 minutes. The platinum precursor, chloroplatinic acid hexahydrate ($H_2PtCl_6.6H_2O$) was added to the suspension to give a

30 wt% Pt catalyst. The suspension was then heated in order to evaporate the solvent and the powder was put in an alumina crucible and reduced for 4 hours in a tube furnace at 400°C with a H_2 atmosphere.

All of the supported catalysts were 30 wt% Pt, so 4 mg of supported catalyst was required for each catalyst solution. In order to increase the conductive pathways throughout the catalyst layer, 10 wt% carbon black (Vulcan XC72R) was added to the 4 mg of Pt/Nb-TiO_2 (to give a total supported catalyst mass of ~4.44 mg in the Pt/Nb-TiO_2-C solution). The carbon was added after deposition of Pt on the Ni-TiO_2 support and is thus not expected to provide support for the catalyst, but rather only electrical continuity within the catalyst layer. After the proper amount of supported catalyst was measured into a vial, deionized (DI) water was added drop-wise to wet the catalyst prior to adding 2 mL of isopropyl alcohol (IPA). Addition of water reduces the risk of igniting IPA vapor during suspension. The catalyst solution was ultrasonicated (Fisher Scientific FS60) briefly to mix the components before a 5 wt% Nafion® solution (Ion Power, Inc. 1100EW) was added to the mixture. The ratio of Nafion® to catalyst support was roughly 0.6 in the Pt/C and PtSn/C solutions and 0.5 in the Pt/Nb-TiO_2-C solution. Each catalyst solution was then ultrasonicated for at least 30 minutes after the preparation was complete. If the solution was left to sit long enough for the supported catalyst particles to settle on the bottom, the solution was ultrasonicated again using the same procedure to ensure proper distribution of the supported catalyst particles.

3.2. Thin Film Electrode Preparation

A glassy carbon (GC) electrode (Princeton Applied Research RDE0008 Glassy Carbon Electrode) with a 0.20 cm^2 surface area was used for all of the electrochemical tests (Figure 3-2). At the start of the electrochemical tests, the GC electrode was polished with 0.06 μm aluminum oxide and deionized water. Before the deposition of each catalyst solution, the GC electrode was cleaned with isopropyl alcohol (IPA). Once the electrode was clean and dry, a syringe was used to dispense 20 μl of catalyst solution onto the GC electrode, pausing after every couple of drops to allow some of the solvent to evaporate. Once all 20 μl were dispensed, the syringe was cleaned with IPA while the thin film electrode was left to dry completely before testing. All of the thin film electrodes had a loading of 0.012 mg Pt (0.06 mg Pt/cm^2) and about 0.017 mg Nafion® (0.085 mg Nafion®/cm^2).

Figure 3-2. Glassy carbon electrode used for electrochemical experiments.

3.3. Electrochemical Measurements of Thin Film Electrodes

The electrochemical measurements involved the use of a rotating system (Princeton Applied Research Model 616) and an electrochemical work station (Solatron Analytical 1480 Multistat with CorrWare software), which are shown in Figure 3-3 and Figure 3-4, respectively. The electrochemical cell was comprised of three electrodes and a liquid electrolyte, shown in Figure 3-5. The glassy carbon electrode was used as the working electrode, Ag/AgCl for the reference electrode (eDAQ 2 mm diameter leakless Ag/AgCl reference electrode), and a graphite rod as the counter electrode. All potentials stated here are reported with respect to RHE. The electrochemical tests were performed in solutions that were purged with N_2 for at least 30 min to remove O_2.

Figure 3-3. Princeton Applied Research rotating disk system.

Figure 3-4. Solatron electrochemical work station.

Figure 3-5. Three electrode electrochemical cell.

Measurements of Electrochemically Active Surface Area. Tests to determine the electrochemically active surface area (EASA) of each catalyst and to check for catalyst

degradation throughout the experiment were conducted in a solution of 0.1 M H_2SO_4 (Fisher Scientific A300C-212 18 M Sulfuric Acid F.W. 98.08) in DI water. The EASA was determined by stationary disk cyclic voltammetry (SDCV) test, comprised of either three or six cyclic voltammetry (CV) sweeps from 0.05 to 1.2 V vs RHE at a 50 mV/s sweep rate. The six-cycle test was used to calculate the initial EASA for a new thin film electrode, and the three-cycle test was used to confirm that the EASA did not decrease during the ethanol solution tests. The resulting voltammograms were analyzed to determine the charge transfer associated with the adsorption of a hydrogen monolayer onto the Pt catalyst surface. Knowing the charge transfer, the area of the monolayer can be determined, and thus the active area of the Pt can be predicted as described in the Results chapter (4.1.1) and as detailed by Cooper *et al.* [46].

Measurement of Ethanol Oxidation. As summarized in Table 3-1, following the initial EASA determination, each catalyst was subjected to a series of tests (SDCV-ETH, SDPS-ETH, RDCV-ETH), in three different solutions of ethanol (Acros Organics Ethyl Alcohol, absolute, 200 proof, 99.5%) in DI water and sulfuric acid. The solutions contained 0.1 M H_2SO_4 mixed with either 0.01 M ethanol, 0.1 M ethanol, or 1 M ethanol.

Table 3-1. Electrochemical test series.

SDCV-6	SDCV-ETH	SDCV-3	SDPS-ETH	SDCV-3	RDCV-ETH	SDCV-3
0.1 M H_2SO_4	0.1 M H_2SO_4 + x.xx M EtOH	0.1 M H_2SO_4	0.1 M H_2SO_4 + x.xx M EtOH	0.1 M H_2SO_4	0.1 M H_2SO_4 + x.xx M EtOH	0.1 M H_2SO_4
Stationary electrode	Stationary electrode	Stationary electrode	Stationary electrode	Stationary electrode	Rotating electrode: 200, 400, 600, 800, 900, 1200, and 1600 RPM	Stationary electrode
6-sweeps: [0.05 -1.2 V] at 50 mV/s	2-sweeps: [0.05 –1.2 V] at 10, 20, 50, 100 mV/s	3-sweeps: [0.05 –1.2 V] at 50 mV/s	Hold at E = 0.5 V unit current is constant	3-sweeps: [0.05 –1.2 V] at 50 mV/s	2-sweeps: [0.05 –1.2 V] at 10 mV/s	3-sweeps: [0.05 –1.2 V] at 50 mV/s
Establish EASA	Characterize ethanol oxidation on the catalyst	Compare to initial results to check for poisoning, degradation	Evaluate rate of catalyst poisoning, degradation	Compare to initial results to check for poisoning, degradation	Characterize ethanol oxidation on the catalyst	Compare to initial results to check for poisoning, degradation

Notes:

SDCV stands for stationary disk cyclic voltammetry; SDPS stands for stationary disk potentiostatic; and RDCV stands for rotating disk cyclic voltammetry.

X.xx indicates ethanol concentration of interest – 0.01 M, 0.1 M, 1.0 M.

At the end of the SDCV-ETH test and after completion of the SDPS-ETH test, three-cycle SDCV tests (SDCV-3) were conducted to determine whether the EASA had been affected by the tests. SDCV-3 tests were also conducted throughout the RDCV-ETH test. If the EASA was seen to have noticeably decreased, due to catalyst poisoning or degradation, the potential was cycled between 0.05 V and 1.2 V vs RHE at a rate of 100 mV/s until the original EASA was recovered. If the original EASA could not be re-established, the GC electrode was cleaned with IPA and a new thin film electrode was deposited.

As shown in Table 3-1, the first set of tests in the ethanol solution (SDCV-ETH) involved two SDCV sweeps from 0.05 to 1.2 V vs RHE at each of four different sweep rates (10, 20, 50, and 100 mV/s). This test was used to examine the voltage ranges during which different ethanol oxidation reactions occurred on the various supported catalysts. This set of tests also looked at the effects of voltage sweep rates on the current density produced and allowed comparison of peak current densities, which are indicative of the oxidation reaction kinetics on each of the different supported catalysts.

Following the SDCV-ETH test and an EASA check (SDCV-3), a potentiostatic test (SDPS-ETH) was run at 0.5 V vs RHE (after an initial 30 second hold at 0.05 V) until the current stabilized. This test was used to evaluate the rate at which the current density decreased on each supported catalyst, which is related to the rate of reactant depletion and catalyst poisoning by intermediate species, such as CO_{ad}.

After the potentiostatic test and another EASA check, a rotating disk CV test (RDCV-ETH) was executed. This test involved rotating the GC electrode in an ethanol solution while sweeping the voltage and measuring the current. Two CV sweeps from 0.05 – 1.2 V vs RHE were completed at each of seven different rotational speeds (200, 400, 600, 800, 900, 1200, and 1600 rpm) at a 10 mV/s sweep rate. EASA checks were conducted throughout the RDCV-ETH test. These rotational tests were used to provide insight into the diffusion limitations of the reaction, which decreased as the rotation rate was increased. In some cases, RDCV tests can also be used to calculate the number of electrons transferred during oxidation reactions on both the forward and reverse voltage sweeps. As noted in the results (section 4.1.4), RDCV tests for this system were inconclusive, most likely due to the combined effects of catalyst poisoning, multiple parallel reactions, and Pt oxide formation.

3.4. MEA Preparation

The catalyst solutions for the membrane electrode assemblies (MEA) were prepared with the same supported catalysts that were analyzed in the thin film electrode tests. All of the MEA cathode catalyst solutions used the commercial Pt/C supported catalyst. The target Pt loading for all of the cathodes was 1 mg Pt/cm^2 MEA active area and the target Pt loading for all of the anodes was 2 mg Pt/cm^2 MEA active area (5

cm^2). As with the thin film catalyst solutions, 10% carbon black was added to the Pt/Nb-TiO_2 catalyst. All of the catalyst solutions were prepared in the same manner as the thin film catalyst solutions. The supported catalyst was first massed into a vial (and carbon black was then added to the Pt/Nb-TiO_2 vials), after which enough DI water was added drop-wise to ensure all of the catalyst was wetted. IPA was then added to the vial, with a 1 mL:6 mg ratio of IPA to supported catalyst. After ultrasonicating the solution for a few minutes, the 5 wt% Nafion® solution was added to give a 0.8 ratio of Nafion® to catalyst support. The catalyst solutions were ultrasonicated for 30 minutes once the Nafion® was added. The solutions were also ultrasonicated for at least 30 minutes prior to being sprayed onto the membrane to ensure good distribution of the supported catalyst within the solution.

The MEAs were prepared by spraying catalyst solutions, using an artist's airbrush, onto an 8 x 8 cm^2 membrane (Nafion® N117). Prior to spraying, each membrane underwent a drying regimen to establish a baseline mass for the membrane. This involved drying the membrane at 80°C for 2 hours and then quickly transferring the membrane to an enclosed mass balance which was purged with N_2 to establish a 0% relative humidity (RH) atmosphere (measured using a Vaisala humidity sensor). When the RH of the chamber was around 0 %, the flow rate of the N_2 was decreased and the mass of the membrane was recorded once it had stabilized. Previous trials were conducted to ensure that 2 hours of drying was sufficient time to remove water from the

membrane and establish a baseline membrane mass. It was seen that extra drying time did not result in a lower membrane mass for the same sample. After drying, the membrane was secured in a spray fixture that was constructed in-house (see Figure 3-6) and was heated to 60°C for the duration of the spraying in order to enhance the solvent evaporation and prevent swelling of the membrane. The spray fixture masked the membrane except for a 5 cm^2 active area.

a. b. c.

Figure 3-6. Spray fixture (a.) front view before spraying, (b.) back view, (c.) front view after spraying

The cathode catalyst solution was then manually sprayed onto the membrane in an up-and-down/side-to-side pattern so as to evenly coat the active area of the membrane. Once the spraying was complete, the MEA underwent another series of drying and weighing steps to determine the dry catalyst layer mass. The catalyst loading

was determined from the difference between the dry catalyst-coated membrane mass and the dry non-coated membrane mass. The catalyst application process was repeated for the anode side using the anode catalyst solution. After assuring that the actual catalyst loading from the differential mass measurement was close to the target loading, a curing step was implemented (15 minutes at 100°C) to encourage the formation of interconnected Nafion® pathways throughout the active area. Two MEAs were prepared for each of the three catalyst solutions tested. The characteristics of the anode catalyst layers for each MEA are displayed in Table 3-2. For the cathode, differential mass measurements were made to verify that the loading was close to the target catalyst loading (1 mg/cm^2) for a sample of cathode catalyst layers. The cathode loadings for all catalyst layers were not measured since the anode is assumed to be limiting for the DEFC.

Table 3-2. Anode catalyst layer characteristics for each MEA.

	MEA 1a	MEA 1b	MEA 2a	MEA 2b	MEA 3a	MEA 3b	MEA 3c
Supported Catalyst	Pt/C	Pt/C	PtSn/C	PtSn/C	Pt/Nb-TiO_2-C	Pt/Nb-TiO_2-C	Pt/Nb-TiO_2-C
Target Pt Loading (mg Pt/cm^2 Active Area)	2	2	2	2	2	2	2
Actual Pt Loading (mg Pt/cm^2 Active Area)	2.1	2.1	1.8	1.7	1.5	1.4	1.7
Actual Nafion® Loading (mg Nafion®/cm^2 Active Area)	0.20	0.20	0.17	0.16	0.18	0.15	0.18

3.5. DEFC Assembly

A schematic of the DEFC fuel cell assembly is shown in Figure 3-7. The fuel cell hardware (graphite blocks with serpentine flow channels, current collectors, and aluminum end plates) was from Fuel Cell Technologies, Inc. The 5 cm^2 active area MEA with anode and cathode catalysts was sandwiched between two E-TEK B1A carbon cloth gas diffusion layers (GDLs). The cathode GDL had 10% wet proofing to help prevent flooding on the cathode side of the fuel cell. The anode GDL contained no wet proofing, so that flow of the ethanol solution was not hindered in any way. In order to keep all of the fuel cell assemblies uniform, a GDL without wet proofing was also used for the H_2/Air anode GDL. Teflon gaskets containing cut outs large enough so as to not block the flow channels and GDLs were placed between the graphite flow channel blocks and the MEA to help seal the fuel cell. The thickness of each gasket (130 μm) was less than the GDL thicknesses (*ca.* 190 μm for the anode GDL and *ca.* 250 μm for the cathode GDL), which ensured contact between the flow channels, GDLs, and catalyst layers. The current collectors were in contact with the graphite flow channel blocks and were separated from the aluminum end plates by PTFE gaskets, which were used to prevent short circuiting of the cell. The end plates contained inlets and outlets for the anode and cathode reactants, as well as openings for a thermocouple and cylindrical heaters. The cell was held together with bolts that were tightened with a torque wrench to 75 in-lbs.

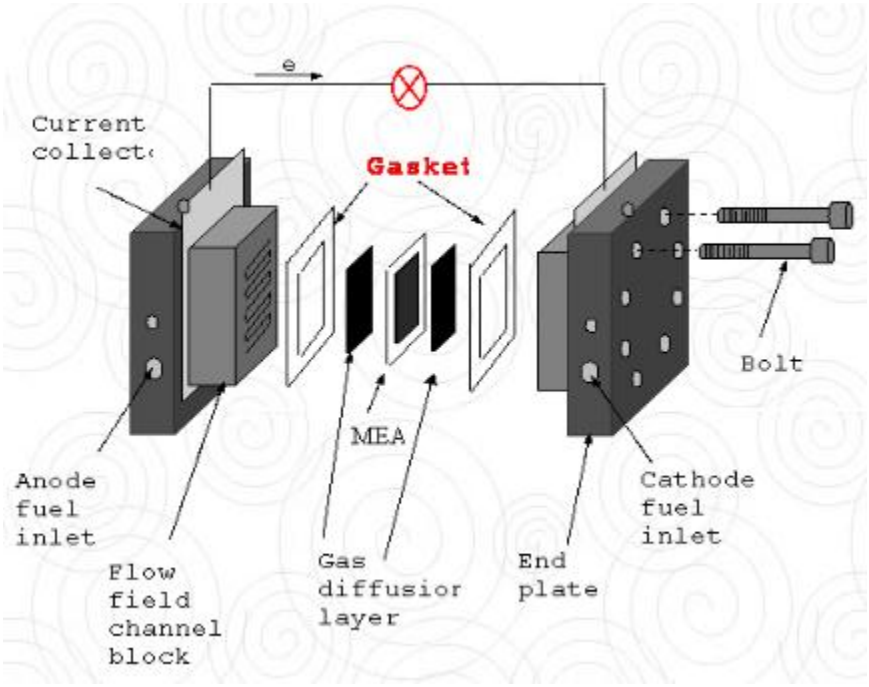

Figure 3-7. Fuel cell assembly [47]

A dual fuel cell test system (Fuel Cell Technologies, Inc.), shown in Figure 3-8, was used to control the backpressure, gaseous reactant humidification, cell temperature, and gaseous reactant flow rates for the fuel cell experiments. The Solatron electrochemical work station that was used for the electrochemical tests discussed earlier, was used to control the voltage and measure the OCV and current for all of the fuel cell tests since the currents produced during the DEFC tests were too small for accurate measurements by the Fuel Cell Technologies test system. A

Masterflex® peristaltic pump, pictured in Figure 3-9, was used to flow DI water and ethanol solution through the fuel cell.

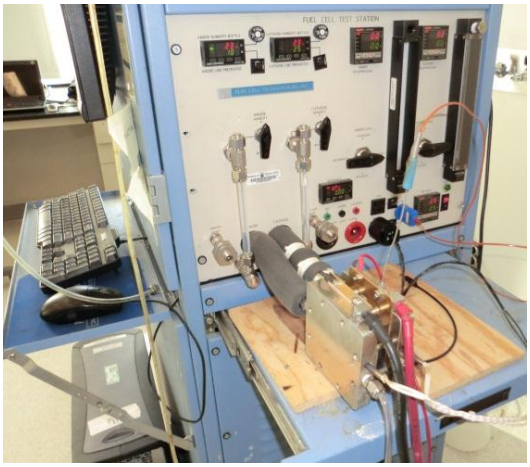

Figure 3-8. Dual fuel cell test system, side view, with fuel cell hardware.

Figure 3-9. Peristaltic pump.

3.6. DEFC EASA Measurements

As with the electrochemical measurements, the EASA was established for each MEA and was checked throughout testing for any degradation. After the fuel cell was assembled, room temperature DI water was pumped (30 mL/min flow rate) through the anode side of the cell for at least 10 minutes in order to hydrate the membrane. Next, both the anode and cathode sides were purged with N_2 at a flow rate of 400 sccm to remove any excess water droplets. For the actual EASA measurement, the flow rate of N_2 through the anode was set to 100 sccm and H_2 was supplied to the cathode at 100

sccm. The anode was set as the working electrode and the cathode as the counter electrode. Once the OCV was near zero (the cell was shorted if the OCV was too high), the voltage was cycled (6 times for the initial EASA measurement and 3 times for EASA checks) from 0.05 – 1.2 V at a rate of 50 mV/s and, during the last cycle, the current was recorded. Following this test, the anode and cathode were again purged with N_2 (400 sccm) for at least 5 minutes. This complete procedure (DI water rinse, N_2 purge, voltage cycling while flowing H_2 and N_2, and a final N_2 purge) was repeated for every EASA check.

3.7. Performance Measurements

H_2/Air Tests. Once the EASA test was complete, fuel cell performance measurements were taken. For the Pt/C MEAs, H_2/Air tests were run after the initial EASA measurement so that the performance of the MEA could be compared to other Pt/C H_2 fuel cell results. For this, unpressurized H_2 was supplied to the anode at 100 sccm (8.6 times stoichiometric flow for a current density of 0.3 A/cm^2) and air to the cathode at 400 sccm (14.5 times stoichiometric flow for a current density of 0.3 A/cm^2). The cell temperature was set to 60°C and the dew point was set to 55°C for both the anode and cathode, resulting in about 80% RH. The voltage was swept at a rate of 2 mV/s from the OCV down to 0.05 V and back up to the OCV with the cathode now

connected as the working electrode. This voltage sweep was repeated until the fuel cell performance remained stable. An EASA check followed the final H_2/Air test.

Ethanol/Air Tests. Two performance curves were recorded in 0.1 M ethanol solution (with DI water and 0.1 M H_2SO_4), one at room temperature and one at 60°C. The 0.1 M concentration of the ethanol solution was chosen since higher concentration solutions have led to increased ethanol crossover and increased electrode poisoning, while lower ethanol concentrations, which have shown increased CO_2 production, have led to unreasonably low current production [6, 15, 17]. The higher temperature performance test was conducted below the boiling point of ethanol (~78°C) in order to reduce ethanol evaporation. For these tests, air was supplied to the cathode at a rate of 950 sccm (34.5 times stoichiometric flow for a current density of 0.3 A/cm^2) with a 15 psig backpressure. The ethanol solution was pumped from a 1 L bottle through the cell and back into the bottle at 8 mL/min (1.7 times stoichiometric flow for a current density of 0.3 A/cm^2). The same solution was used for both performance tests for one MEA. Between the two ethanol tests, the EASA was checked to ensure no degradation of the MEA had occurred during the room temperature voltage sweep. During both DEFC tests, the dew point temperature of the cathode was set for 25°C because it was assumed the flow of ethanol through the anode side would fully hydrate the membrane. Operating conditions for all of the fuel cell performance tests are listed in Table 3-3.

During each test, the voltage was swept from the OCV down to 0.05 V and back up to the OCV with the cathode connected as the working electrode.

Table 3-3. Fuel cell operating conditions for performance measurements.

	H_2/Air	0.1 M Ethanol/Air_1	0.1 M Ethanol/Air_2
Cell Temperature	60°C	25°C	60°C
Anode Flow Rate	100 sccm	8 mL/min	8 mL/min
Cathode Flow Rate	400 sccm	950 sccm	950 sccm
Cathode Backpressure	0 psig	15 psig	15 psig
Anode Reactant RH	80%	100%	100%
Cathode Gas RH	80%	100%	16%
Ethanol Temperature	-	25°C	60°C

Immediately following the DEFC performance tests, without any change in operating conditions, a high frequency resistance (HFR) test was performed to measure the resistance of the cell. The resistance can be due to contact resistance in the cell, resistance to ion conductivity through the membrane, and resistance to electron transport throughout the cell. Initially, the HFR measurements were recorded along the complete voltage range of the cell (OCV to 0.05 V), but since the resistance was stable throughout the range, future HFR measurements were made solely at the OCV. The cell contact resistance and electron transport resistance are not dependent on the current of the cell, so the stable resistance measurements indicated that the ionic

conductivity resistance was also independent of the cell current. A constant ionic conductivity resistance implied the membrane hydration did not change across the current range, since a decrease in membrane hydration would lead to a decrease in ionic conductivity. This is not surprising since the presence of liquid water at the anode should maintain a constant level of hydration.

4. RESULTS

In this work, a novel catalyst for ethanol oxidation, Pt/Nb-TiO_2-C, was evaluated and compared to two common ethanol oxidation catalysts, Pt/C and PtSn/C. The TiO_2 support was expected to increase ethanol oxidation and decrease catalyst layer poisoning and the addition of Nb and C was meant to increase the conductivity of the TiO_2 support. It was hoped that results from the use of the novel catalyst would be at least comparable, if not better, than those from the use of Pt/C. The electrochemical activity of all three catalysts was examined using stationary disk cyclic voltammetry experiments at various potential scan rates, stationary disk potentiostatic holds at 0.5 V vs RHE, and rotating disk electrode tests at various rotational rates in three different ethanol concentration solutions. A manual spraying technique was used to prepare the MEAs with each of the different catalysts and the performance of the MEAs was measured in a DEFC at both room temperature and 60°C.

4.1. Pt/C Catalyst

4.1.1. Electrochemically Active Surface Area for a Pt/C Thin Film Electrode

A cyclic voltammetry (CV) test in 0.1 M H_2SO_4 with a Pt/C electrode is shown in Figure 4-1 where the voltage is plotted vs RHE (all following voltages are reported vs RHE). The current measured between 0.05 and 0.4 V is due to desorption of H_2 on Pt

(on the forward, positive scan) and to adsorption of H_2 on Pt (on the reverse, negative scan). Oxide formation begins around 0.75 V and continues until the scan is reversed and oxide reduction occurs, with a peak seen around 0.75 V. The double layer charge region is attributable to the charging and discharging of the interface and is not associated with electrochemical reactions. On the plot, the voltage range for double layer charging lies between the end of hydrogen adsorption (prior to the onset of PtOx formation) and the beginning of hydrogen adsorption (after completion of PtO_x reduction).

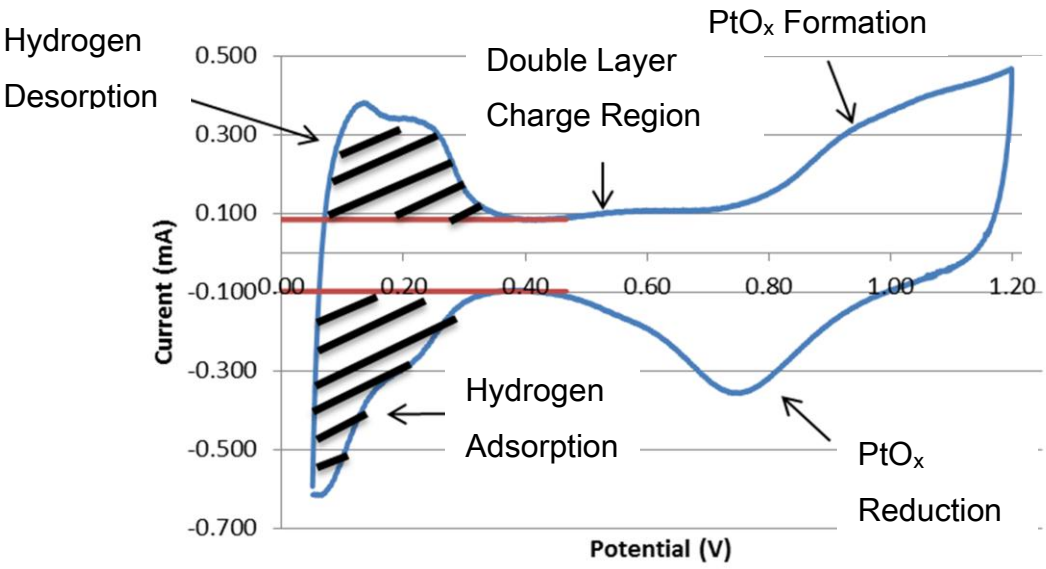

Figure 4-1. Description of CV on a Pt/C electrode in 0.1 M H_2SO_4.

The area under the portions of the initial SDCV in 0.1 M H_2SO_4 associated with hydrogen adsorption (the shaded sections from 0.4 V – 0.05 V vs RHE of the reverse

potential sweep in Figure 4-1) was estimated using the trapezoidal rule and was used to calculate the specific electrochemically active surface area (EASA). The portion of the hydrogen adsorption area due to the double layer charge region was subtracted to give the net charge transfer related to hydrogen adsorption. This value can be used with (4.1) to determine the specific EASA of the electrode. In the equation, q $\left[\frac{C}{cm^2}\right]$ is the hydrogen adsorption charge density, Γ $\left[\frac{\mu C}{cm^2\ Pt}\right]$ is the charge required to reduce a monolayer of protons on Pt, and L $\left[\frac{mg\ Pt}{cm^2\ electrode}\right]$ is the Pt loading in the electrode.

$$EASA\left[\frac{cm^2}{mg\ Pt}\right] = \frac{q}{\Gamma L} \tag{4.1}$$

The charge required to reduce a single layer of protons on Pt is 210 μC/cm^2 Pt [48, 49]. The Pt loading was determined from the catalyst solutions, which were prepared such that the Pt loading was ~1.2 mg per 2 mL of catalyst solution. The EASA [cm^2 Pt] of the Pt was calculated by dividing the charge due to hydrogen adsorption by the charge required to reduce a single layer of protons on Pt. Results of the final sweep of 0.1 M H_2SO_4 SDCV-6 for the Pt/C thin film is shown in Figure 4-2 and is similar to results found in literature [18, 44].

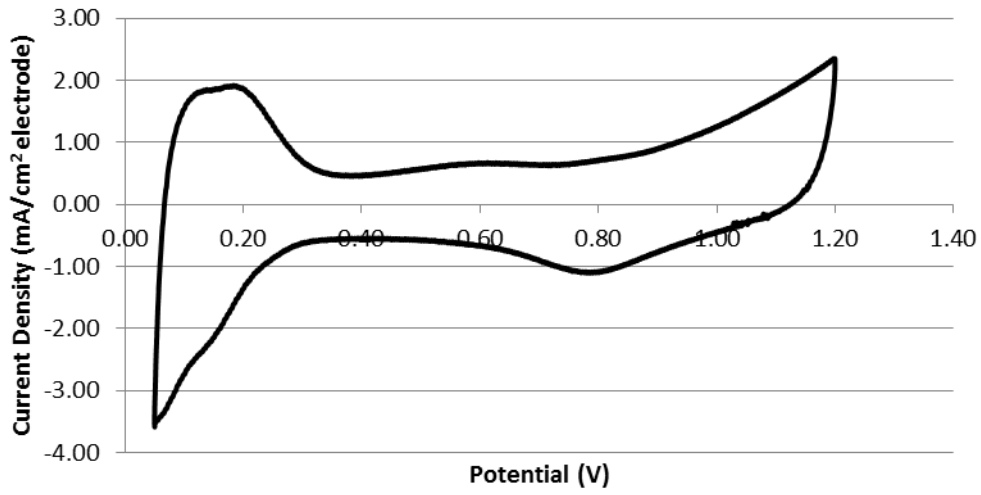

Figure 4-2. Final sweep of SDCV-6 in 0.1 M H_2SO_4 for the Pt/C thin film A electrode.

Four thin film electrodes were used during the course of the Pt/C electrode experiments. Average values of the thin film electrode EASAs are reported in Table 4-1. As the experiments progressed, the EASA for each thin film electrode changed by a maximum of ± 25%. All results which are normalized by EASA were calculated with the most recent EASA value, each of which was calculated based on the electrochemical reduction of protons and the adsorption of hydrogen on the catalyst during a 0.1 M H_2SO_4 SDCV test. The specific EASAs for the various thin film electrodes range from 315 – 580 cm^2 Pt/mg Pt and the EASAs of the thin films range from 5.2 – 7.2 cm^2 Pt. *CVs in 0.1 M H_2SO_4 with a Pt/C electrode are reproducible and resemble those reported in the literature. The EASA for the Pt/C thin film electrodes varies slightly but is much higher than the surface area of the GC electrode (0.1963 cm^2) in all cases.*

Table 4-1. Pt/C thin film electrode properties.

Thin Film	A	B	C	D
Pt Loading [mg Pt/cm^2 electrode]	0.06	0.06	0.06	0.06
C_{dl} [C]	7.30E-04	4.86E-04	7.14E-04	6.67E-04
H^+ Adsorption Charge [C]	1.27E-03	1.53E-03	8.13E-04	6.80E-04
Specific EASA [cm^2 Pt/mg Pt]	490	580	315	470
EASA [cm^2 Pt]	6.0	7.2	5.2	5.8

4.1.2. SDCV Tests for Ethanol Oxidation for a Pt/C Thin Film Electrode

A SDCV in 0.01 M ethanol on a Pt/C electrode at 10 mV/s is shown in Figure 4-3 in the typical format used for CV studies (forward/reverse scans shown over the same range). Figure 4-4 is the same plot as Figure 4-3, but the data is shown linearly rather than as a cycle, with a description of what is occurring at various voltages along the sweep. The voltage is plotted along the horizontal axis, increasing from 0.05 V to 1.2 V and then decreasing back to 0.05 V. This method presents a clearer picture of the reactions that are taking place during the forward and reverse sweeps. The ethanol oxidation process on Pt/C in acid media has been described by Lai *et al.* [50], Wang *et a.*/[51], and Sun *et al.* [17]. Between 0.10 and 0.45 V, CH_{ad} is converted to CO_{ad}, which can then further oxidize to CO_2 (between ~0.40 and 0.75 V in Figure 4-3 below). The slight shoulder that is circled on the plot in Figure 4-3 is due to CO_2 formation. The

peak seen near 0.85 V on the forward scan is due to incomplete ethanol oxidation to acetaldehyde and acetic acid. The surface of the electrode is blocked after 0.85 V on the forward scan by PtO_x and OH_{ad} until just after 1.0 V, when the increase in voltage leads to the further oxidation of acetaldehyde to acetic acid and an increase in current density. Reduction of the oxides that are blocking the Pt surface occurs on the reverse sweep and, around 0.85 V, the Pt surface begins to clear, allowing oxidation of ethanol to acetaldehyde and acetic acid to occur with a peak around 0.6 V. The formation of CO_2 is not seen on the reverse scan, at least not at room temperature, due to the absence of CO_{ad}. In Figure 4-3, a small amount of reduction is seen around 0.9 V, noted by the slightly negative current density, but at other voltages more incomplete oxidation of ethanol is occurring than reduction of PtO_x, thus positive current density values are produced.

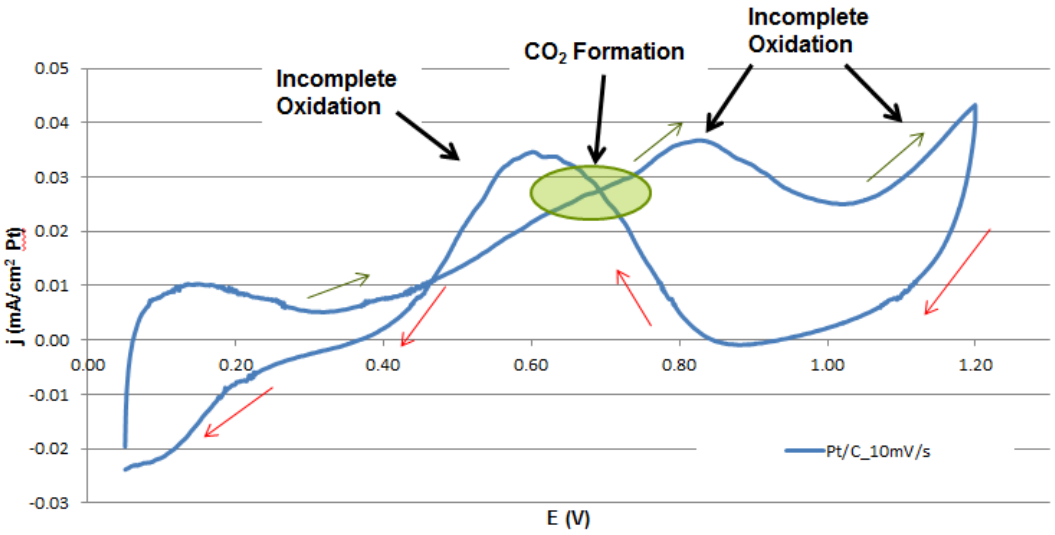

Figure 4-3. SDCV sweep at 10 mV/s on a Pt/C electrode in 0.01 M ethanol solution.

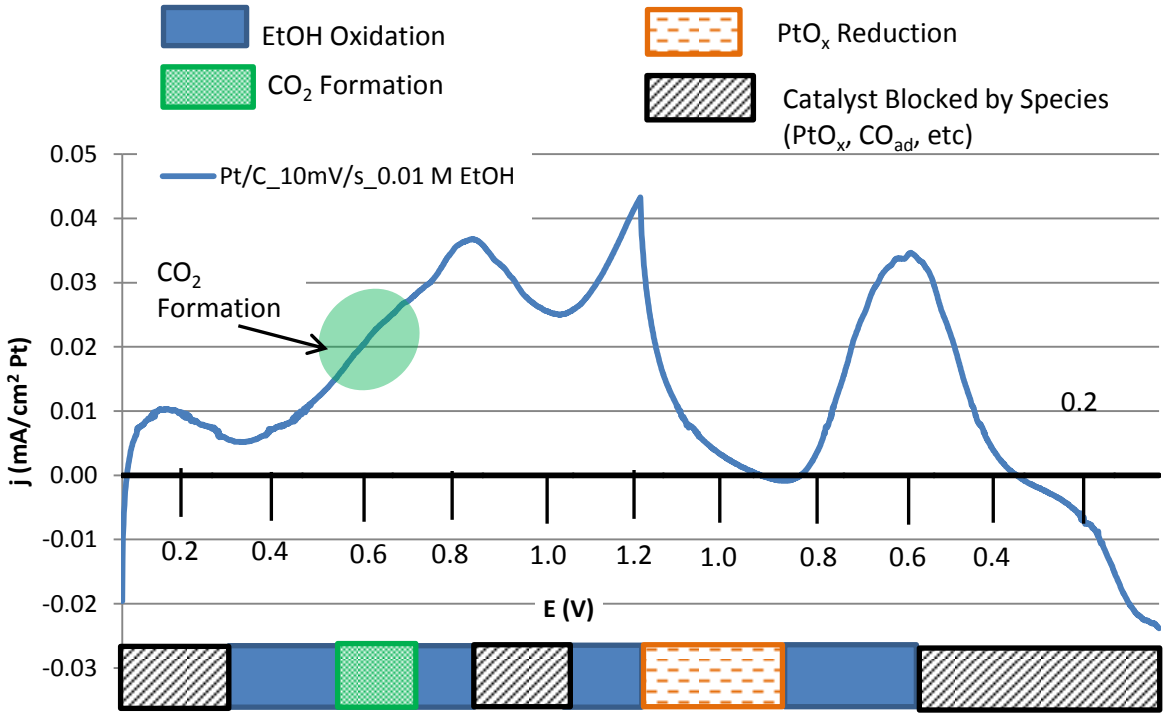

Figure 4-4. Annotated SDCV sweep at 10 mV/s on a Pt/C electrode in 0.01 M ethanol solution displayed as a linear voltammogram.

The SDCVs in the ethanol solutions were conducted at four sweep rates in the three different ethanol concentration solutions and are comparable to other CV plots recorded in similar conditions on Pt/C electrodes [18, 51]. The SDCVs in 0.01 M ethanol solution are shown in Figure 4-5 on a Pt/C thin film electrode. As the voltage sweep rate increases, the current density becomes more positive on the forward scan and more negative on the backward scan, which is highlighted by the orange arrows in Figure 4-5. A peak occurs when the concentration of the reactant near the surface of the working electrode reaches zero. During the slower sweep rate, more time is spent in the voltage ranges where oxidation is occurring, leading to an increase in the rate of reactant depletion and a decrease in peak current values. On the reverse scan, PtO_x reduction and ethanol oxidation are both occurring and the difference between the reduction and oxidation peaks is more significant than the actual peak values. As the scan rate increases, the difference in peak current density values (around 0.8 V and 0.6 V on the reverse scan) increases. even though the difference in current density between the reduction peak around 0.8 V and the oxidation peak around 0.6 V becomes larger as the scan rate is increased, the actual current density around 0.6 V decreases with an increase in the CV scan rate due to the larger (more negative) reduction peak that has to be overcome. In the forward scan, the peak due to CO_2 formation is visible at 0.6 V and is highlighted on the higher scan rates.

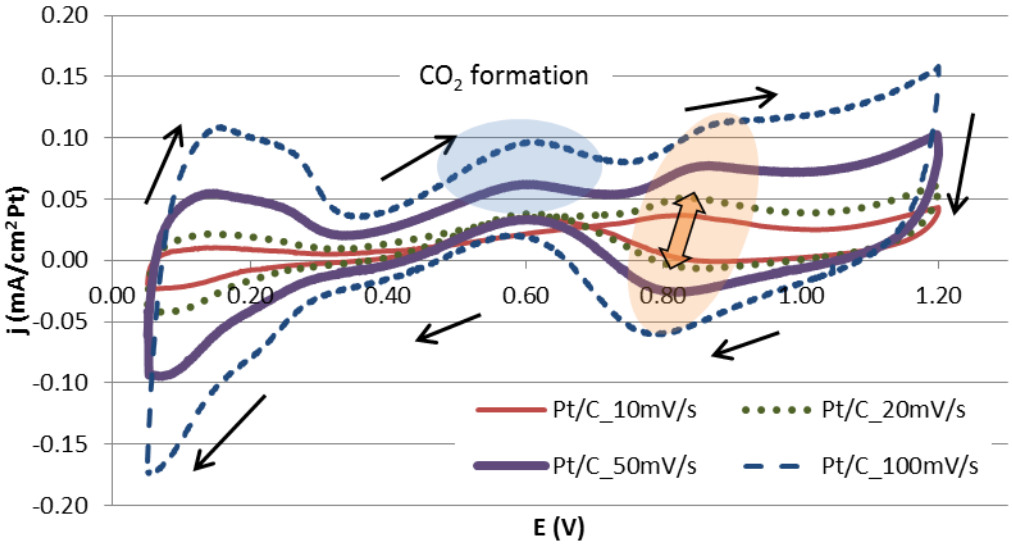

Figure 4-5. SDCV sweeps on a Pt/C thin film electrode in 0.01 M ethanol solution.

In 0.1 M ethanol solution, a similar trend is seen, with the maximum current density increasing as the CV scan rate is increased. Figure 4-6 displays the plots for the SDCV sweeps at all four scan rates on a Pt/C electrode in 0.1 M ethanol solution. The peak currents due to complete and incomplete ethanol oxidation in 0.1 M ethanol solution are higher than those in 0.01 M ethanol solution and the peak due to PtO_x reduction is no longer seen because of the increase in ethanol oxidation. The peak (shoulder) due to CO_2 formation is still situated around 0.6 V on the forward scan and is highlighted in the 50 and 100 mV/s sweeps, where the peak is more noticeable. The potential of the forward scan peak shifted to the right as the voltage scan rate

increased, while the reverse scan peak potential shifted to the left as the scan rate increased. This can be explained by the fact that a larger voltage range is covered in a given time period when scanning the potential at a higher rate. If it takes a set amount of time for the reactant to deplete (based on the reaction and diffusion rates) once ethanol oxidation begins, then a larger voltage range will be covered before the reactant is depleted when at a higher voltage scan rate.

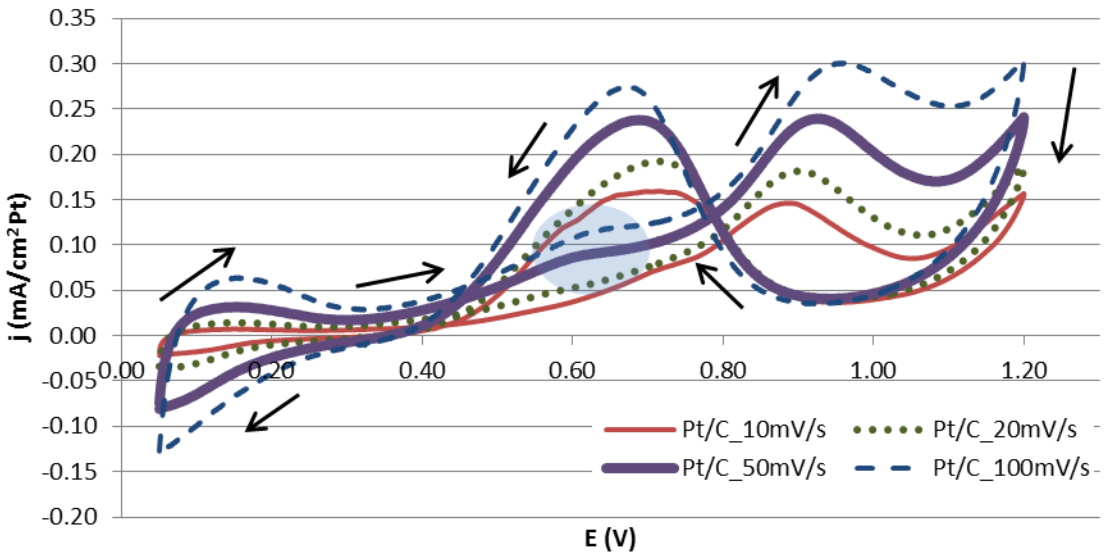

Figure 4-6. SDCV sweeps on a Pt/C thin film electrode in 0.1 M ethanol solution.

Figure 4-7 contains plots of the SDCV sweeps on Pt/C in 1.0 M ethanol solution. The CV sweeps show an even larger increase in maximum current density and peak potential in 1.0 M ethanol. The CO_2 formation peak, for which the amplitude was less

than 1 mA/cm^2 Pt on the 0.01 M and 0.1 M ethanol solution plots, is no longer visible on the forward scan now that the current densities are larger, though a shoulder is noticeable after the oxidation peak on the reverse sweep. This shoulder is also likely due to incomplete ethanol oxidation to acetaldehyde and acetic acid.

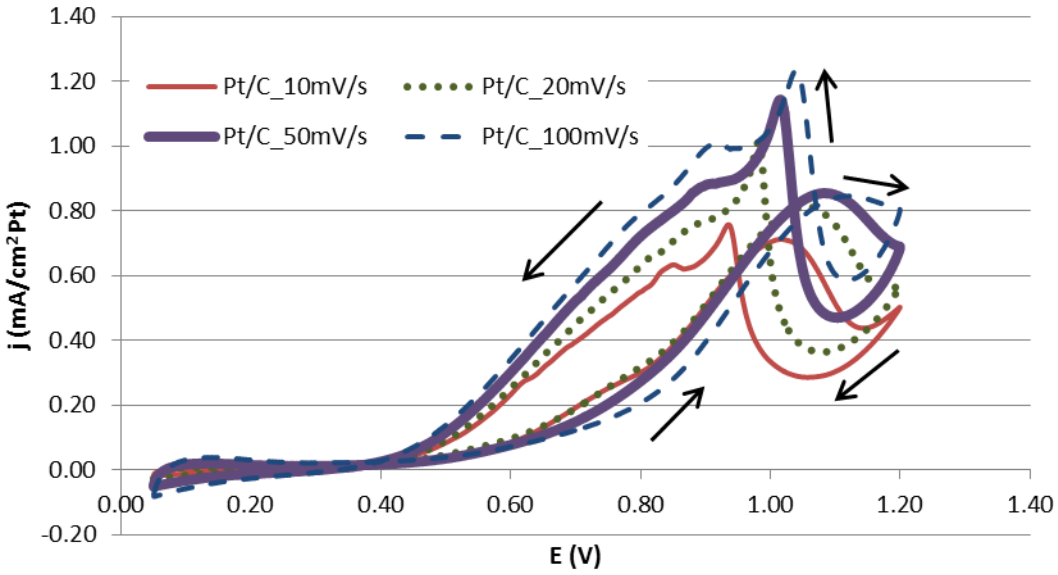

Figure 4-7. SDCV sweeps on a Pt/C thin film electrode in 1.0 M ethanol solution.

In order to better compare the variations of the CV plots in the three different ethanol concentration solutions, the 10 mV/s sweeps in each solution are shown together in Figure 4-8. This allows the peak magnitudes and potential shifts to more easily be seen. It also emphasizes the differences between the 1.0 M ethanol sweep and the other, lower ethanol concentration sweeps. In the higher ethanol concentration

solutions, the reactant depleted more slowly, which led to larger oxidation peaks. This large increase in current density seen with an increase in ethanol concentration from 0.1 M to 1.0 M is consistent with the findings of Camara *et al.* [15]. It was also observed that the oxidation peaks shifted to higher potentials as the ethanol concentration increased. *In general, two main oxidation peaks are seen on a Pt/C electrode (one on the forward scan and one on the reverse scan), with a shoulder due to CO_2 production noticeable at higher voltage scan rates. The oxidation current densities increase as the voltage scan rate and ethanol concentration increase. An increase in scan rate and ethanol concentration also leads to shifts in the voltage where the oxidation peaks occur.*

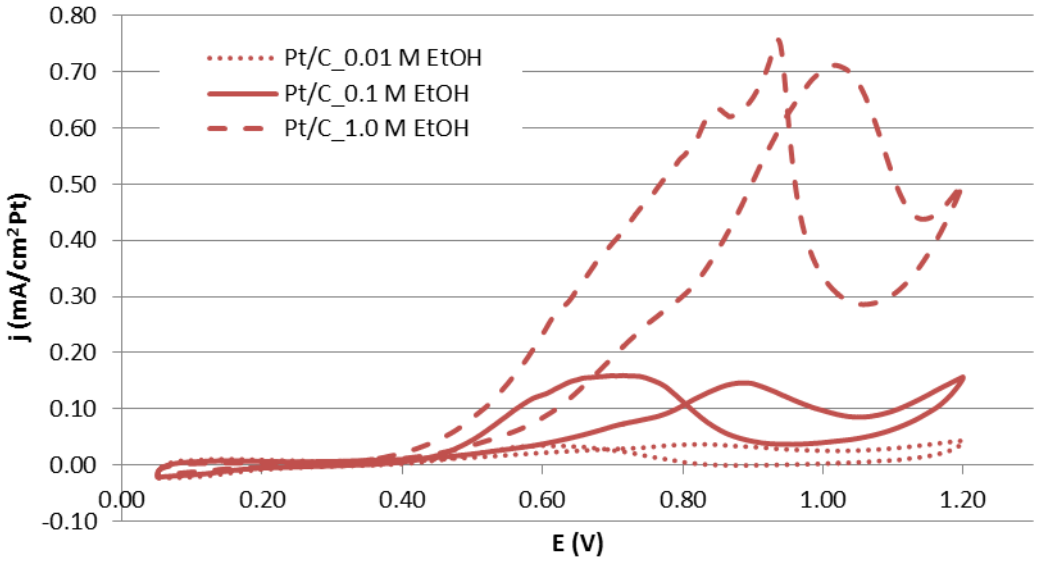

Figure 4-8. SDCV sweeps on a Pt/C thin film electrode at 10 mV/s in 0.01, 0.1, and 1.0 M ethanol solutions.

4.1.3. SDPS Tests for Ethanol Oxidation on a Pt/C Thin Film Electrode

The results of the potentiostatic measurements in 0.01 M, 0.1 M, and 1.0 M ethanol concentration solutions are shown in Figure 4-9, beginning one second after the potential was increased to 0.5 V. The complete data for these tests can be found in the Appendix (7.2). At the moment the voltage is increased, the current is much higher, making it difficult to see the trend in current change at longer times. Also, the instrument only records data at a rate of 1 point every 0.2 seconds, which most likely does not accurately capture the rapid increase and decrease in current seen when the voltage changes. For these reasons, the results are presented beginning one second (t = 1 s) after the voltage change. As was expected, slightly larger currents are seen with higher ethanol concentration solutions.

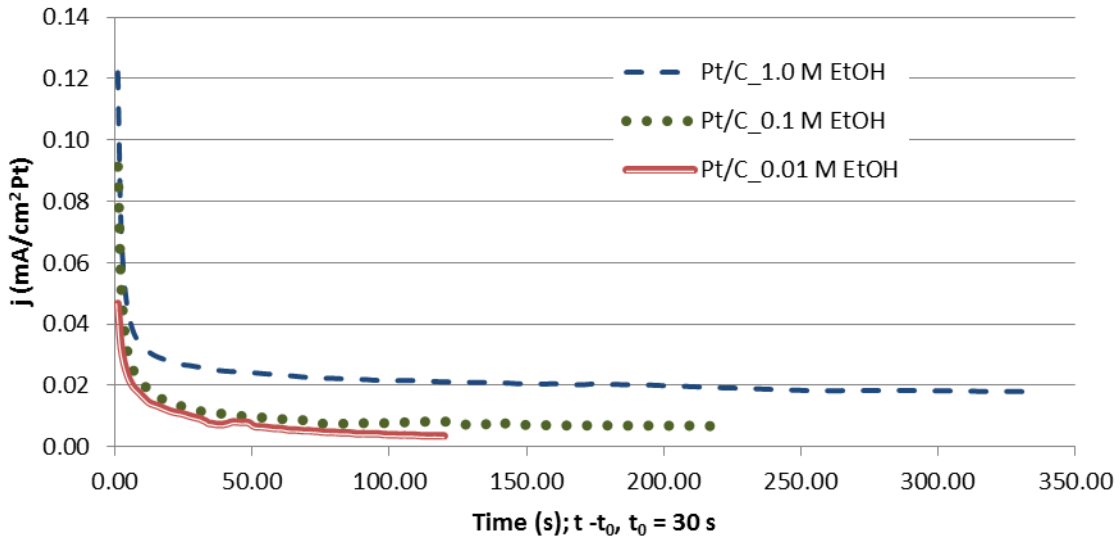

Figure 4-9. SDPS test at 0.5 V vs RHE for a Pt/C thin film in 0.01, 0.1, and 1.0 M ethanol solutions.

The Cottrell equation is discussed by Bard and Faulkner [52] and models the theoretical diffusion limited current during a step from a potential where to electrolysis is occurring to a potential where the electrochemical reaction is dependent on the reactant diffusion. Equation 4.2 shows the Cottrell equation and a simplified form of the equation, where the diffusion limited current is a function of time ($t^{-1/2}$) and A is a constant.

$$\boldsymbol{i_d = \frac{nFAD_O^{1/2}C_O^*}{\pi^{1/2}} t^{-1/2} = At^{-1/2}} \qquad (4.2)$$

Power curves of the form shown in Equation 4.3 were fit to the SDPS results in the range of 1 to 10 seconds after the voltage change, where ethanol oxidation rapidly decreases as the catalyst surface is poisoned and the reactant is depleted.

$$\boldsymbol{i = At^{-b}} \tag{4.3}$$

The power curve fits are plotted alongside the data in Figure 4-10 and the equations for the fits are listed in Table 4-2., where a value of b greater than 0.5 indicates that factors other than diffusion limitations are contributing to the decrease in current density (e.g. poisoning of the catalyst layer).

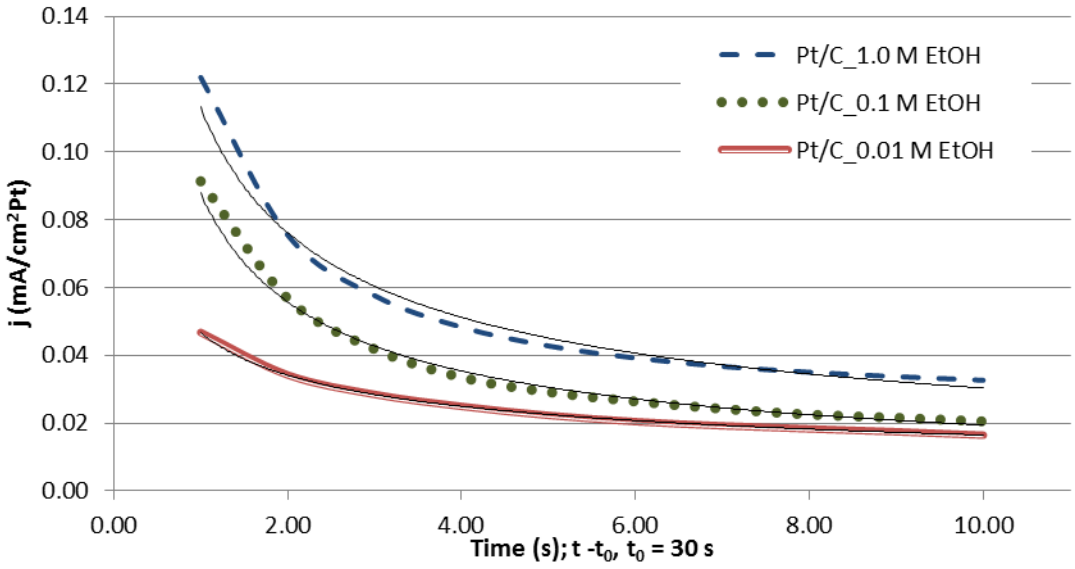

Figure 4-10. Power law fits to the SDPS data on Pt/C from t = 1 – 10 s in various ethanol concentration solutions.

Table 4-2. Equations of the power law fits to the SDPS data shown in Figure 4-10.

Ethanol Concentration [M]	Power Law Equations
0.01	$Y = 0.0467x^{-0.454}$
0.1	$Y = 0.0879x^{-0.657}$
1.0	$Y = 0.1132x^{-0.573}$

In the equations, $\boldsymbol{A}$ is the current density at t = 1 second. The exponent relates to the rate of decrease of the curve. The more negative the exponent, the faster the current density is decreasing. The drop in current density within this time frame is due to diffusion limits, where the ethanol is reacting faster than it is being replenished, and to electrode poisoning, where intermediate species, such as CO_{ad}, are blocking the

platinum surface. For the case of Pt/C, the 0.1 M ethanol solution power law fit has the largest (most negative) exponent, implying that catalyst poisoning is greatest in the 0.1 M ethanol solution during the first 10 seconds at 0.5 V. This quick decrease can also be seen in Figure 4-10. *As was expected, higher concentrations of ethanol produce higher initial current densities. Interestingly, the poisoning was most pronounced in the 0.1 M ethanol solution.*

4.1.4. RDCV Tests for Ethanol Oxidation on a Pt/C Thin Film Electrode

Plots of both CV sweeps at each of the rotation rates in 0.01 M ethanol solution on a Pt/C electrode are shown in Figure 4-11 and Figure 4-12. There is a noticeable increase in the magnitude of the current peaks from 400 rpm to 900 rpm, but the peak current values for 900, 1200, and 1600 rpm are very similar. This implies that the reaction is not dependent on the rotational rate above speeds of 900 rpm. Once this speed is reached, the reactant is supplied at a rate faster than it is consumed and therefore the current density peaks must be due to limitations other than mass transfer from the solution to the outer surface of the electrode. Other limitations include the kinetics of the ethanol oxidation reaction and the diffusion of the reactant through the thin film electrode, both of which are independent of rotational rate. For this reason, the RDE tests were repeated on a new Pt/C electrode at lower rates, with EASA tests in

between each rate to keep track of any active area degradation. Although a dependence of current density on rotational rate can be seen in the lower rotational rate tests, the correlation remains poor, indicating that other factors are affecting the current density besides just the electrode rotation.

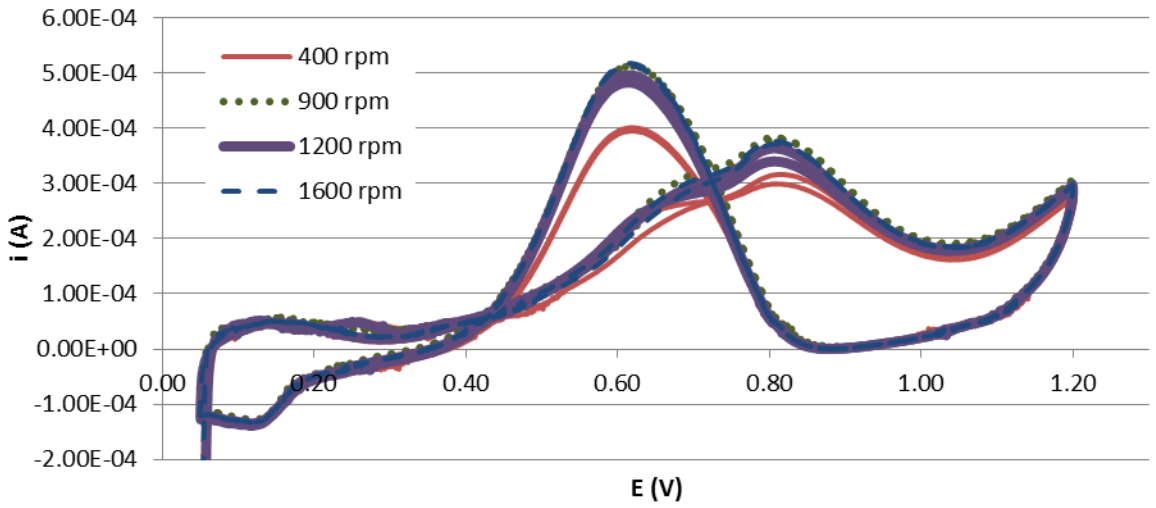

Figure 4-11. RDCV results for higher rotation rates on a Pt/C thin film electrode in 0.01 M ethanol solution at 10 mV/s.

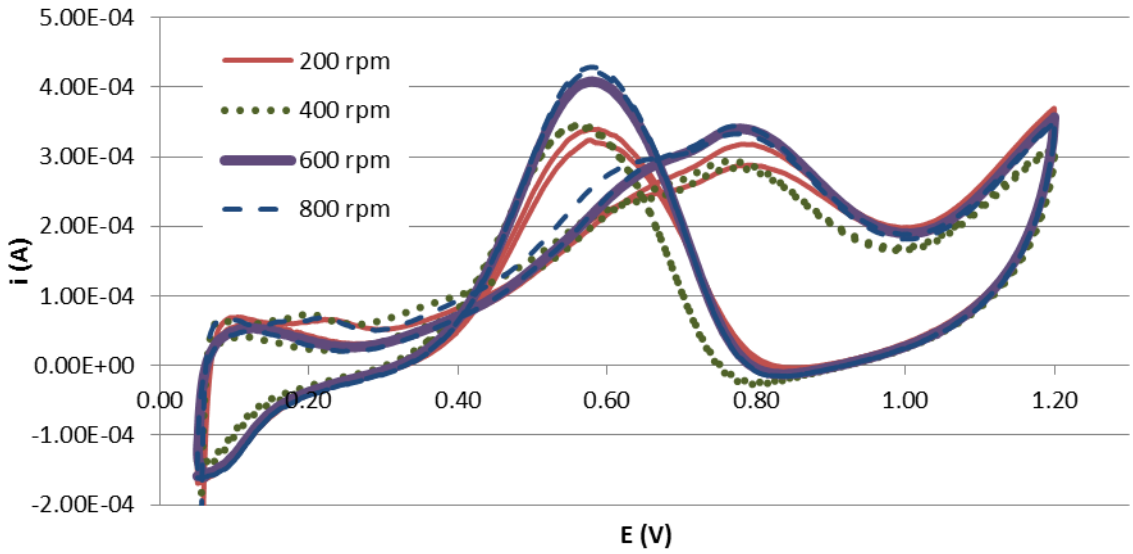

Figure 4-12. RDCV results for lower rotation rates on a Pt/C thin film electrode in 0.01 M ethanol solution at 10 mV/s.

The Koutecký – Levich (K-L) equation describes the limiting current based on mass-transfer limitations at the surface of a RDE, which is a function of rotational rate, along with other limitations that are independent of the rate of rotation [52]. Bard and Faulkner [52] state that the K-L equation applies to totally irreversible reactions that involve one step and the transfer of one electron, though others have applied this equation to reactions that are more complex and involve more than one electron transfer. This equation was applied to the data from the RDE tests to calculate the number of electrons transferred per mole of ethanol when the current density peaks (around 0.8 V on the forward sweep and 0.6 V on the reverse sweep in Figure 4-12). In

the K-L equation, which is shown below, the inverse of the current is a function of the inverse of the square root of the rotational rate.

$$\frac{\mathbf{1}}{\boldsymbol{i}} = \frac{\mathbf{1}}{\boldsymbol{i_k}} + \left(\frac{\mathbf{1}}{\mathbf{0.62}\boldsymbol{nFAD_O^{2/3}\nu^{-1/6}C_O^*}}\right)\left(\frac{\mathbf{1}}{\boldsymbol{\omega^{1/2}}}\right) \tag{4.4}$$

In the above equation, i is the measured current (A), i_k is the mass-transfer independent current (A), n is the number of electrons transferred, F is Faraday's constant (96,500 C/mol e^-), A is the area of the electrode (m^2), D_O is the diffusion of ethanol in the solution (1.20E-09 m^2/s – 1.09E-09 m^2/s, depending on the concentration [53]), ν is the viscosity of ethanol (9.90E-07 m^2/s [54]), C_O^* is the concentration of the bulk solution (mol/m^3) and ω is the rate of rotation (rad/s).

The K-L equation accounts for both rotational rate dependent and independent limitations. As the rotational rate increases, the current approaches the reaction kinetics-limited current. In this case, other limitations besides reaction kinetics are lumped into the y-intercept value, $\frac{1}{i_k}$. As mentioned previously, diffusion is occurring through the ethanol solution, as well as through the thin film layer. While the movement of ethanol from the bulk solution to the surface of the electrode is dependent on the

rotational rate of the electrode, movement of ethanol through the thin film layer, which also includes the Nafion® film layer, is not.

The peak currents for the forward and reverse peaks during two voltage sweeps at 200, 400, 600, and 800 rpm are presented in Figure 4-13. While a linear equation was fit to the data, it is apparent that the measured current during the 400 rpm test was lower than expected based on the trend formed by the other three rotational rates. A few factors could account for a lower than expected current value. While the electrode surface was checked for bubbles before a test was initiated, it is possible that a particle or bubble (formed by ethanol oxidation) unseen by the naked eye could have partially blocked the electrode surface, thereby decreasing the catalyst active area and the measured current. It is also possible in any of the tests that other chemical reactions, which did not involve electron transfer, could have been occurring among the species in the solution.

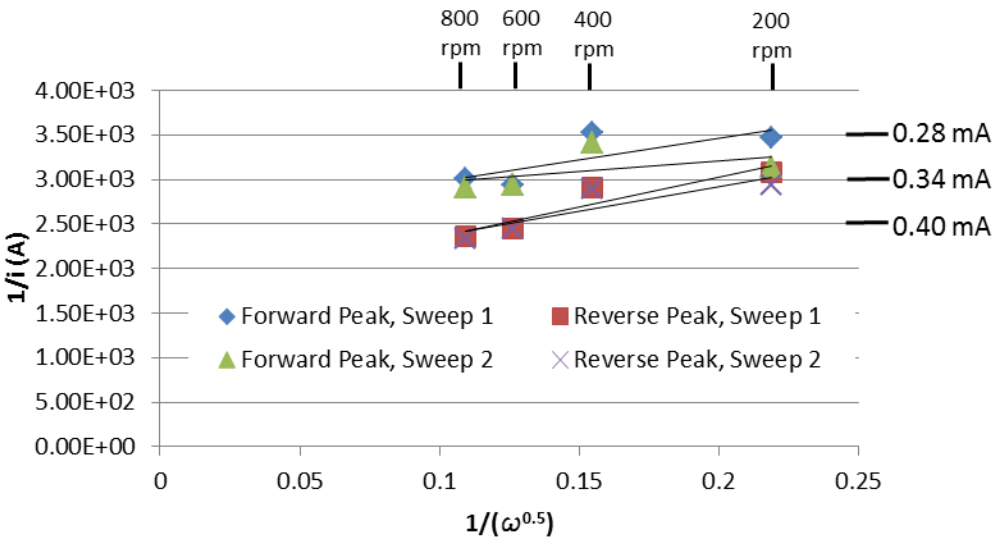

Figure 4-13. K-L plot using RDCV data from four rotational rates (200, 400, 600, and 800 rpm) in 0.01 M ethanol solution on a Pt/C thin film electrode.

It was apparent from the RDCV tests on each of the three catalysts, in all three solutions, that a correlation between measured current and rotational rate was not seen. In some cases, the current increased with an increase in rotational rate, but in others the current decreased when the rotational rate increased. It seems most likely that this was due to the complexity of the ethanol oxidation reaction. The 200 rpm sweep in Figure 4-12 demonstrated that two sweeps during the same test at the same rate could result in different peak currents. The reactions that occurred within each sweep were not identical and the differences were possibly due to the catalyst surface being blocked by (or freed from) intermediate ethanol oxidation reaction species, such as CO, and products from the reaction of sulfuric acid on Pt, like PtO_x. The results of the RDCV

tests were not as expected and because of the inconsistencies in the measured currents with respect to the electrode rotational rate, the RDCV data was not able to be used to calculate the number of electrons transferred per mole of ethanol reacted. RDCV results will not be discussed for the other two catalysts tested, but the data can be found in the Appendix (7.3). A review of the literature did not identify examples of successful applications of RDCV to determine electron transfer rates for the electrochemical oxidation of ethanol. *The results of the RDCV tests were inconclusive and it seems likely that the ethanol oxidation reaction is too complex to be modeled by the K-L equation.*

4.1.5. Evaluation of a Pt/C Catalyst MEA for Ethanol Oxidation in a DEFC

Polarization curves were plotted for each of the conditions tested and the current was normalized based on the MEA active area (5 cm^2) in order to be consistent with values reported in the literature. The forward and reverse voltage scans were averaged over the current range for the plots, but the initial OCV (before the sweep started) is also shown on the plots. The voltage in all of the performance plots shown in this document is iR-corrected based on the resistance that was measured using the high frequency sweep. The resistance measurements for the Pt/C MEAs ranged from 0.170 ohms to 0.183 ohms (0.85 – 0.915 Ωcm^2), which had a minor effect on the iR-corrected

voltage (as compared to the uncorrected voltage). The low resistance measurements indicated that the voltage drop in the cell was not primarily due to the membrane or fuel cell assembly, but rather to other factors including low reaction kinetics and incomplete ethanol oxidation, both of which contribute to low numbers of transferred electrons and less than optimal current output. Flooding and poisoning of the cathode from the transport/crossover of water and ethanol through the membrane would also cause a drop in the fuel cell performance. Poisoning of the catalyst by intermediate species, which was discussed in the thin film electrode experiments, can also cause a decrease in fuel cell performance. Power density was calculated by multiplying each current density value by its corresponding voltage value. Figure 4-14 shows the performance of the Pt/C MEAs when flowing hydrogen and air.

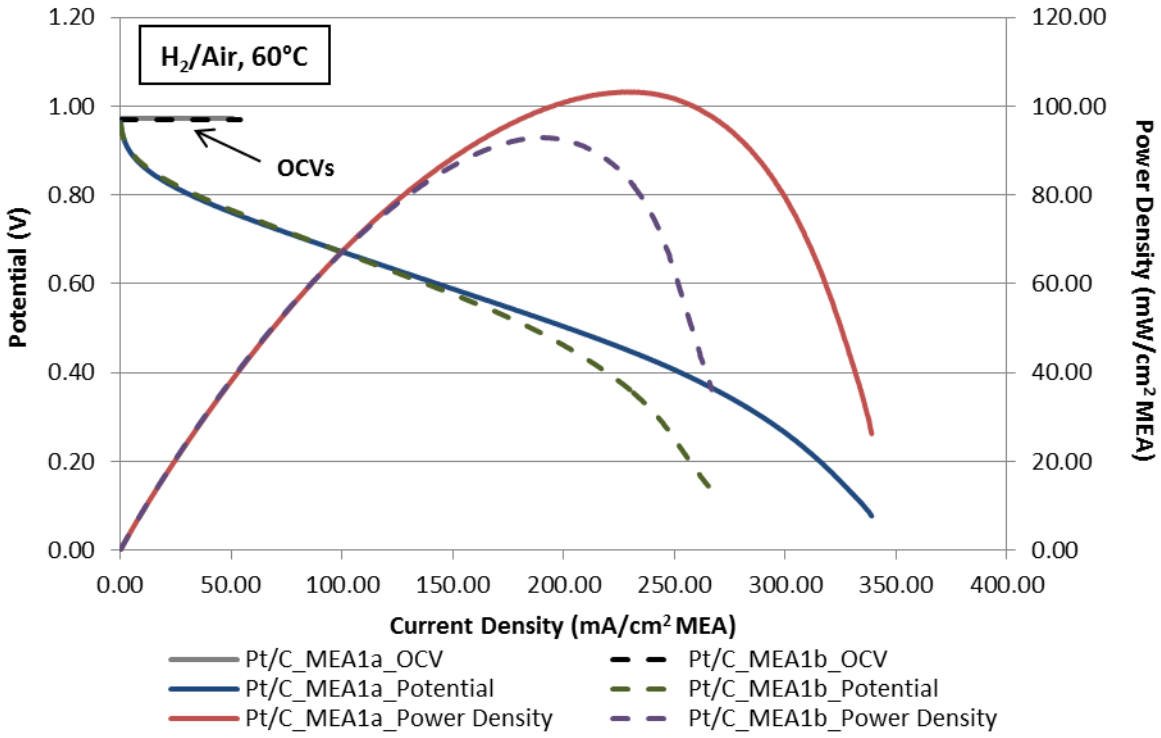

Figure 4-14. H_2-Air fuel cell performance on Pt/C electrodes (MEA 1a and MEA 1b); cell temperature = 60°C, dew point$_{a,c}$ = 55°C (80% RH), unpressurized reactants, air flow rate = 400 sccm, H_2 flow rate = 100 sccm .

While the OCVs of MEAs 1a and 1b are at or above average (0.97 V for both MEAs), the performance was worse than is seen in a typical hydrogen PEM fuel cell. Even when accounting for the overpotential due to the increased membrane resistance for the thicker (about 200 μm) membrane used in this experiment, the current density reported here only reached about 300 mA/cm^2 at 0.2 V. OCVs between 0.8 and 0.9 V with a maximum current density of about 700 mA/cm^2 at 0.2 V were reported by Siegel [55] in a hydrogen-air fuel cell at similar operating conditions (60°C, unpressurized reactants, and 75% RH) with a thinner (50 μm) membrane and a lower Pt loading (0.325

mg Pt/cm^2 MEA). Siegel did use a different catalyst layer application technique (decal transfer) that included a hot press step to consolidate and bond the catalyst layer to the membrane. While the results presented here for the H_2/Air performance tests were lower than previous results from Virginia Tech efforts, suggesting improvements may be needed in our spraying and catalyst layer consolidation steps, the MEA preparation procedures were judged to be sufficient for make MEA comparisons.

The EASA measurements taken prior to the room temperature ethanol experiments for MEAs 1a and 1b are plotted together in Figure 4-15. The EASA and effective surface area were calculated from the EASA plots and the results are shown in Table 4-9, which can be found in section 4.4.4. The EASA plots are similar for both MEAs, though MEA 1a has higher hydrogen desorption and adsorption peaks in this plot and a slightly higher double layer capacitance charge.

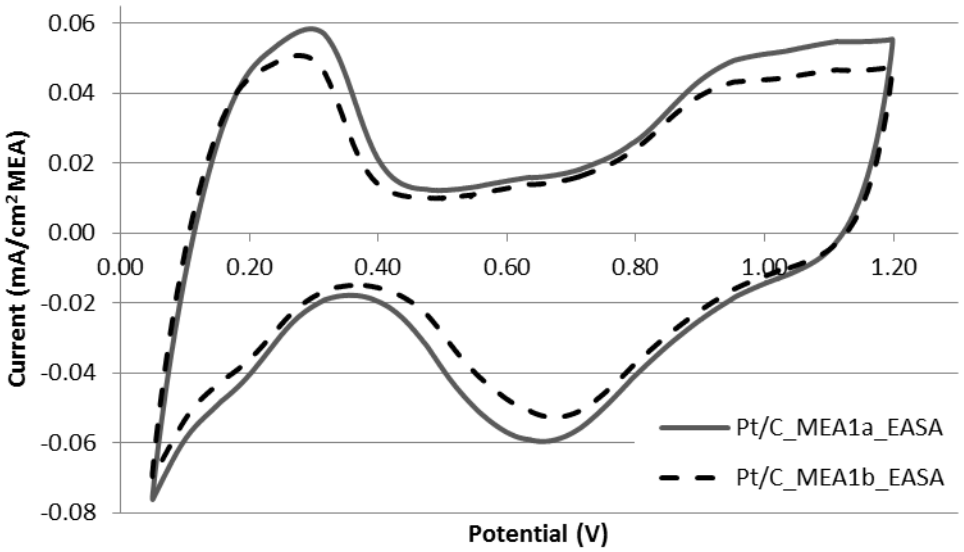

Figure 4-15. EASA measurements for the Pt/C electrodes (MEA 1a and MEA 1b) before the 25°C ethanol polarization curve, cell temperature = 25°C, dew point$_{a,c}$ = 25°C, unpressurized reactants, H_2 flow rate = 100 sccm, N_2 flow rate = 100 sccm.

The performance of the Pt/C MEAs when flowing 0.1 M ethanol solution and air at room temperature and 60°C is shown in Figure 4-16 and Figure 4-17, respectively. The OCVs at room temperature were 0.79 V for MEA 1a and 0.77 V for MEA 1b. At 60° C, the OCVs increased slightly to 0.81 V (1a) and 0.80 V (1b). The current densities for the Pt/C electrodes reached between 15 and 20 mA/cm^2 MEA active area at room temperature and about 57 mA/cm^2 MEA active area at 60°C by the end of the potential range. The OCVs of the Pt/C MEAs during the 60°C test were higher than those reported by Vigier *et al.* [24] and Zhou *et al.* [9] in a 90°C fuel cell flowing oxygen and 1.0 M ethanol solution with similar anode Pt loading. The maximum current density attained in the Vigier *et al.* [24] experiment was 80 mA/cm^2, which is similar to the

results reported here, and that achieved by Zhou *et al.* [9] was about 100 mA/cm^2, which is higher than the results from this experiment. The differences in the current densities are likely attributable to the operating conditions and experimental setup. The maximum power densities achieved by the Pt/C MEAs at room temperature were 2.4 mW/cm^2 MEA active area (MEA 1a) and 2.8 mW/cm^2 MEA active area (MEA 1b) and were achieved at 10.5 mA/cm^2 MEA active area. At 60°C, the power density maxima occurred around 40 mA/cm^2 MEA active area and were 8.2 and 9.0 mW/cm^2 MEA active area for MEA 1a and MEA 1b, respectively, and are similar to results in the literature [9, 24]. *While the performance of the Pt/C MEAs was lower than expected for the H_2/Air tests, the results in a DEFC are similar to those in literature, which gives confidence in our MEA preparation procedure used for the performance experiments.*

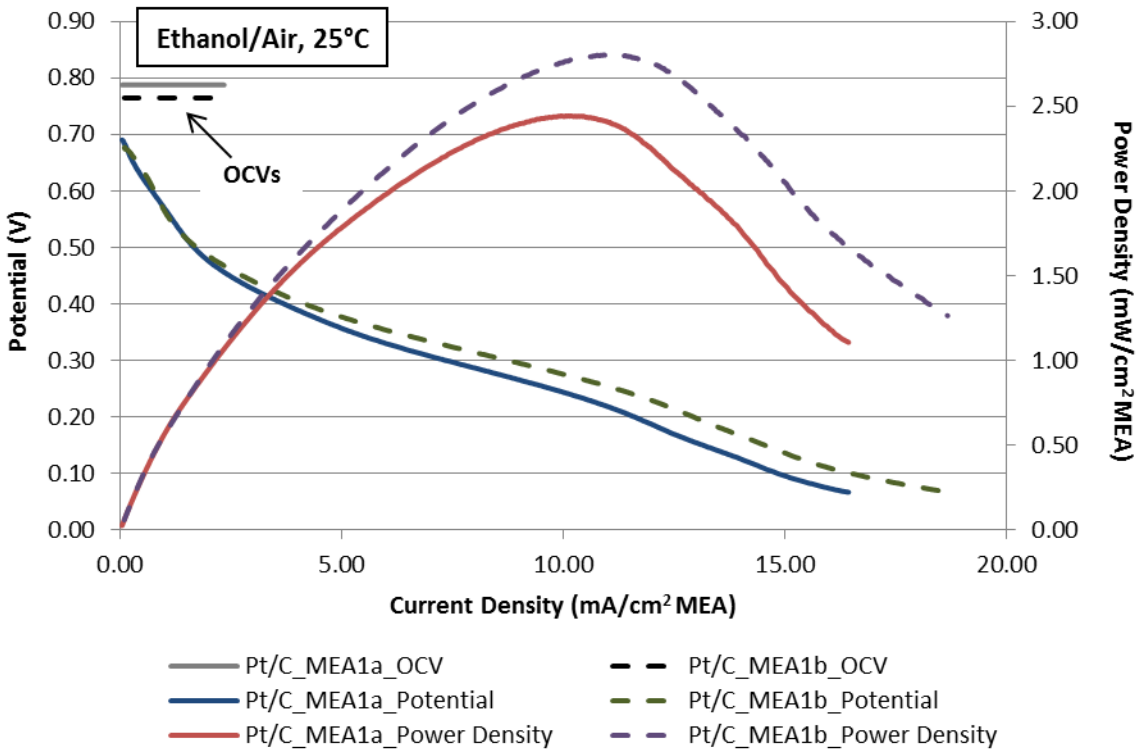

Figure 4-16. 0.1 M ethanol solution iR-corrected fuel cell performance on Pt/C electrodes (MEA 1a and MEA 1b); cell temperature = 25°C, dew point$_c$ = 25°C, back pressure = 15 psig, air flow rate = 950 sccm, EtOH temperature = 25°C, EtOH flow rate = 8 mL/min, MEA 1a ASR = 0.915 Ωcm^2, MEA 1b ASR = 0.85 Ωcm^2.

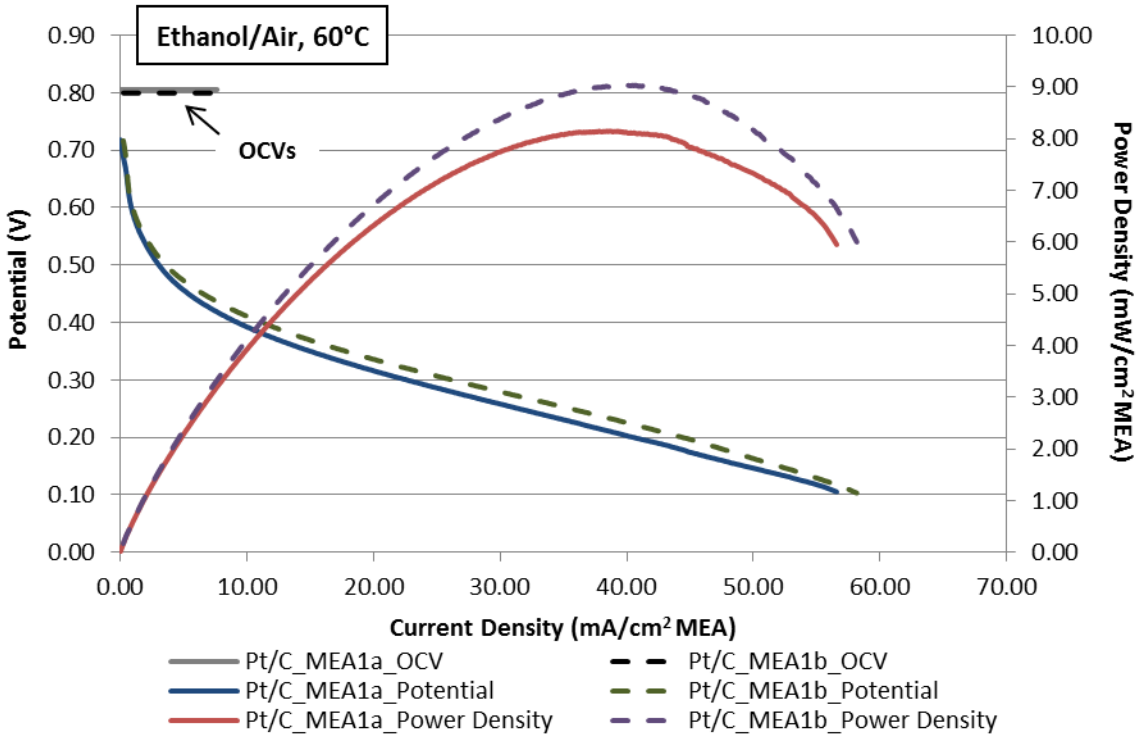

Figure 4-17. 0.1 M ethanol solution iR-corrected fuel cell performance on Pt/C electrodes (MEA 1a and MEA 1b); cell temperature = 60°C, dew point$_c$ = 25°C, back pressure = 15 psig, air flow rate = 950 sccm, EtOH temperature = 60°C, EtOH flow rate = 8 mL/min, MEA 1a ASR = 0.915 Ωcm^2, MEA 1b ASR = 0.865 Ωcm^2.

4.2. PtSn/C Catalyst

4.2.1. Electrochemically Active Surface Area for a PtSn/C Thin Film Electrode

The final sweep of SDCV-6 on a PtSn/C thin film electrode is plotted in Figure 4-18. As was done for the Pt/C thin film electrodes, the properties from all of the EASA tests for each of the two PtSn/C thin film electrodes were averaged and are displayed in Table 4-3.

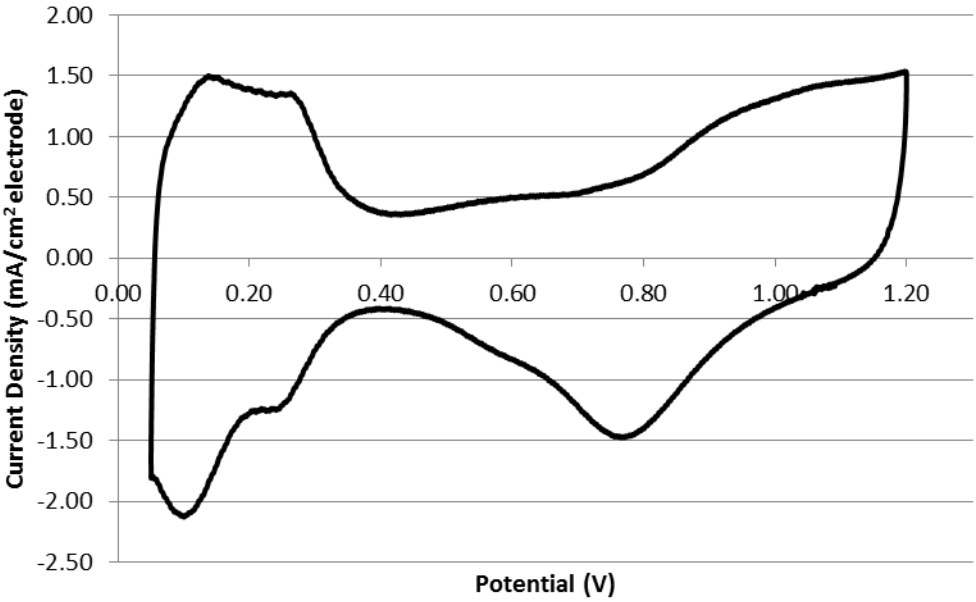

Figure 4-18. Final sweep of SDCV-6 in 0.1 M H_2SO_4 for the PtSn/C thin film A electrode.

Table 4-3. PtSn/C thin film electrode properties.

Thin Film	A	B
Pt Loading [mg Pt/cm^2 electrode]	0.06	0.06
C_{dl} [C]	5.22-04	6.32E-04
H^+ Adsorption Charge [C]	8.93E-04	1.44E-03
Specific EASA [cm^2 Pt/mg Pt]	340	560
EASA [cm^2 Pt]	4.2	6.9

As the experiments progressed, the EASA for each thin film electrode changed by a maximum of ± 25%. Thin film B had almost double the specific EASA as thin film A (560 versus 340 cm^2 Pt/mg Pt) and had an EASA of 6.9 cm^2 Pt versus 4.2 cm^2 Pt for

thin film A. *Overall, the results demonstrate that the experimental procedure can yield high specific area thin film electrodes but that the surface area may vary significantly between PtSn/C electrodes. Thus, it is essential to normalize results based on catalyst surface area, not catalyst loading.*

4.2.2. SDCV Tests for Ethanol Oxidation on a PtSn/C Thin Film Electrode

The SDCVs at 10 and 100 mV/s sweep rates on a PtSn/C thin film electrode in 0.01 M ethanol concentration solution are shown in Figure 4-19. Data for all of the sweep rates is in the Appendix (7.1). An increase in the voltage scan rate led to a wider current density range in the 0.01 M ethanol solution, which is emphasized by the orange arrows in Figure 4-19. The oxidation peaks are larger on the forward scan and the reduction peaks are larger on the reverse scan. The peak around 0.6 V on the reverse sweep dropped slightly, though the current density difference between the preceding reduction peak and the oxidation peak (at 0.6 V) increased during the faster scan rate. The peak due to CO_2 formation is very visible in the 100 mV/s CV and is highlighted in Figure 4-19. Also, the oxidation peak on the forward scan shifted to higher potentials as the scan rate increased, and the oxidation peak on the reverse scan shifted to slightly lower potentials as the scan rate increased. This was also seen with the Pt/C thin film

electrode and can be explained by the fact that a larger voltage range is covered in a given time period when scanning the potential at a higher rate.

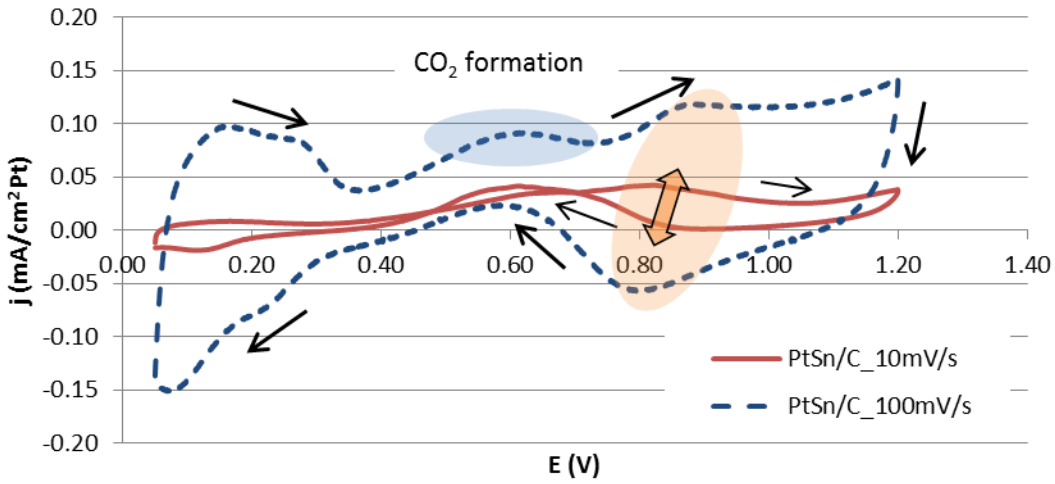

Figure 4-19. SDCV 10 mV/s and 100 mV/s sweeps on a PtSn/C thin film electrode in 0.01 M ethanol solution.

In 0.1 M and 1.0 M ethanol solution, shown in Figure 4-20 and Figure 4-21, the oxidation peaks are clearly seen (one on the forward scan and one on the reverse scan) at both scan rates. The shoulder due to CO_2 formation is visible on both the 10 mV/s and the 100 mV/s sweep rates in 0.1 M ethanol solution, but not in the 1.0 M ethanol solution.

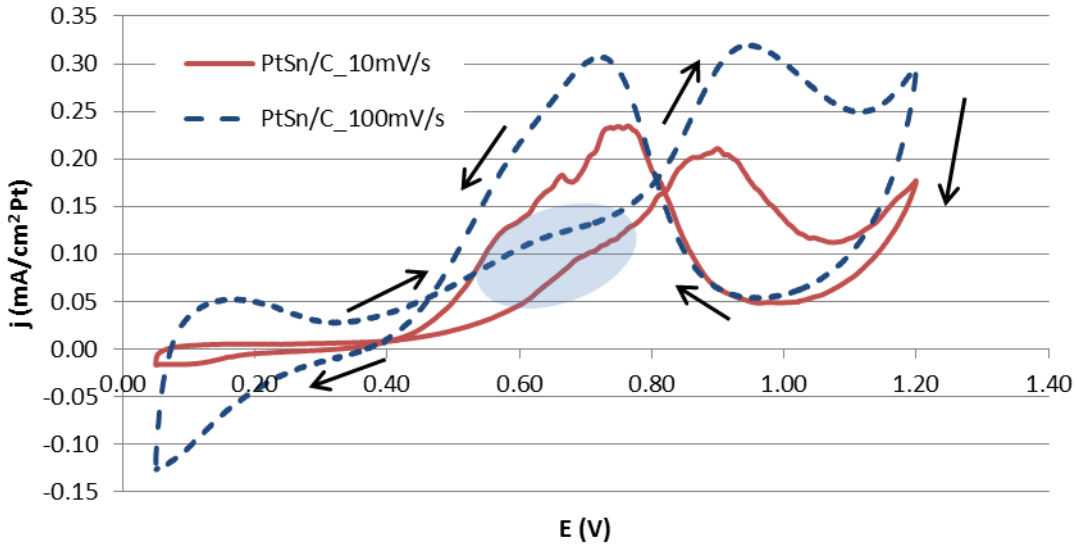

Figure 4-20. SDCV 10 mV/s and 100 mV/s sweeps on a PtSn/C thin film electrode in 0.1 M ethanol solution.

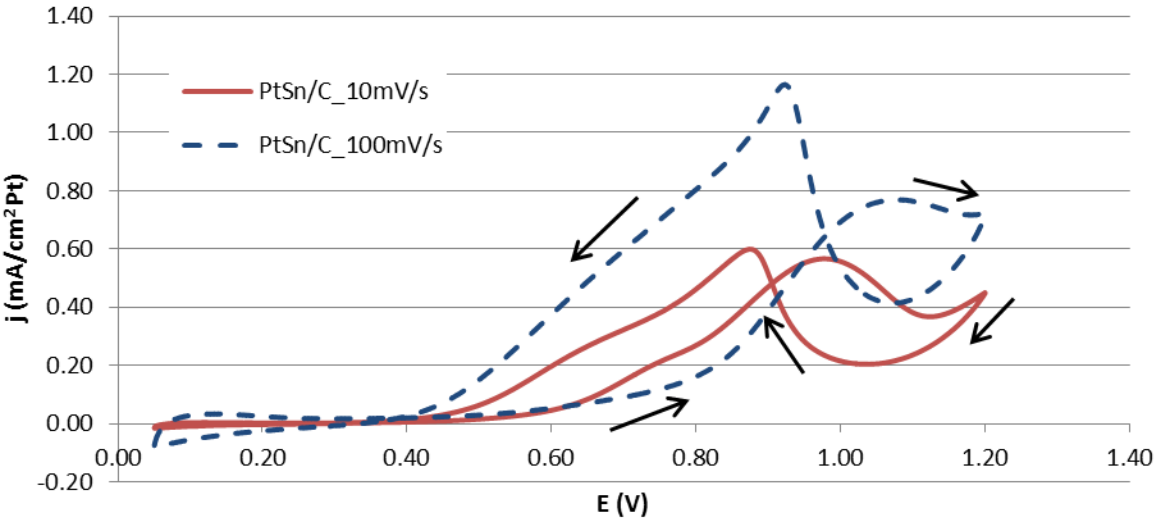

Figure 4-21. SDCV 10 mV/s and 100 mV/s sweeps on a PtSn/C thin film electrode in 1.0 M ethanol solution.

As can be seen from the 0.01 M and 0.1 M ethanol solution plots, the CO_2 formation peak or shoulder has an amplitude of less than 0.05 mA/cm^2 Pt and therefore may not be visible in the 1.0 M ethanol solution measurements due to the much larger current density values recorded. As was seen in 0.01 M ethanol solution, the oxidation peak on the forward sweep shifted to the right with an increase in voltage scan rate, while the oxidation peak on the reverse sweep shifted slightly to the left. In the 1.0 M ethanol solution, both peaks shifted to the right as the scan rate increased.

Figure 4-22 displays the 10 mV/s CVs for all three ethanol concentration solutions when a PtSn/C thin film electrode was used. The SDCV plots are similar in shape to those reported in the literature for PtSn/C, but exhibited slightly lower current densities than are reported for similar catalyst preparation and experimental conditions [18]. As was seen with the Pt/C thin film electrode, the current density increased with an increase in ethanol concentration and the oxidation peaks shifted to the right as the ethanol concentration increased. *The PtSn/C catalyst exhibited higher current densities than the Pt/C catalyst in 0.01 M and 0.1 M ethanol solution, which demonstrates a greater effectiveness of the PtSn/C catalyst for ethanol oxidation in low ethanol concentration solutions.*

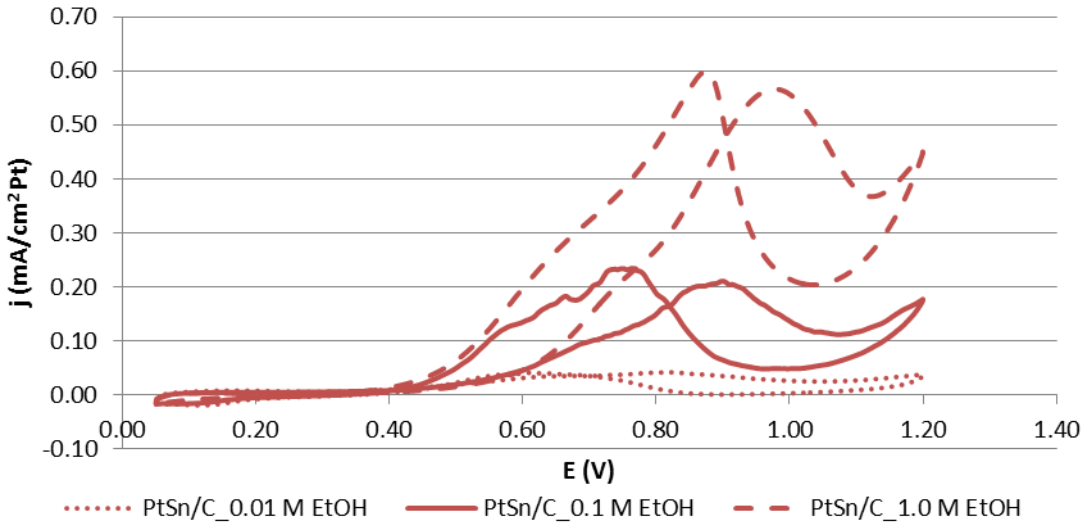

Figure 4-22. SDCV sweeps on a PtSn/C thin film electrode at 10 mV/s in 0.01, 0.1, and 1.0 M ethanol (EtOH) solutions.

4.2.3. SDPS Tests for Ethanol Oxidation on a PtSn/C Thin Film Electrode

The following two plots, Figure 4-23 and Figure 4-24, report the results from the SDPS tests on a PtSn/C thin film electrode in 0.01 M, 0.1 M, and 1.0 M ethanol solutions. The complete data for these tests can be found in the Appendix (7.2). As seen with the Pt/C electrode, higher ethanol concentration solutions gave rise to slightly higher current densities one second after the voltage reached 0.5 V. The slope of each curve and the current density values at t = 1 s are more clearly seen in Figure 4-24, which reports the data recorded for nine seconds, beginning one second after the voltage was stepped to 0.5 V.

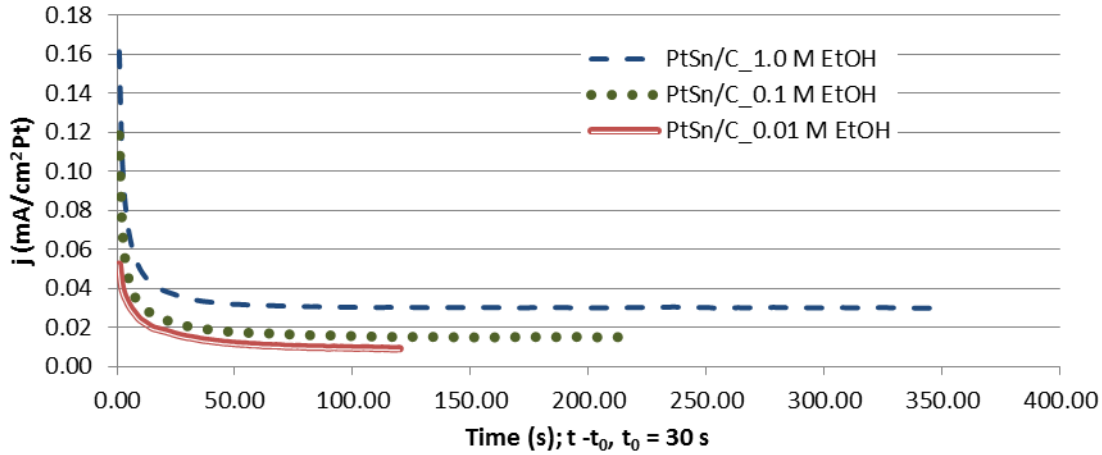

Figure 4-23. SDPS test on a PtSn/C thin film in 0.01, 0.1, and 1.0 M ethanol solutions.

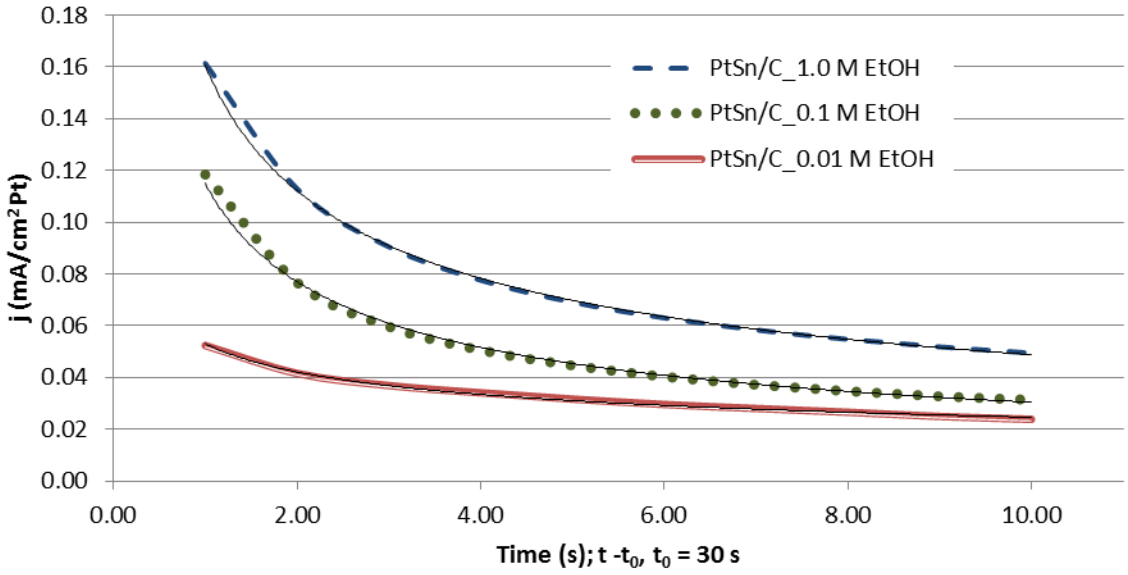

Figure 4-24. Power law fits to the SDPS data on PtSn/C from t = 1 – 10 s in various ethanol concentration solutions.

The equations for the power law fits to the data plotted in Figure 4-24 are given in Table 4-4. The quickest decrease in current density is seen in the 0.1 M ethanol solution and is indicated by the largest (most negative) exponent in the power law fit equation. This suggests the thin film electrode in 0.1 M ethanol solution was most affected by electrode poisoning by intermediate species. The exponent in the equation fit to the data from the 0.01 M ethanol solution SDPS test is less than 0.5, which is the exponent in the Cottrell equation which describes the theoretical diffusion limited current. All exponents were expected to be greater than 0.5 in order to account for both diffusion limitations as well as catalyst poisoning. It is unclear why the exponent for this particular case was less than 0.5. *As Figure 4-33 and Figure 4-34 illustrate, higher concentrations of ethanol lead to more rapid poisoning of the catalyst layer but also yield higher steady-state current densities. Further, the PtSn/C steady-state values are larger when compared to the Pt/C catalyst results.*

Table 4-4. Equations of the power law fits to the SDPS data shown in Figure 4-24.

Ethanol Concentration [M]	Power Law Equations
0.01	$Y = 0.0531x^{-0.334}$
0.1	$Y = 0.115x^{-0.578}$
1.0	$Y = 0.1604x^{-0.517}$

4.2.4. Evaluation of a PtSn/C Catalyst MEA for Ethanol Oxidation in a DEFC

The results of the EASA tests for both PtSn/C MEAs (2a and 2b) before the 25°C ethanol test are found in Figure 4-25. The PtSn/C MEAs have similar EASA plots.

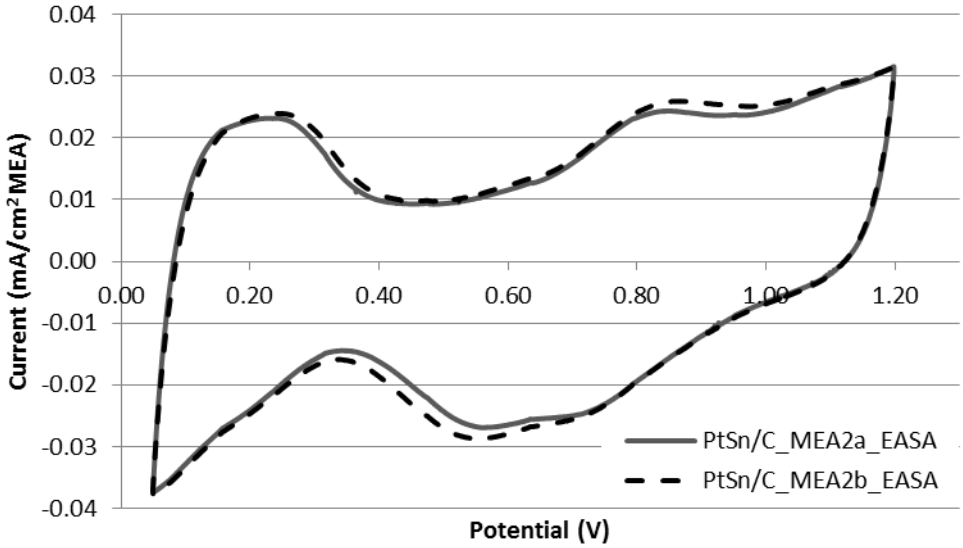

Figure 4-25. EASA measurements for the PtSn/C electrodes (MEA 2a and MEA 2b) before the 25°C ethanol polarization curve, cell temperature = 25°C, dew point$_{a,c}$ = 25°C, unpressurized reactants, H_2 flow rate = 100 sccm, N_2 flow rate = 100 sccm.

Figure 4-26 and Figure 4-27 display the iR-corrected polarization curves and calculated power densities for the PtSn/C MEAs, along with the initial OCVs, for the 25°C and 60° C 0.1 M ethanol solution experiments. The plots in this section are normalized to the MEA active area, as was done with the Pt/C MEAs, in order to be consistent with performance values reported in the literature. The resistance values ranged from 0.163

ohms to 0.205 ohms (0.815 – 1.025 Ωcm^2) for the two MEAs at the two temperatures examined.

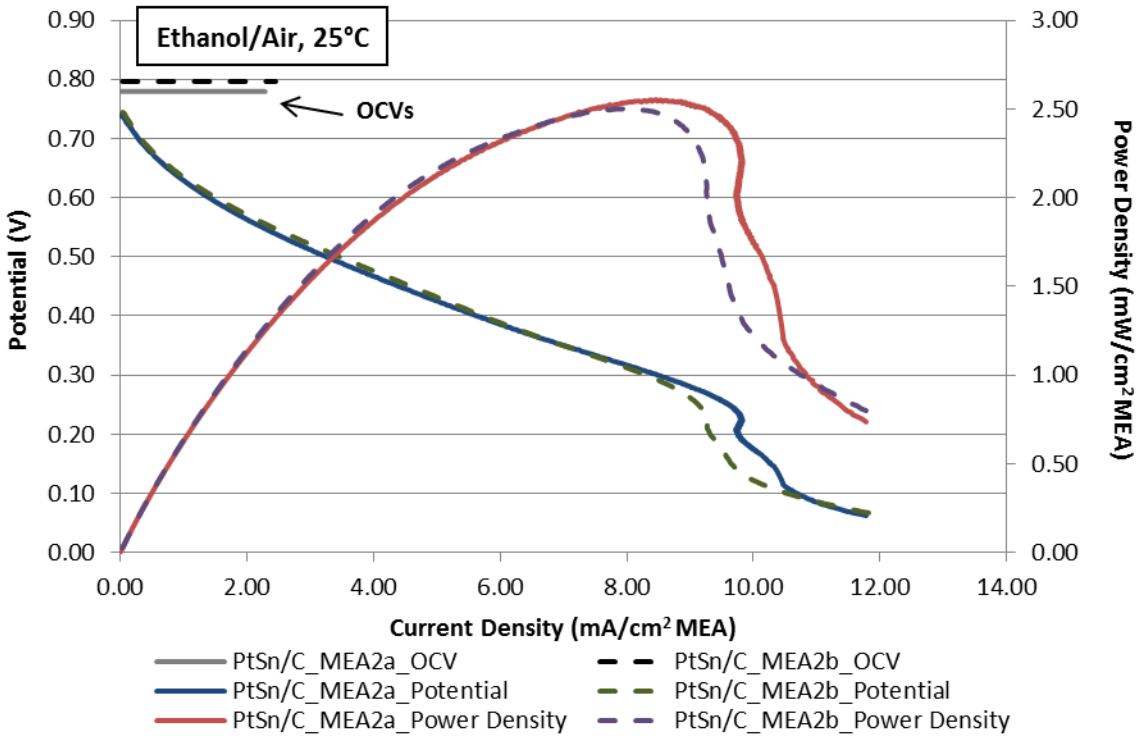

Figure 4-26. 0.1 M ethanol solution iR-corrected fuel cell performance on PtSn/C electrodes (MEA 2a and MEA 2b); cell temperature = 25°C, dew point$_c$ = 25°C, back pressure = 15 psig, air flow rate = 950 sccm, EtOH temperature = 25°C, EtOH flow rate = 8 mL/min, MEA 2a ASR = 0.815 Ωcm^2, MEA 2b ASR = 1.025 Ωcm^2.

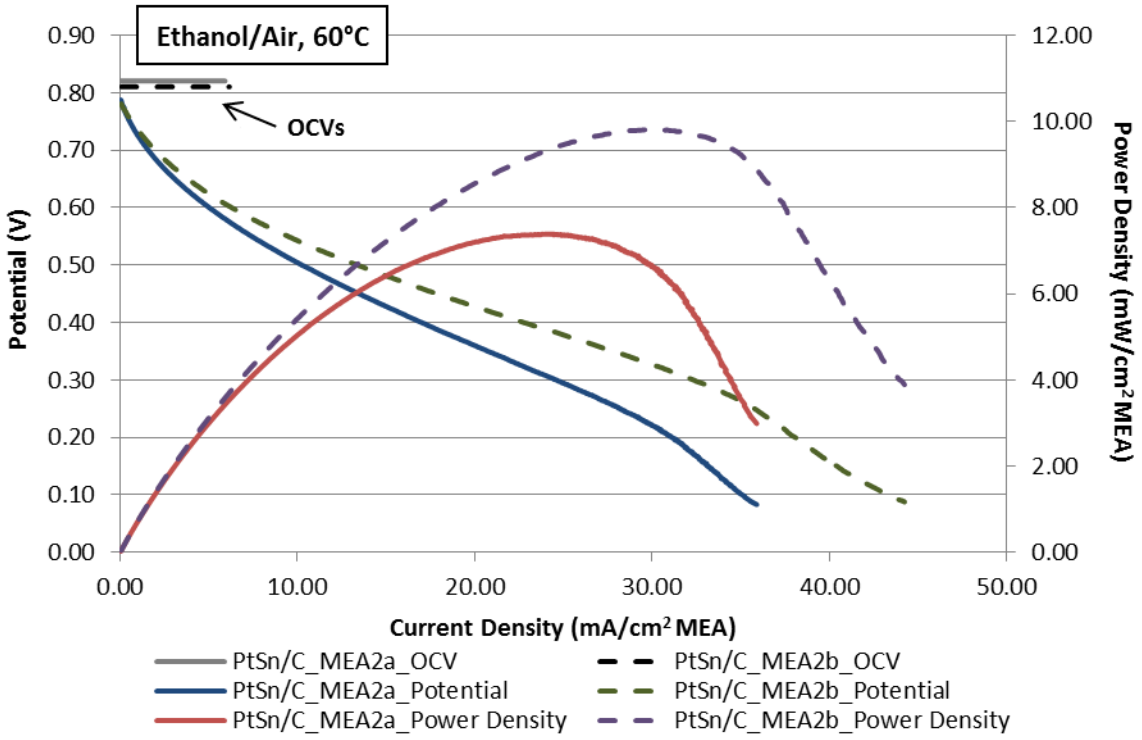

Figure 4-27. 0.1 M ethanol solution iR-corrected fuel cell performance on PtSn/C electrodes (MEA 2a and MEA 2b); cell temperature = 60°C, dew point$_c$ = 25°C, back pressure = 15 psig, air flow rate = 950 sccm, EtOH temperature = 60°C, EtOH flow rate = 8 mL/min, MEA 2a ASR = 0.830 Ωcm^2, MEA 2b ASR = 0.815 Ωcm^2.

The OCVs for MEA 2a and 2b at 25°C were 0.78 V and 0.80 V, respectively, and 0.82 V and 0.81 V, respectively, while at 60°C, similar to those reported in the literature [3, 5, 9, 14, 24, 32]. The maximum current density increased from about 12 mA/cm^2 to around 40 mA/cm^2 with the increase in fuel cell operating temperature. The maximum power densities produced were 2.5 mW/cm^2 MEA active area for both MEAs at room temperature at about 8.0 mA/cm^2 MEA active area. The peak power density reached 7.4 mW/cm^2 MEA active area for MEA 2a and 9.8 mW/cm^2 MEA active area for MEA 2b

around 27 mW/cm^2 MEA active area at 60°C. The maximum current densities and peak power densities in the 60°C polarization curve are on par with results from similar experiments that used 0.1 M ethanol solution and slightly lower than results from experiments that tested 1.0 M ethanol solution [3, 24]. On the PtSn/C polarization curves, more so at room temperature, a drastic drop in cell voltage occurred when the cell reached 0.25 V. Before the end of the test, the rate of the voltage drop decreased to a more reasonable rate (based on the rate of voltage drop at potentials higher than 0.25 V). The reason for this brief but sudden drop is unknown, but it occurred in both PtSn/C MEAs around the same voltage and was not seen when the other MEAs were tested. *As is seen in the literature, performance measurements with PtSn/C MEAs result in higher OCVs, current densities, and power densities than is seen with Pt/C MEAs.*

4.3. Pt/Nb-TiO_2-C Catalyst

4.3.1. Electrochemically Active Surface Area for a Pt/Nb-TiO_2-C Thin Film Electrode

The final sweep of SDCV-6 on the Pt/Nb-TiO_2-C thin film A electrode is presented in Figure 4-28. The plot has a similar shape to the EASA plots using Pt/C and PtSn/C thin film electrodes, indicating the same reactions are occurring on all of the

electrodes. Once again, changes were seen in the thin film electrode properties as the experiments progressed, so the average properties for each of the Pt/Nb-TiO_2-C thin films tested are organized in Table 4-5. The EASA value changed by a maximum of ± 13% for each thin film electrode. The properties are very similar among all of the thin films, with the specific EASA ranging from 130 – 160 cm^2 Pt/mg Pt and the EASA spanning 1.6 – 2 cm^2 Pt. *Thus, the Nb-TiO_2-C support is confirmed to be capable of forming thin film electrodes with high active areas. It should be noted that there was an attempt to prepare thin film electrodes with Nb-TiO_2 support (i.e. without carbon), but it was found that the EASAs were quite small, suggesting that, in the absence of carbon to contribute a conductive matrix, the Nb-TiO_2 support does not have sufficient conductivity to make high performance electrodes.*

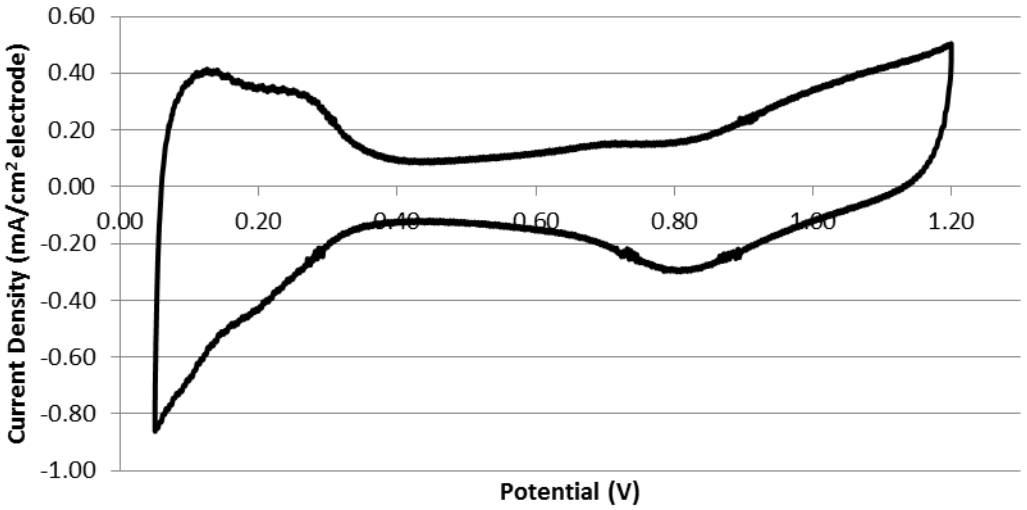

Figure 4-28. Final sweep of SDCV-6 in 0.1 M H_2SO_4 for the Pt/Nb-TiO_2-C thin film A electrode.

Table 4-5. Pt/Nb-TiO_2-C thin film electrode properties.

Thin Film	A	B	C	D	E
Pt Loading [mg Pt/cm^2 electrode]	0.06	0.06	0.06	0.06	0.06
C_{dl} [C]	1.66E-04	1.84E-04	1.72E-4	1.72E-4	1.70E-4
H^+ Adsorption Charge [C]	3.63E-04	4.11E-03	4.02E-4	3.85E-4	3.37E-4
Specific EASA [cm^2 Pt/mg Pt]	140	160	150	150	130
EASA [cm^2 Pt]	1.7	2	1.8	1.8	1.6

4.3.2. SDCV Tests for Ethanol Oxidation for a Pt/Nb-TiO_2-C Thin Film Electrode

Similar trends are seen with the Pt/Nb-TiO_2-C electrode as were seen with the previous electrodes. An increase in scan rate resulted in increased oxidation and reduction peaks. In the 0.01 M ethanol solution SDCVs, the reverse peak around 0.6 V was actually slightly higher in the 100 mV/s CV than in the 10 mV/s CV, both of which are depicted in Figure 4-29, unlike what was seen with the previous electrodes. As with the other SDCV plots, the peak due to CO_2 formation is highlighted in the 100 mV/s CV and occurred at 0.6 V on the forward scan in 0.01 M ethanol solution. The increase in current density range is also emphasized by the orange arrows.

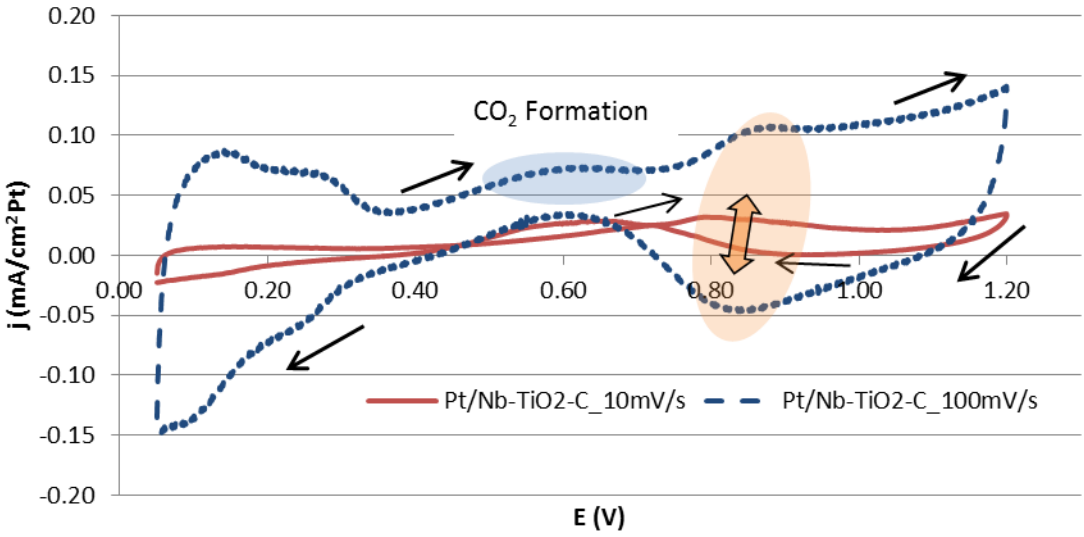

Figure 4-29. SDCV 10 mV/s and 100 mV/s sweeps on a Pt/Nb-TiO_2-C thin film electrode in 0.01 M ethanol solution.

The CO_2 formation shoulder is still visible in the 100 mV/s CV in 0.1 M ethanol solution and is highlighted in Figure 4-30, though it is almost directly behind the reverse peak of the 10 mV/s CV. There is no distinct CO_2 formation shoulder in the 1.0 M ethanol solution CVs shown in Figure 4-31. Minor shifts in the potentials at which the forward oxidation peaks and, to a lesser extent the reverse oxidation peaks, occurred are noticeable in each of the ethanol concentration plots and can be explained by the increase in voltage range covered during a set time frame as the scan rate was increased. The results of all of the sweep rates tested are located in the Appendix (7.1).

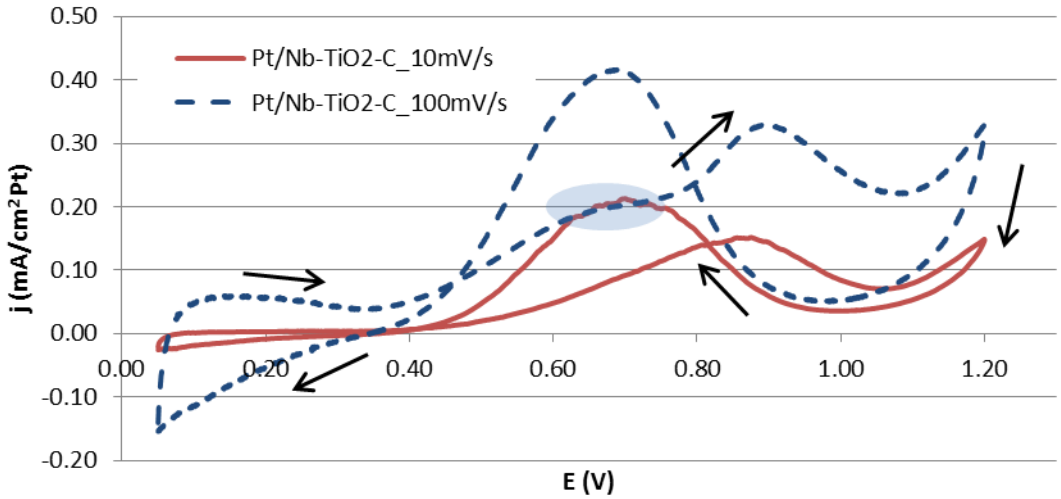

Figure 4-30. SDCV 10 mV/s and 100 mV/s sweeps on a Pt/Nb-TiO2-C thin film electrode in 0.1 M ethanol solution.

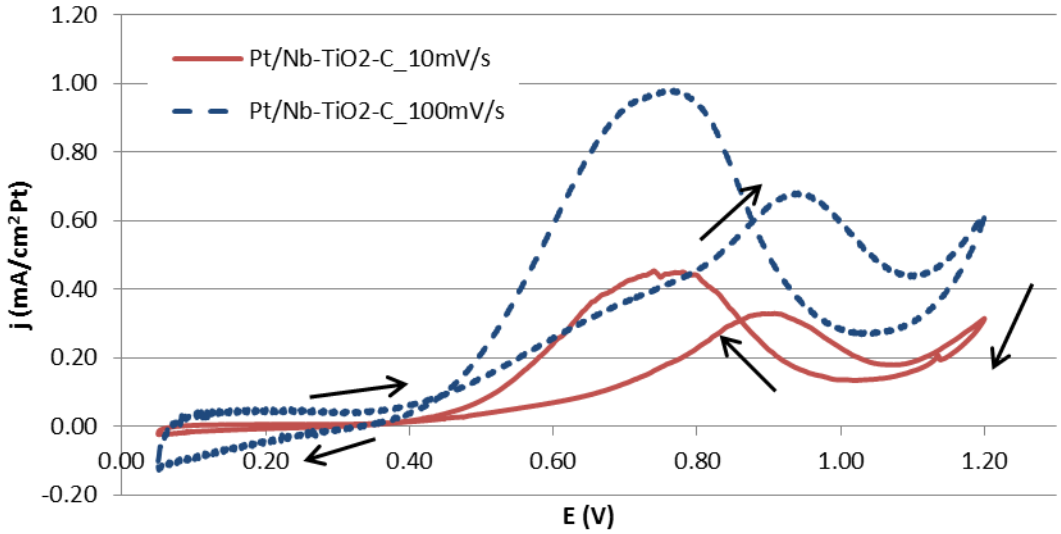

Figure 4-31. SDCV 10 mV/s and 100 mV/s sweeps on a Pt/Nb-TiO2-C thin film electrode in 1.0 M ethanol solution.

The 10 mV/s CVs in each ethanol concentration solution with a Pt/Nb-TiO_2-C thin film electrode are plotted together in Figure 4-32. Similarly to the Pt/C and PtSn/C electrodes, both the forward and reverse scan current peaks shifted to slightly higher potentials as the concentration of ethanol increased. *It is apparent that complete ethanol oxidation to CO_2, as well as incomplete oxidation to acetaldehyde and acetic acid, occurs on the Pt/Nb-TiO_2-C catalyst based on the similarities of the SDCV plots among the three catalysts investigated. In general, the SDCVs with a Pt/Nb-TiO_2-C thin film electrode most closely resemble those of the PtSn/C thin film electrode based on current densities, overall shape, and voltages at which peak currents occur.*

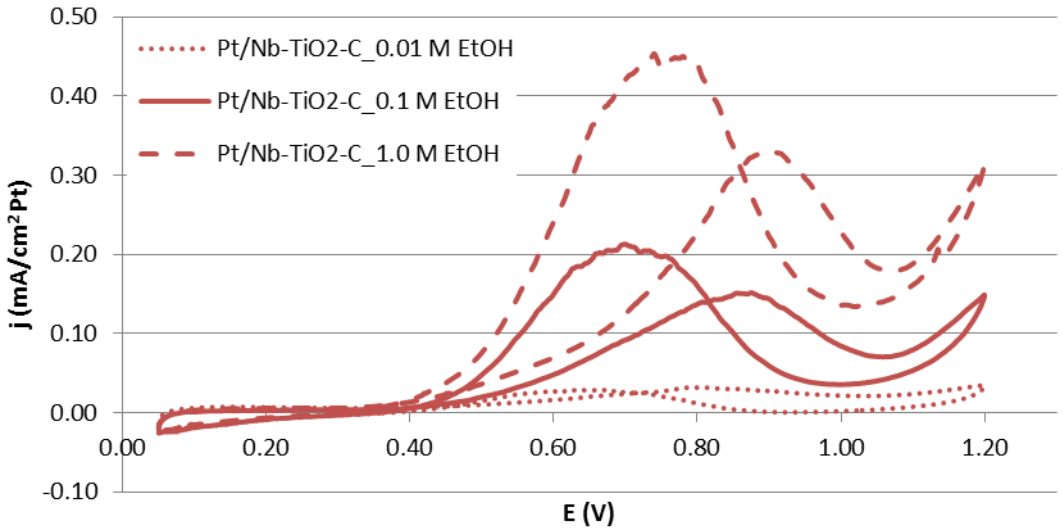

Figure 4-32. SDCV sweeps on a Pt/Nb-TiO_2-C thin film electrode at 10 mV/s in 0.01, 0.1, and 1.0 M ethanol solutions.

4.3.3. SDPS Tests for Ethanol Oxidation on a Pt/Nb-TiO_2-C Thin Film Electrode

The SDPS data recorded using a Pt/Nb-TiO_2-C thin film electrode is plotted for all three ethanol concentrations, after the voltage was stepped to 0.5 V, in Figure 4-33, with the complete data reported in the Appendix (7.2). As with the Pt/C and PtSn/C electrodes, higher current densities were reached in the higher ethanol concentration solutions. The current density values and power law fits are displayed for 1 to 10 seconds after the voltage increased to 0.5 V in Figure 4-34.

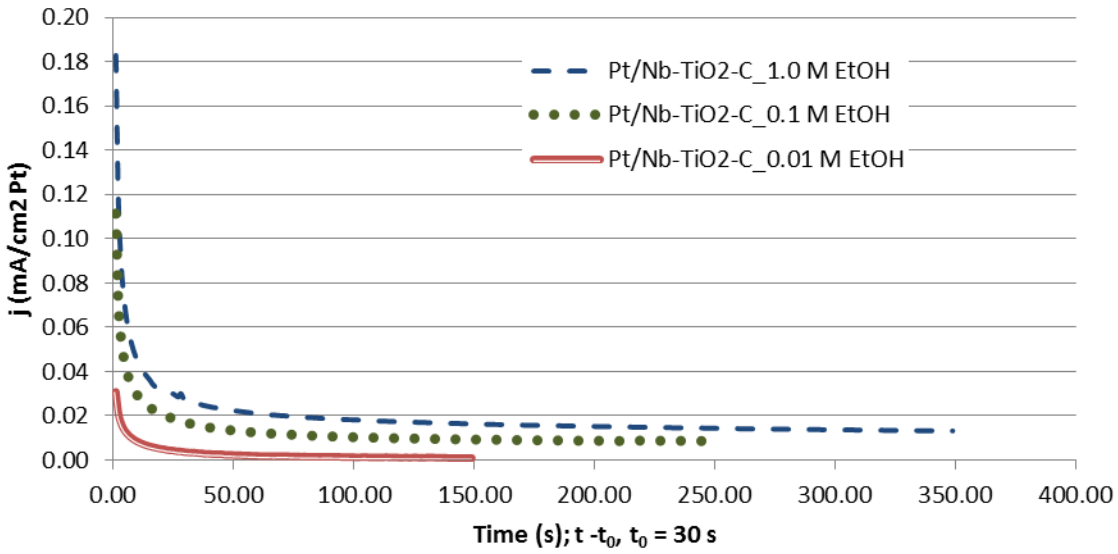

Figure 4-33. SDPS test on a Pt/Nb-TiO_2-C thin film in 0.01, 0.1, and 1.0 M ethanol solutions.

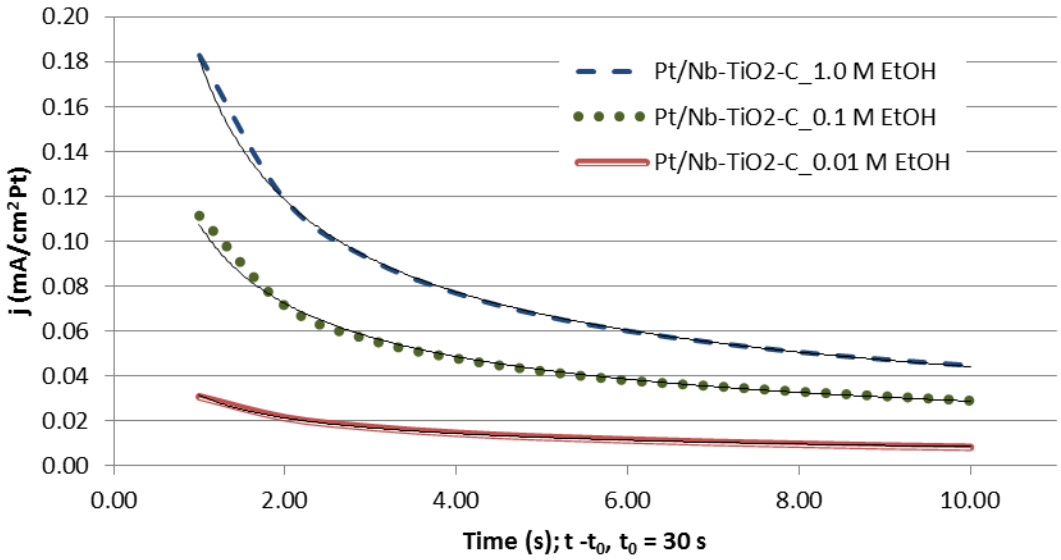

Figure 4-34. Power law fits to the SDPS data on Pt/Nb-TiO_2-C from t = 1 – 10 s in various ethanol concentration solutions.

The power law equations for each ethanol concentration are listed in Table 4-6 and, unlike with the Pt/C and PtSn/C electrodes, there was a direct correlation between catalyst layer poisoning and ethanol concentration, with the poisoning increasing as the concentration increased. The value of b (from Equation 4.3) for the 1.0 M ethanol solution fit was 0.612 as compared to 0.573 for the 0.1 M ethanol solution power law equation and 0.567 for the 0.01 M ethanol solution equation. As stated previously, the larger b is, the more the catalyst layer is affected by poisoning. *Similarly to the Pt/C and PtSn/C electrodes, the initial current density on a Pt/Nb-TiO_2-C electrode increases with*

an increase in ethanol concentration. The catalyst poisoning also increases as the ethanol concentration increases on a Pt/Nb-TiO_2-C catalyst.

Table 4-6. Equations of the power law fits to the SDPS data shown in Figure 4-34.

Ethanol Concentration [M]	Power Law Equations
0.01	$Y = 0.0316x^{-0.567}$
0.1	$Y = 0.1077x^{-0.573}$
1.0	$Y = 0.1812x^{-0.612}$

4.3.4. Evaluation of a Pt/Nb-TiO_2-C Catalyst MEA for Ethanol Oxidation in a DEFC

Data from the EASA measurements of the Pt/Nb-TiO_2-C MEAs (3a, 3b, and 3c) are plotted in Figure 4-35. The double layer capacitance region is quite small for all of the MEAs, though the calculated specific EASA values (140, 120, and 110 cm^2 Pt/mg Pt) are similar and are reasonable values based on those seen with the other catalysts.

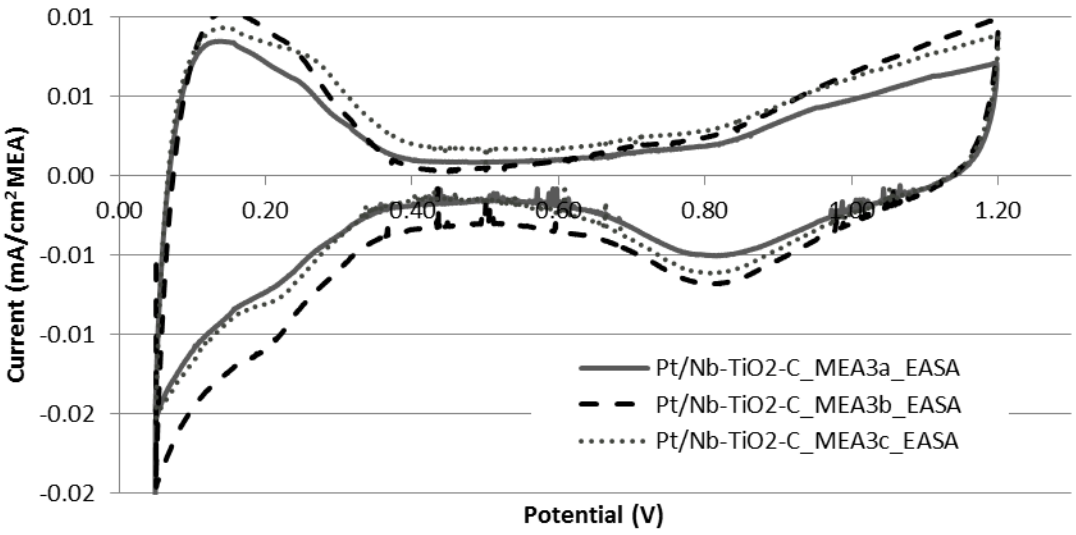

Figure 4-35. EASA measurements for the Pt/Nb-TiO2-C electrodes (MEA 3a, MEA 3b. and MEA 3c) before the 25°C ethanol polarization curve, cell temperature = 25°C, dew point$_{a,c}$ = 25°C, unpressurized reactants, H2 flow rate = 100 sccm, N2 flow rate = 100 sccm.

The 0.1 M ethanol/air iR-corrected fuel cell performance results are displayed in Figure 4-36, for the room temperature test, and Figure 4-37, for the 60°C test. The resistance measurements ranged from 0.06 ohms to 0.18 ohms (0.30 – 0.90 Ωcm^2) for the Pt/Nb-TiO_2-C MEAs.

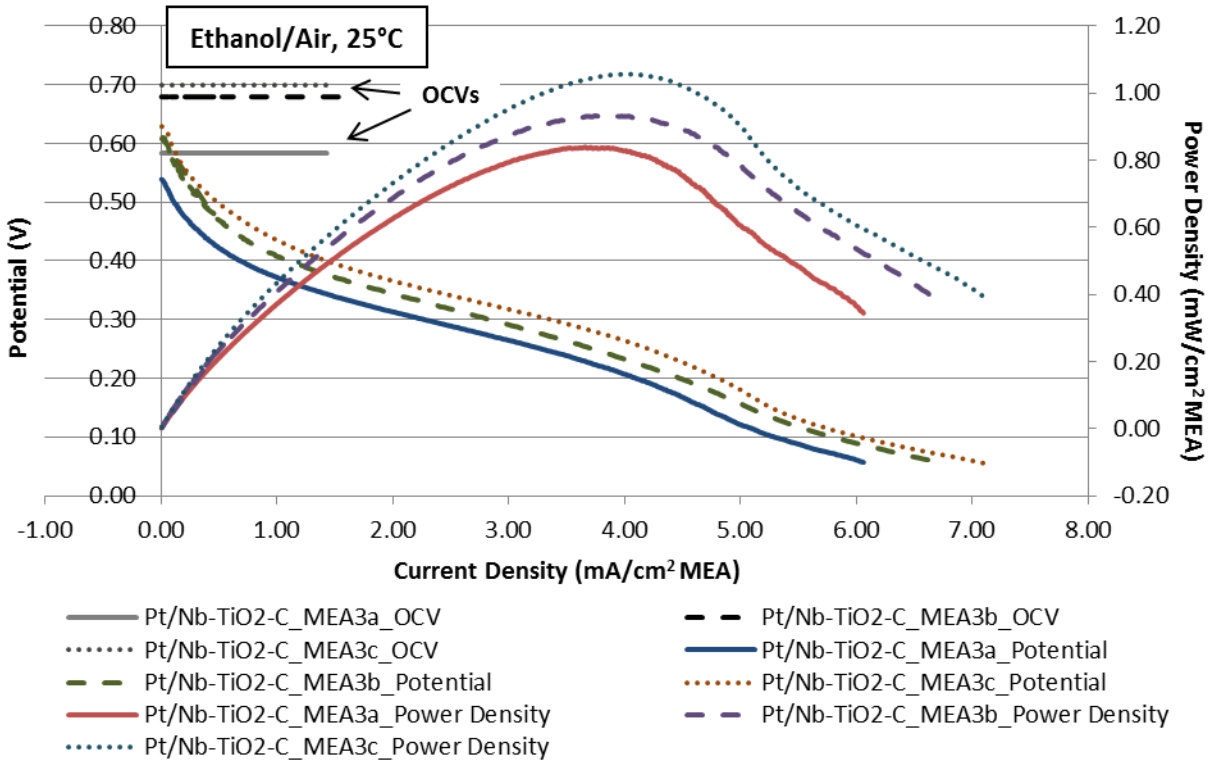

Figure 4-36. 0.1 M ethanol solution iR-corrected fuel cell performance on Pt/Nb-TiO2-C electrodes (MEA 3a, MEA 3b, MEA 3c); cell temperature = 25°C, dew pointc = 25°C, back pressure = 15 psig, air flow rate = 950 sccm, EtOH temperature = 25°C, EtOH flow rate = 8 mL/min, MEA 3a ASR = 0.885 Ωcm^2, MEA 3b ASR = 0.545 Ωcm^2, MEA 3c ASR = 0.550 Ωcm^2.

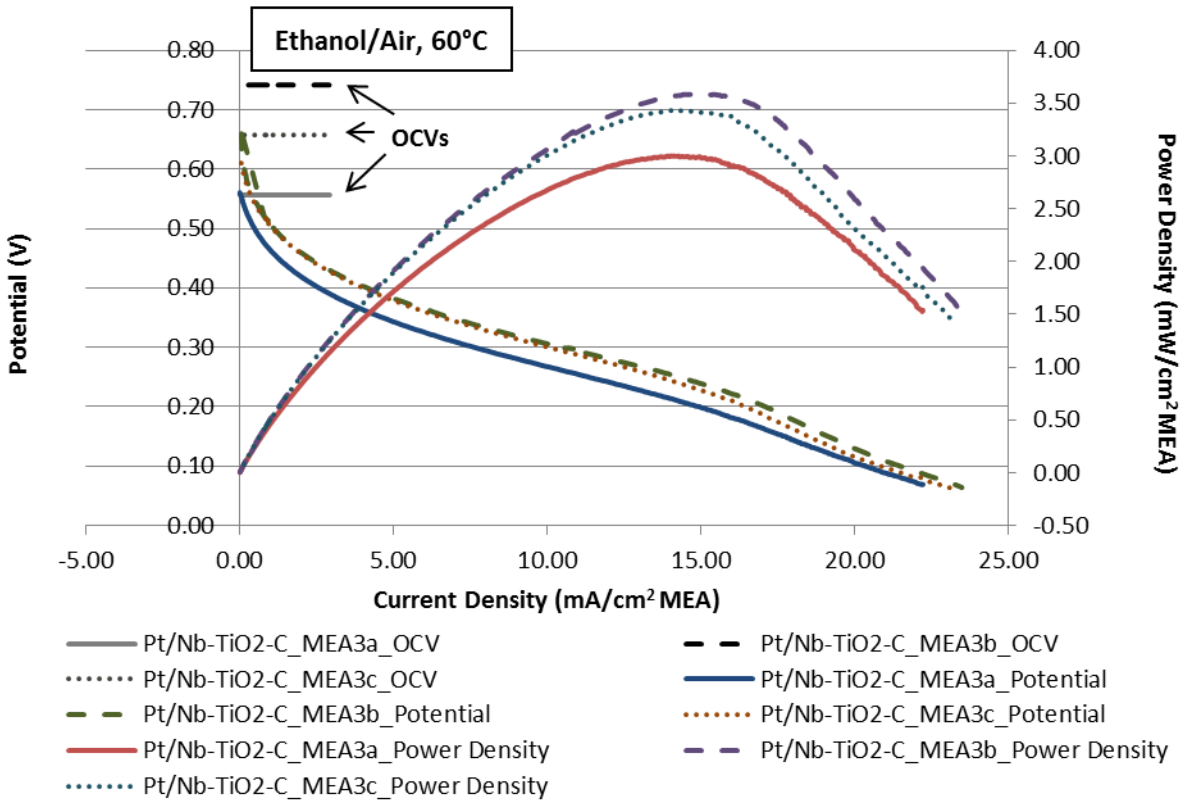

Figure 4-37. 0.1 M ethanol solution iR-corrected fuel cell performance on Pt/Nb-TiO2-C electrodes (MEA 3a, MEA 3b, MEA 3c); cell temperature = 60°C, dew pointc = 25°C, back pressure = 15 psig, air flow rate = 950 sccm, EtOH temperature = 60°C, EtOH flow rate = 8 mL/min, MEA 3a ASR = 0.780 Ωcm^2, MEA 3b ASR = 0.300 Ωcm^2, MEA 3c ASR = 0.650 Ωcm^2.

The OCVs were for 0.58 V (MEA 3a), 0.68 V (MEA 3b), and 0.70 V (MEA 3c) at room temperature and 0.56 V (MEA 3a), 0.74 V (MEA 3b), and 0.66 V (MEA 3c) at 60° C. The current density peaked between 6.0 – 7.1 mA/cm^2 MEA active area for the MEAs during the room temperature test. At 60°C, the maximum current density increased to about 23 mA/cm^2 MEA active area for all of the Pt/Nb-TiO_2-C MEAs. The power densities produced by the Pt/Nb-TiO_2-C MEAs were lower than those seen on Pt/C and PtSn/C MEAs due to the low currents produced, which is partly due to the low

EASA measured on the Pt/Nb-TiO_2-C MEAs. The power density peaked at 0.839, 0.935, and 1.06 mW/cm^2 MEA active area for MEA 3a, 3b, and 3c, respectively, at room temperature around 3.8 mA/cm^2 MEA active area. The peak power increased to 3.0, 3.6, and 3.4 mW/cm^2 MEA active area near 15 mA/cm^2 MEA active area for MEA 3a, 3b, and 3c, respectively, at 60°C. *The similar performances among the three Pt/Nb-TiO_2-C MEAs with known Pt loadings demonstrate that reproducible results can be achieved with this catalyst by the sample preparation and test methods used for the other catalysts in this investigation. The peak current densities and power densities achieved by the Pt/Nb-TiO_2-C MEAs, based on the 5 cm^2 MEA active area, are lower than those seen with Pt/C and PtSn/C MEAs.*

4.4. Catalyst Comparison

In the following sections, the results of the electrochemical and performance tests are compared among the three catalysts investigated. A Pt/Nb-TiO_2-C catalyst was tested in hopes that the catalyst would perform equally as well, or better, than a Pt/C catalyst since the TiO_2 is more resistant to corrosion than the commonly used carbon support. It was also thought that the TiO_2 could assist in providing sites for OH_{ad}, similar to Sn, and therefore help increase catalytic activity toward ethanol oxidation. The results of the Pt/Nb-TiO_2-C catalyst are compared to those of Pt/C and

PtSn/C catalysts, both of which have been examined as catalysts for ethanol oxidation in the literature. For the fuel cell performance comparison, the results are normalized based on the Pt active area rather than the MEA active area since the electrochemically active surface area varied greatly among the three catalysts.

4.4.1. Electrochemically Active Surface Area for Various Thin Film Electrodes

Table 4-7 lists the average thin film properties for the three catalysts examined. Pt/C thin film electrodes had, on average, the highest EASA. It was expected that PtSn/C electrodes would have a slightly lower EASA than the Pt/C thin film electrodes based on reports in the literature [18], though the values are very close to that seen with a Pt/C electrode. The average EASA of a Pt/Nb-TiO_2-C thin film electrode was lower than that of a Pt/C electrode by more than a factor of 3. The double layer charge for the Pt/Nb-TiO_2-C thin film electrode was also quite low, which indicated that the conductivity through the Pt/Nb-TiO_2-C thin film was lower than that through the other catalyst thin films. As noted previously, in the absence of a carbon matrix, the Pt/Nb-TiO_2 catalyst had an even lower active area. The Nb was added to the TiO_2 (which is non-conductive) by the procedure described earlier (see Section 3.1) in an effort to establish sufficient conductivity for use in electrodes, though clearly the Nb by itself did not provide sufficient conductivity enhancement. *The addition of 10 wt% carbon provided*

sufficient conductivity to allow preparation of high surface area electrodes but still not enough conductivity to achieve EASAs comparable to those achieved with common carbon supported catalysts.

Table 4-7. Average properties of each thin film electrode.

Catalyst	Pt/C	PtSn/C	Pt/Nb-TiO_2-C
Pt Loading [mg Pt/cm^2 electrode]	0.06	0.06	0.06
CdI [C]	6.49E-04	5.77E-04	1.73E-04
H^+ Adsorption Charge [C]	1.07E-03	1.17E-03	3.79E-04
Specific EASA [cm^2 Pt/mg Pt]	460	450	146
EASA [cm^2 Pt]	5.7	5.5	1.8

4.4.2. SDCV Tests for Ethanol Oxidation for Various Thin Film Electrodes

The SDCV results for each catalyst are compared at the 10 mV/s scan rate in each ethanol concentration. The current densities in each figure were normalized to the thin film effective surface area, as was done in the previous SDCV plots. In 0.01 M ethanol solution (Figure 4-38), the earliest onset of ethanol oxidation was seen on the PtSn/C electrode during the forward scan, and on both the PtSn/C and Pt/Nb-TiO_2-C electrodes during the negative scan. The earlier onset of oxidation indicated that either poisoning of the catalyst surface was decreased (for the PtSn/C electrode on the forward scan) or that any intermediate species that were blocking the catalyst surface

were removed sooner (for both of the scans on the PtSn/C electrode, as well as the Pt/Nb-TiO_2-C electrodes on the reverse scan). A shoulder around 0.6 V on the forward scan, presumably due to CO_2 formation, was apparent but only on the PtSn/C electrode CV. The peak current densities are highest for the PtSn/C catalyst and lowest for the Pt/Nb-TiO_2-C catalyst. Higher current densities can be attributed to increased reaction kinetics (increased rate of ethanol oxidation) and/or more complete ethanol oxidation (formation of products that result in a larger number of electrons transferred per mole of ethanol), both of which lead to a higher number of total electrons transferred and a larger current output. Higher current densities on a PtSn/C electrode over a Pt/C electrode were also achieved by Jiang *et al.* [18] during a room temperature 10 mV/s sweep in a solution of 0.01 M ethanol and 0.5 M H_2SO_4.

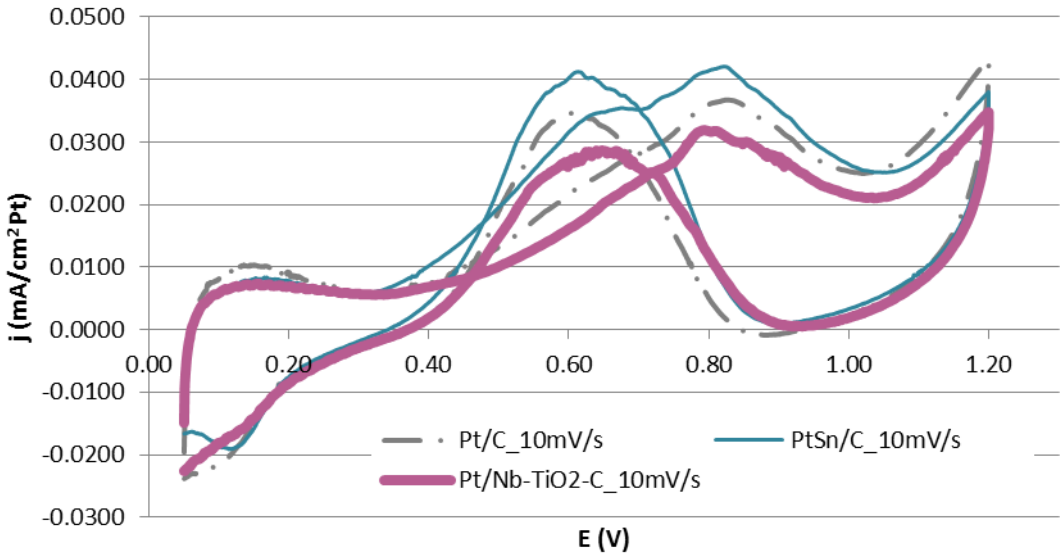

Figure 4-38. SDCV 10 mV/s sweeps in 0.01 M ethanol solution for each catalyst.

In 0.1 M ethanol solution (Figure 4-39), the highest current densities were recorded using the PtSn/C electrode, but the Pt/Nb-TiO_2-C catalyst had the next highest peak current (on the reverse scan). While the forward scan peak on the Pt/Nb-TiO_2-C catalyst CV just barely surpassed the peak value recorded on a Pt/C catalyst, the reverse scan peak was definitively higher on the Pt/Nb-TiO_2-C electrode CV, which is consistent with the observation in the 0.01 M ethanol solution sweep, where the Pt/Nb-TiO_2-C catalyst was clear of blocking species earlier in the reverse scan.

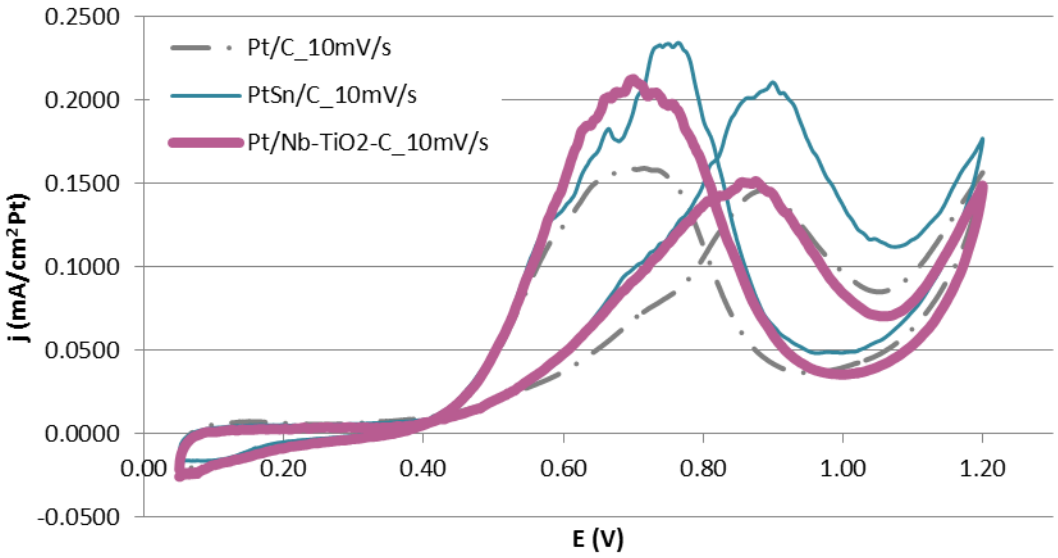

Figure 4-39. SDCV 10 mV/s sweeps in 0.1 M ethanol solution for each catalyst.

The last SDCV plot (Figure 4-40) contains data from tests in 1.0 M ethanol solution. Interestingly, the Pt/C thin film electrode CV resulted in the highest current densities, followed by the PtSn/C thin film electrode CV. It has been shown that acetaldehyde is the primary product in ethanol concentration solutions greater than 0.2 M [15], which may form more easily on a Pt/C catalyst rather than a PtSn/C catalyst. It is also noted that the forward and reverse peaks occur at different potentials for each of the catalysts. *Overall, the shape of the SDCVs is similar for all three catalysts at all three ethanol concentrations, indicating similar ethanol oxidation reaction mechanisms on all of the catalysts. While the PtSn/C thin film electrode results in the highest current densities in the solutions with lower ethanol concentration, the Pt/C electrode outperforms the other catalysts in 1.0 M ethanol solution. As the concentration of ethanol increases, the potentials at which the oxidation peaks occur begin to vary among the catalysts, with peak current densities occurring at different voltages for each of the catalyst in 1.0 M ethanol solution.*

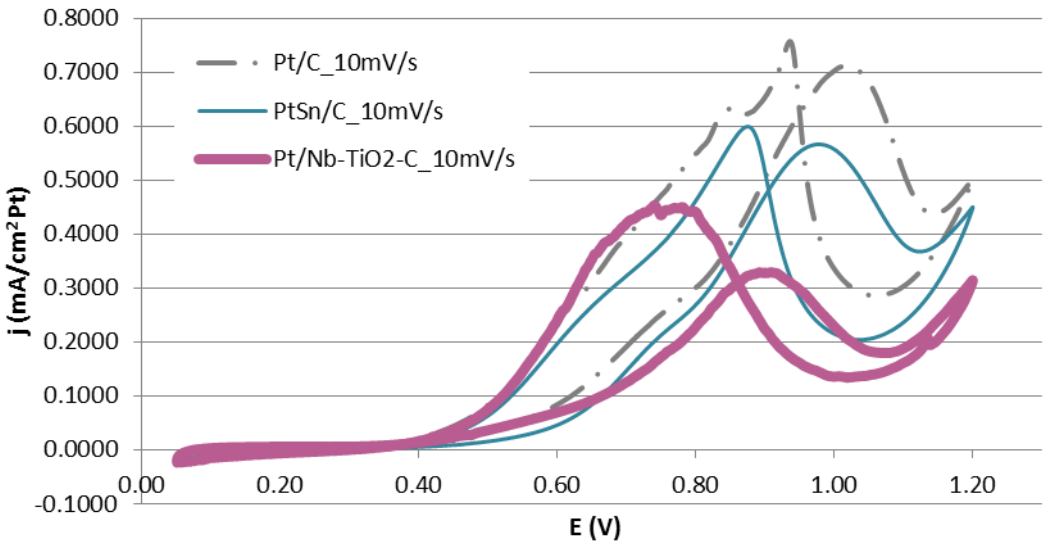

Figure 4-40. SDCV 10 mV/s sweeps in 1.0 M ethanol solution for each catalyst.

4.4.3. SDPS Tests for Ethanol Oxidation on Various Thin Film Electrodes

The results of the SDPS tests for all three catalysts are compared in various ethanol solutions in Figure 4-41, Figure 4-42, and Figure 4-43, with the steady-state current density for each catalyst displayed to the right of the plot. The current density was higher in the 9-second range plotted for the PtSn/C catalyst in 0.01 M ethanol solution, though in 0.1 M and 1.0 M ethanol solutions, both the PtSn/C catalyst and Pt/Nb-TiO_2-C catalyst results produced similar currents, which were higher than those produced on the Pt/C catalyst.

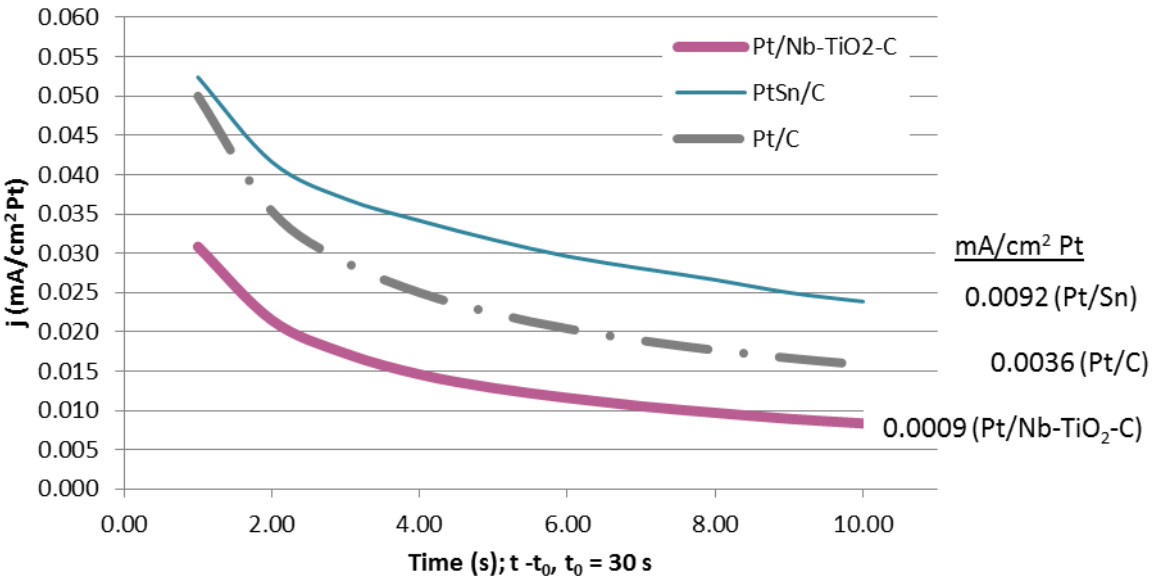

Figure 4-41. SDPS test results for all three catalysts in 0.01 M ethanol solution.

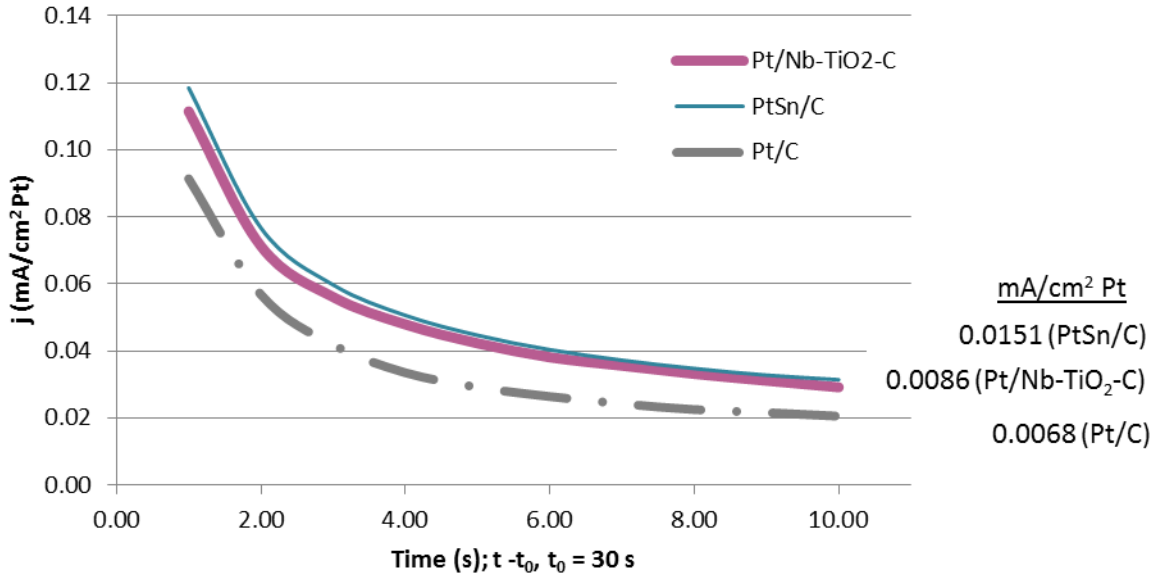

Figure 4-42. SDPS test results for all three catalysts in 0.1 M ethanol solution.

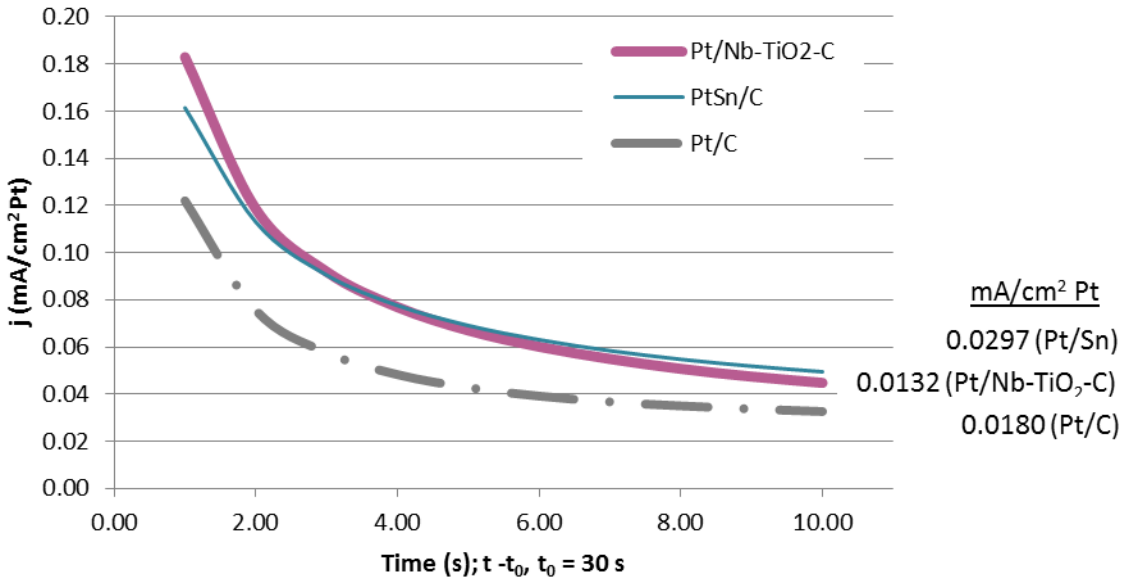

Figure 4-43. SDPS test results for all three catalysts in 1.0 M ethanol solution.

The exponents from the power law curves that were fit to the data and discussed in previous sections are compared in Table 4-8. The current density decreased at the slowest rate (indicating greater resistance to catalyst layer poisoning) on a PtSn/C thin film electrode in both 0.01 M and 1.0 M ethanol solutions. While the catalyst layer poisoning was most pronounced on a Pt/Nb-TiO_2-C thin film electrode in 0.01 M and 1.0 M ethanol solutions, the slowest rate of poisoning (lowest value of b) occurred on this electrode in 0.1 M ethanol solution. The catalyst layer poisoning was always lower on a PtSn/C electrode than on a Pt/C electrode at all ethanol concentrations tested. *Based on these experiments, a Pt/C electrode results in the lowest initial current density in all three ethanol concentrations. The use of a Pt/C electrode leads to the highest rate of*

catalyst poisoning in the 0.1 M ethanol concentration solution, whereas a Pt/Nb-TiO_2-C electrode has the highest rate of poisoning in 0.01 M and 1.0 M ethanol solutions.

Table 4-8. Exponents from the power law fits to the SDPS test results.

Ethanol Concentration	Pt/C Exponents	PtSn/C Exponents	Pt/Nb-TiO_2-C Exponents
0.01 M	-0.454	-0.334	-0.567
0.1 M	-0.657	-0.578	-0.573
1.0 M	-0.573	-0.517	-0.612

4.4.4. Evaluation of Various Catalysts for Ethanol Oxidation in a DEFC

Properties of the MEAs determined from the EASA measurements are listed in Table 4-9. The EASA was largest for the Pt/C MEAs and about equal on the PtSn/C and Pt/Nb-TiO_2-C MEAs. The double layer capacitance region was smallest for the Pt/Nb-TiO_2-C MEAs (3a, 3b, and 3c) and MEA 3b had the lowest hydrogen adsorption charge.

Table 4-9. MEA EASA results.

Catalyst	Pt/C		PtSn/C		Pt/Nb-TiO_2-C		
MEA	1a	1b	2a	2b	3a	3b	3c
Anode Loading [mg Pt/cm^2 MEA]	2.1	2.1	1.8	1.7	1.5	1.4	1.7
C_{dl} [C]	6.9E-01	5.5E-01	5.7E-01	6.5E-01	6.6E-02	1.2E-01	5.5E-02
H^+ Adsorption Charge [C]	6.4E-01	6.3E-01	2.4E-01	1.9E-01	2.3E-01	1.8E-01	1.9E-01
Specific EASA [cm^2 Pt/mg Pt]	290	280	130	100	140	120	110
EASA [cm^2 Pt]	3.0E03	3.0E03	1.1E03	9.1E02	1.1E03	8.7E02	9.1E02

The ethanol fuel cell performance for each of the MEAs tested is shown in Figure 4-44 and Figure 4-45, at 25°C and 60°C, respectively. The current was normalized to the EASA of the MEA tested so the fuel cell performance could be compared for each of the catalysts based on the measured catalyst active area, which was very different for each of the three catalysts.

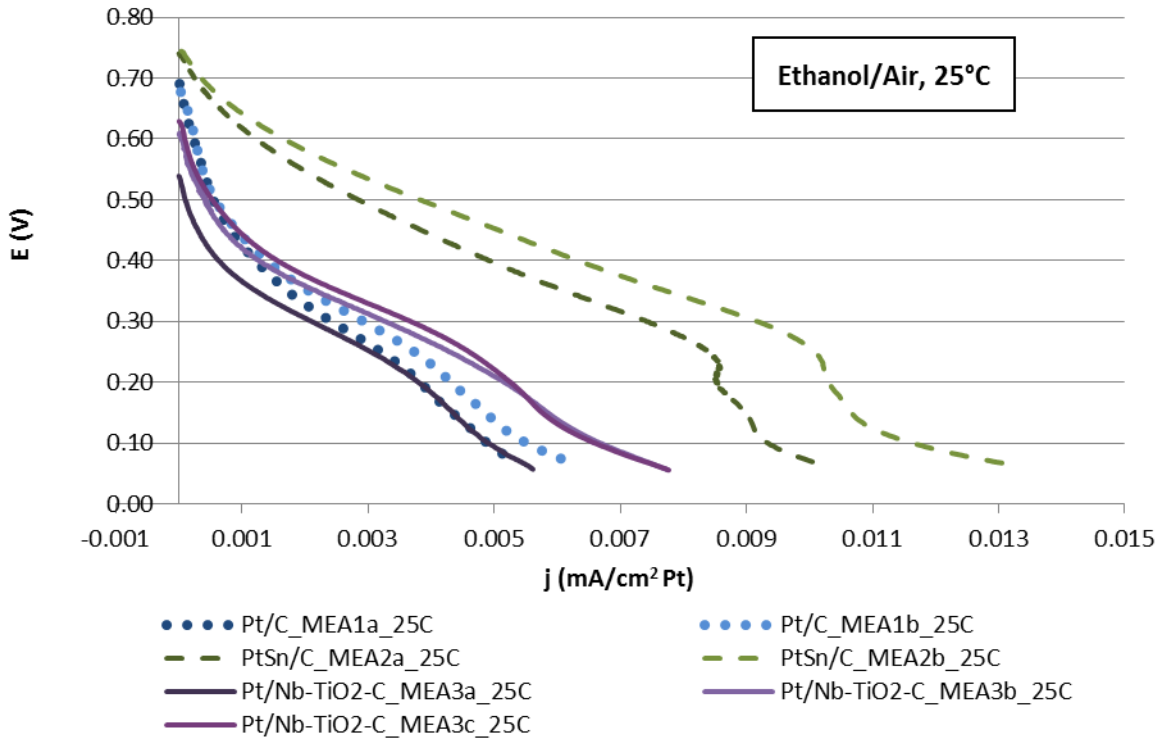

Figure 4-44. 0.1 M ethanol solution fuel cell performance comparing all MEAs; cell temperature = 25°C, dew pointc = 25°C, back pressure = 15 psig, air flow rate = 950 sccm, EtOH temperature = 25°C, EtOH flow rate = 8 mL/min.

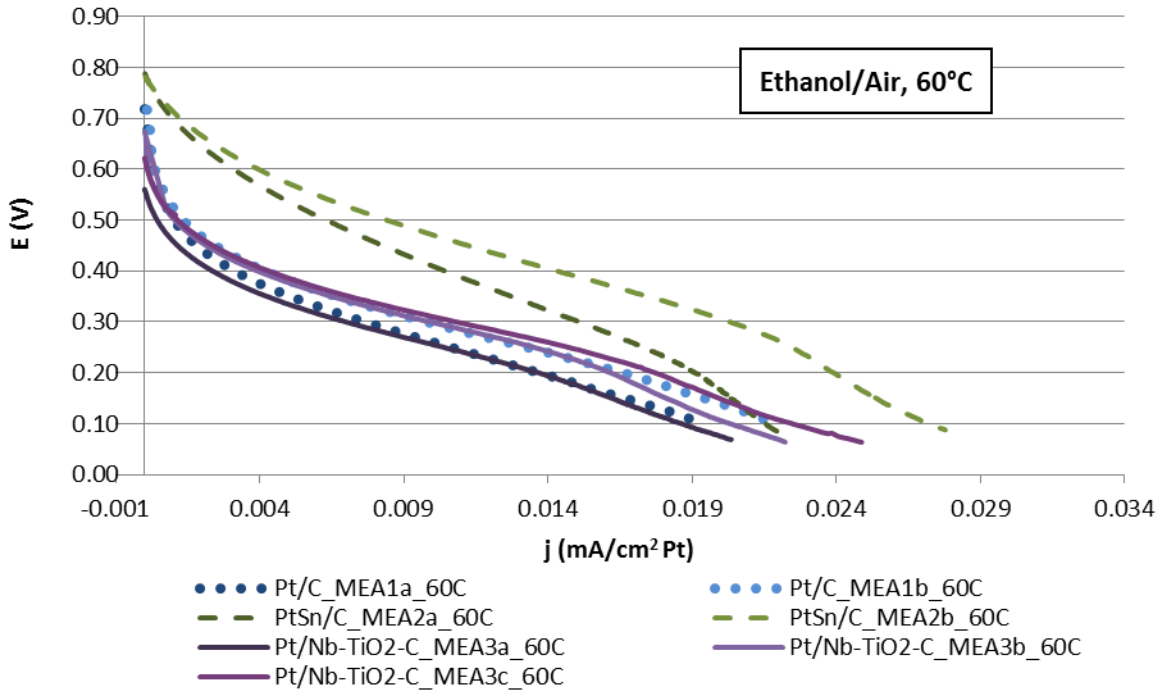

Figure 4-45. 0.1 M ethanol solution fuel cell performance comparing all MEAs; cell temperature = 60°C, dew point$_c$ = 25°C, back pressure = 15 psig, air flow rate = 950 sccm, EtOH temperature = 60°C, EtOH flow rate = 8 mL/min.

At room temperature, the PtSn/C MEAs had the highest OCVs, followed by Pt/C, and lastly Pt/Nb-TiO_2-C. The PtSn/C MEAs also had the maximum current density, with two of the Pt/Nb-TiO_2-C MEAs (3b and 3c) having the next highest maximum current density over the Pt/C MEAs. The other Pt/Nb-TiO_2-C MEA (3a) reached a maximum current density similar to that reached by the Pt/C MEAs. At 60°C, the OCVs for all of the MEAs increased slightly. The maximum current densities were also higher. The highest current density (about 0.028 mA/cm^2 Pt) occurred when the PtSn/C MEA 2b was used, though a Pt/Nb-TiO_2-C MEA (MEA 3c) reached the 2nd highest current

density of 0.025 mA/cm^2 Pt. The other Pt/Nb-TiO_2-C MEAs (3a and 3b) reached similar current densities as the Pt/C MEAs and the PtSn/C MEA 2a. The shape of the IV curves of the Pt/Nb-TiO2-C MEAs matched that of the Pt/C MEAs over the range of current densities measured.

The peak power densities (max, min, and mean values) calculated from the ethanol/air polarization curves just discussed are plotted on a Pt active area basis in Figure 4-46 and Figure 4-47 at 25°C and 60°C, respectively. The PtSn/C MEAs had the largest peak power density values at both temperatures. The Pt/Nb-TiO_2-C MEAs resulted in an average peak power density slightly higher than that of the Pt/C MEAs at both temperatures. The Pt/C MEAs had the lowest peak power density values at both temperatures.

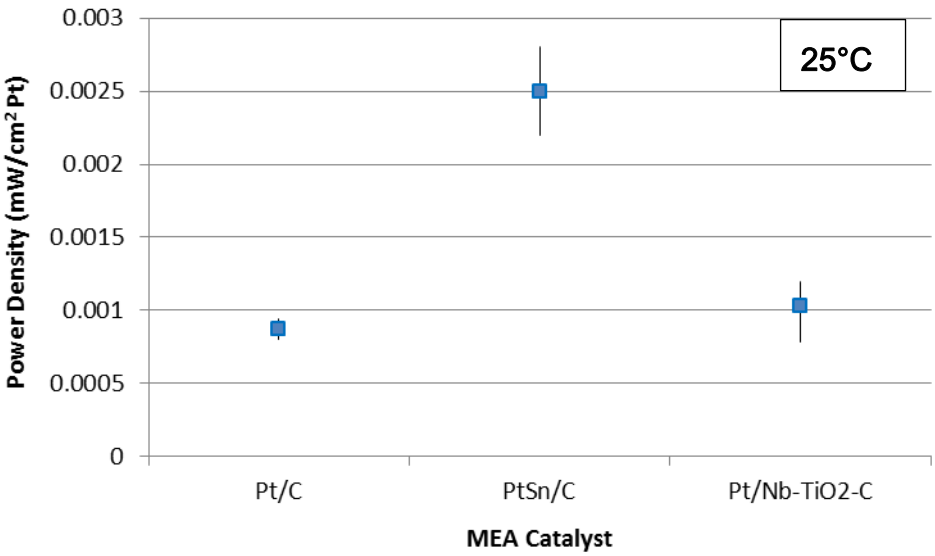

Figure 4-46. Max, min, and mean power densities per Pt active area for each catalyst at 25°C.

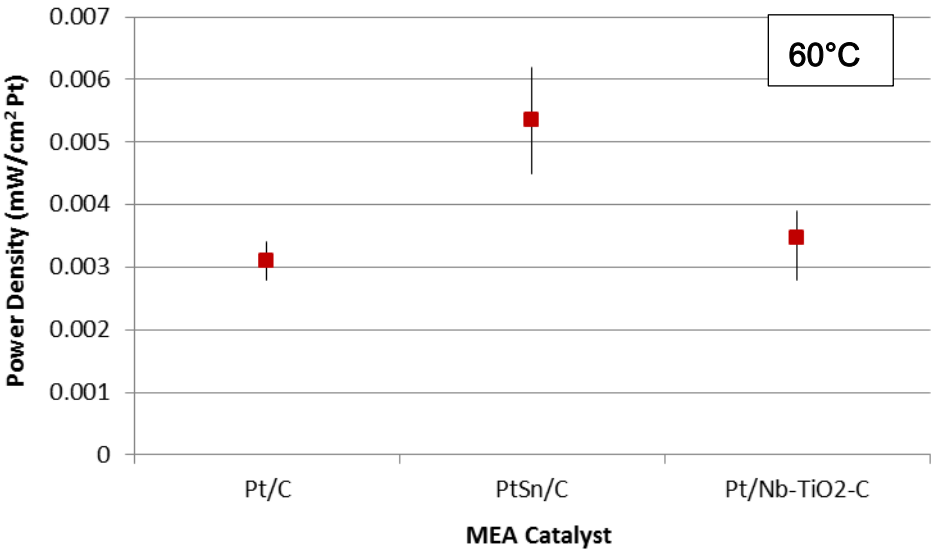

Figure 4-47. Max, min, and mean power densities per Pt active area for each catalyst at 60°C.

Figure 4-48 and Figure 4-49 display the max, min, and average peak power density values based on the MEA active area so that the results can be compared to performances reported in the literature (see Table 2-1). At 25°C, the Pt/C MEAs reached the highest average power density, though the PtSn/C catalyst just barely achieved the best performance at 60°C. At both temperatures, the Pt/Nb-TiO_2-C MEAs produced the least amount of power based on the MEA active area. *The Pt/Nb-TiO_2-C catalyst resulted in the lowest peak power densities based on the MEA active area but, on average, exhibited somewhat better performance than the Pt/C catalyst based on the active area of Pt. The Pt/Nb-TiO_2-C catalyst was consistently outperformed by the PtSn/C catalyst.*

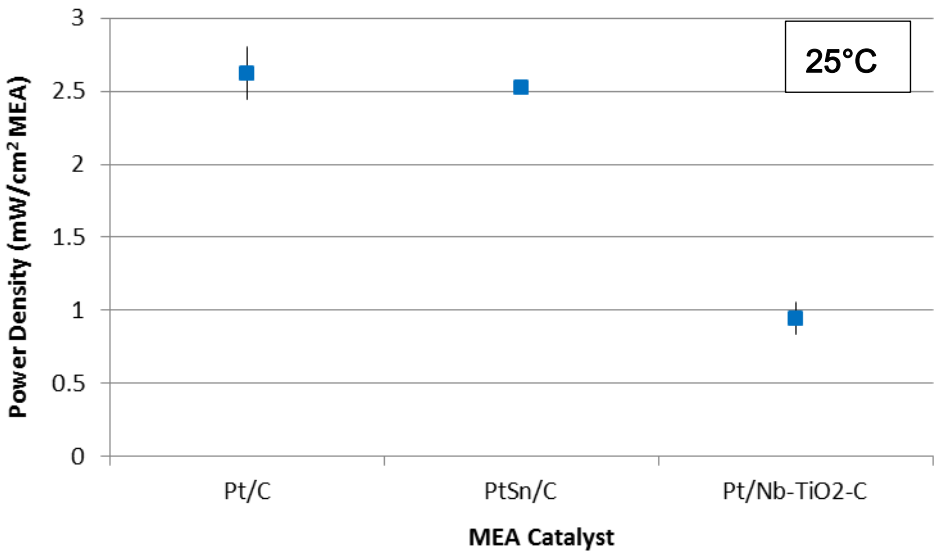

Figure 4-48. Max, min, and mean power densities per MEA active area for each catalyst at 25°C.

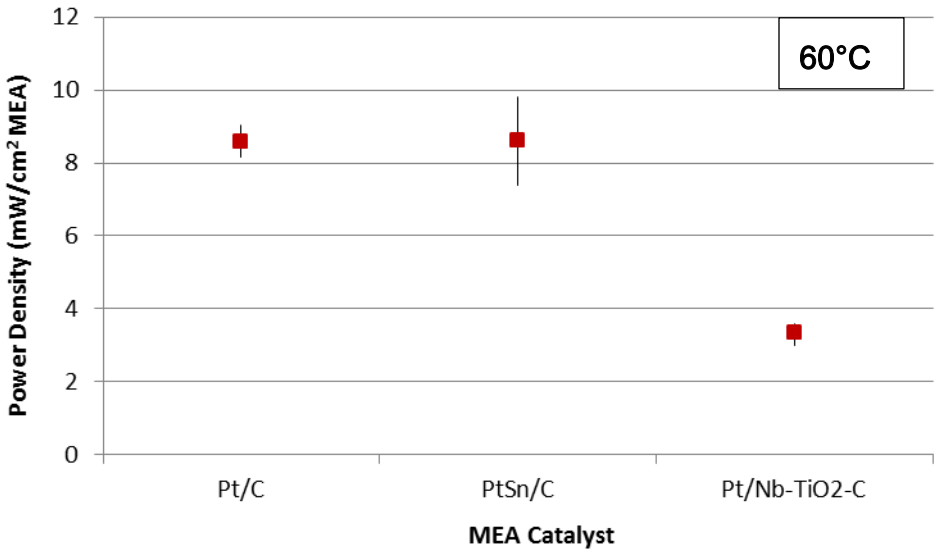

Figure 4-49. Max, min, and mean power densities per MEA active area for each catalyst at 60°C.

5. CONCLUSIONS

The ethanol oxidation reaction was investigated on three catalysts using multiple electrochemical tests in various ethanol concentration solutions. The results from these experiments gave some insight into the ethanol oxidation reaction on a Pt/Nb-TiO_2-C and allowed comparison of the catalytic activity on this novel catalyst to that of two common catalysts, Pt/C and PtSn/C. The performance of the three catalysts in a direct ethanol fuel cell (DEFC) was also examined and a comparison between the catalysts led to some promising results. Overall, three main conclusions can be drawn from this work.

Nb-TiO_2-C was shown to be a feasible support for Pt catalysts used for ethanol oxidation. Even though the electrochemically active surface area (EASA) of the Pt/Nb-TiO_2-C thin film electrode was low, the Pt/Nb-TiO_2-C electrode stationary disc cyclic voltammetry (SDCV) results were on par with those of the other two electrodes once the current was normalized based on effective surface area. All three of the electrodes had SDCVs that were similar in shape, with two main ethanol oxidation peaks (one on the forward scan and one on the reverse scan) and a slight shoulder due to CO_2 formation that was visible at higher potential scan rates. During the fuel cell performance tests, the Pt/Nb-TiO_2-C MEAs had EASAs comparable to that of the PtSn/C membrane electrode assemblies (MEAs). The shape of the polarization curve for the novel catalyst was also similar to that of DEFC polarization curves for other common catalysts.

Oxidation of ethanol on Pt supported by Nb-TiO_2-C was not significantly different than oxidation on Pt when supported by carbon. The peak current densities in 0.01 M and 0.1 M ethanol solutions were comparable or better on the Pt/Nb-TiO_2-C electrode as compared to the Pt/C electrode. In 1.0 M ethanol solution, the catalytic activity on the Pt/C thin film electrode was higher than that of both the PtSn/C and the Pt/Nb-TiO_2-C electrodes, which was surprising. This could be attributed to the fact that acetaldehyde has been observed as the main product formed in ethanol concentrations greater than 0.2 M on a Pt/C electrode [15]. This may partially be due to the decrease in acetaldehyde formation seen on PtSn/C catalysts compared to Pt/C catalysts [13, 31]. It has also been discussed that adding Sn and TiO_2 to the Pt catalysts can increase the number of sites available for OH_{ad}, which assists in clearing the Pt sites of CO_{ad} by further oxidizing the CO_{ad} to CO_2 [5, 9, 30, 32, 39]. If the C-C bond in acetaldehyde is not broken, CH_{ad}, and therefore CO_{ad}, are not formed and the benefit of the OH_{ad} sites is not seen.

In the fuel cell performance tests, the Pt/Nb-TiO_2-C MEAs had comparable performance (based on the Pt active area) to that of the Pt/C MEAs at room temperature and 60°C, with MEAs 3b and 3c reaching higher current densities. At 60° C, Pt/Nb-TiO_2-C MEAs 3b and 3c reached maximum current densities near those of the PtSn/C MEAs. The peak power densities at both 25°C and 60°C for the Pt/Nb-TiO_2-C

MEAs were at least comparable to that of the Pt/C MEAs (based on the Pt active area), though lower than those of the PtSn/C MEAs. It was noted that the addition of TiO_2 did not increase the open circuit voltage (OCV), EASA, or cell performance compared to that of the Pt/C catalyst as has been discussed in the literature [40].

Pt/Nb-TiO_2-C showed low specific activity and most likely requires improved conductivity. The double layer capacitance region and effective surface area of the Pt/Nb-TiO_2-C thin film electrode were much lower than those of the Pt/C and PtSn/C electrodes. The EASAs of the Pt/Nb-TiO_2-C MEAs were similar to those of the PtSn/C MEAs, but much lower than those of the Pt/C MEAs. The double layer capacitance region for the novel catalyst was also much lower than that for both the Pt/C and PtSn/C MEAs, suggesting lower electron conductivity for the Pt/Nb-TiO_2-C catalyst. An increase in the conductivity through the TiO_2 supported catalyst could lead to an increase in EASA and fuel cell performance.

Future work could lead to the development of a TiO_2 supported Pt catalyst with an improved performance over that of a Pt/C catalyst. Further investigation into the preparation of TiO_2 could lead to a support that is more electrically conductive than the one used in this work. It may be necessary to mix the TiO_2 support with other elements, as was attempted here with Nb, to reach an acceptable level of conductivity. Variations in the preparation procedure of the support and in the pairing of catalysts could also lead to an increase in catalytic activity if the oxides can assist in adsorbing OH and

freeing the Pt of CO_{ad}. Kim *et al*. [38] reported encouraging results when they paired a PtRu/C catalyst with Au/TiO_2. They saw an increase in the catalytic activity with the addition of the Au/TiO_2, though they commented on the fact that Au and TiO_2 are not active for CO oxidation when each is used separately.

Another recommendation would be to support a bimetallic catalyst, such as PtSn, which, when supported with carbon, has been reported to be one of the top choices of bimetallic catalysts for ethanol oxidation [3, 30, 31]. It would be interesting to see if the change in catalyst support affects the ethanol oxidation reaction on this bimetallic catalyst and whether or not the performance is comparable to that seen by PtSn/C catalysts. If both the Sn and TiO_2 can provide OH_{ad} sites and assist in further oxidizing CO_{ad} to CO_2, the performance of the TiO_2 supported PtSn catalyst may be improved over that of the carbon supported catalyst.

In summary, the results of the Pt/Nb-TiO_2-C catalyst, in both the electrochemical tests and the DEFC experiments, were very promising. Overall, the performance of the Pt/Nb-TiO_2-C catalyst appeared to be at least as good as that of the Pt/C catalyst based on the area of Pt available. A catalyst that is not supported on carbon, which is susceptible to corrosion and degradation in the fuel cell, could lead to greater durability and an extended lifetime of the catalyst layer, and therefore fuel cell as a whole. Further investigation into increasing the conductivity and specific EASA of the Pt/Nb-TiO_2-C catalyst could lead to increased performance in a DEFC.

6. REFERENCES

1. (January/February 2003) *Fuel for thought on cars of the future*. Scientific Computing World.
2. Lai, S.C.S., et al., *Effects of electrolyte pH and composition on the ethanol electro-oxidation reaction.* Catalysis Today, 2010. **154**(1-2): p. 92-104.
3. Lamy, C., et al., *Recent progress in the direct ethanol fuel cell: development of new platinum-tin electrocatalysts.* Electrochimica Acta, 2004. **49**: p. 3901-3908.
4. Li, Y.S., T.S. Zhao, and Z.X. Liang, *Performance of alkaline electrolyt-membrane-based direct ethanol fuel cells.* Journal of Power Sources, 2009. **187**: p. 387-392.
5. Mann, J., N. Yao, and A.B. Bocarsly, *Characterization and analysis of new catalysts for a direct ethanol fuel cell.* Langmuir, 2006. **22**: p. 10432-10436.
6. Rao, V., et al., *Electro-oxidation of ethanol at gas diffusion electrodes a DEMS study.* Journal of the Electrochemical Society, 2007. **154**(11): p. B1138-B1147.
7. Wang, J., S. Wasmus, and R.F. Savinell, *Evaluation of ethanol, 1-propanol, and 2-propanol in a direct oxidation polymer-electrolyte fuel cell.* Journal of the Electrochemical Society, 1995. **142**(12): p. 4218-4224.
8. Kim, I., et al., *Catalytic reactions in direct ethanol fuel cells.* Angewandte Chemie International Edition, 2011. **50**(10): p. 2270-2274.
9. Zhou, W.J., et al., *Bi- and tri-metallic Pt-based anode catalysts for direct ethanol fuel cells.* Journal of Power Sources, 2004. **131**: p. 217-223.
10. An, L., et al., *A novel direct ethanol fuel cell with high power density.* Journal of Power Sources, 2011. **196**: p. 6219-6222.
11. Colmati, F., et al., *The role of the steps in the cleavage of the C-C bond during ethanol oxidation on platinum electrodes.* Physical Chemistry Chemical Physics, 2009. **11**(40): p. 9114-9123.
12. Ghumman, A., et al., *Online analysis of carbon dioxide from a direct ethanol fuel cell.* Journal of Power Sources, 2009. **194**(1): p. 286-290.

13. Rousseau, S., et al., *Direct ethanol fuel cell (DEFC): Electrical performances and reaction products distribution under operating conditions with different platinum-based anodes.* Journal of Power Sources, 2006. **158**(1): p. 18-24.
14. Song, S.Q., et al., *Direct ethanol PEM fuel cells: The case of platinum based anodes.* International Journal of Hydrogen Energy, 2005. **30**: p. 995-1001.
15. Camara, G.A. and T. Iwasita, *Parallel pathways of ethanol oxidation: The effect of ethanol concentration.* Journal of Electroanalytical Chemistry, 2005. **578**(2): p. 315-321.
16. Ghumman, A. and P.G. Pickup, *Efficient electrochemical oxidation of ethanol to carbon dioxide in a fuel cell at ambient temperature.* Journal of Power Sources, 2008. **179**: p. 280-285.
17. Sun, S., et al., *Ethanol electrooxidation on a carbon-supported Pt catalyst at elevated temperature and pressure: A high-temperature/high-pressure DEMS study.* Journal of Power Sources, 2009. **190**: p. 2-13.
18. Jiang, L., et al., *Ethanol electro-oxidation on Pt/C and PtSn/C catalysts in alkaline and acid solutions.* International Journal of Hydrogen Energy, 2010. **35**: p. 365-372.
19. Antolini, E. and E.R. Gonzalez, *Alkaline direct alcohol fuel cells.* Journal of Power Sources, 2010. **195**: p. 3431-3450.
20. Yu, E.H., U. Krewer, and K. Scott, *Principles and materials aspects of direct alkaline alcohol fuel cells.* Energies, 2010. **3**: p. 1499-1528.
21. Fujiwara, N., et al., *Direct ethanol fuel cells using an anion exchange membrane.* Journal of Power Sources, 2008. **185**(2): p. 621-626.
22. EG&G Technical Services, I., *Fuel Cell Handbook*. Seventh ed. 2004, Morgantown, WV.
23. Kongstein, O.E., et al., *Polymer electrolyte fuel cells based on phosphoric acid doped polybenzimidazole (PBI) membranes.* Energy, 2007. **32**: p. 418-422.
24. Vigier, F., et al., *Development of anode catalysts for a direct ethanol fuel cell.* Journal of Applied Electrochemistry, 2004. **34**: p. 439-446.

25. Willsau, J. and J. Heitbaum, *Elementary steps of ethanol oxidation on Pt in sulfuric acid as evidenced by isotope labelling.* Journal of Electroanalytical Chemistry, 1985. **194**: p. 27-35.
26. Andreadis, G., et al., *Direct ethanol fuel cells: The effect of the cell discharge current on the products distribution.* Applied Catalysis B-Environmental, 2010. **100**(1-2): p. 157-164.
27. Götz, M. and H. Wendt, *Binary and ternary anode catalyst formulations including the elements W, Sn and Mo for PEMFCs operated on methanol or reformate gas.* Electrochimica Acta, 1998. **43**(24): p. 3637-3644.
28. Gasteiger, H.A., N.M. Markovic, and P.N. Ross, *Electrooxidation of CO and H_2/CO mixtures on a well-characterized Pt_3Sn electrode surface.* Journal of Physical Chemistry, 1995. **99**(22): p. 8945-8949.
29. Li, G. and P. Pickup, *The promoting effect of Pb on carbon supported Pt and Pt/Ru catalysts for electro-oxidation of ethanol.* Electrochimica Acta, 2006. **52**: p. 1033-1037.
30. Zhou, W., et al., *Pt based anode catalysts for direct ethanol fuel cells.* Applied Catalysis B: Environmental, 2003. **46**: p. 273-285.
31. Antolini, E., *Catalysts for direct ethanol fuel cells.* Journal of Power Sources, 2007. **170**: p. 1-12.
32. Jiang, L., et al., *Structure and chemical composition of supported Pt-Sn electrocatalysts for ethanol oxidation.* Electrochimica Acta, 2005. **50**: p. 5384-5389.
33. Bianchini, C., et al., *Selective oxidation of ethanol to acetic acid in highly efficient polymer electrolyte membrane-direct ethanol fuel cells.* Electrochemistry Communications, 2009. **11**(5): p. 1077-1080.
34. Kim, D.S., E.F.A. Zeid, and Y.T. Kim, *Additive treatment effect of TiO_2 as supports for Pt-based electrocatalysts on oxygen reduction reaction activity.* Electrochimica Acta, 2010. **55**: p. 3628-3633.
35. Dowlapalli, M., et al., *Electrochemical oxidation resistance of carbonaceous materials.* ECS Transactions, 2006. **1**(8): p. 41.

36. Kangasniemi, K.H., D.A. Condit, and T.D. Jarvi, *Characterization of Vulcan electrochemically oxidized under simulated PEM fuel cell conditions.* Journal of the Electrochemical Society, 2004. **151**.
37. Xu, F., et al., *Investigation of the carbon corrosion process for polymer electrolyte fuel cells using a rotating disk electrode technique.* Journal of the Electrochemical Society, 2010. **157**(8): p. B1138-B1145.
38. Kim, H.-J., et al., *PtRu/C-Au/TiO_2 electrocatalyst for a direct methanol fuel cell.* Journal of Power Sources, 2006. **159**: p. 484-490.
39. Shim, J., et al., *Electrochemical characteristics of Pt-WO_3 and Pt-TiO_2/C electrocatalysts in a polymer electrolyte fuel cell.* Journal of Power Sources, 2001. **102**(1-2): p. 172-177.
40. Xiong, L. and A. Manthiram, *Synthesis and characterization of methanol tolerant Pt/TiO_x/C nanocomposites for oxygen reduction in direct methanol fuel cells.* Electrochimica Acta, 2004. **49**(24): p. 4163-4170.
41. Sheppard, L.R., T. Bak, and J. Nowotny, *Electrical properties of niobium-doped titanium dioxide. 1. Defect disorder.* Journal of Physical Chemistry B, 2006. **110**: p. 22447-22454.
42. Kissinger, P.T. and W.R. Heineman, *Cyclic voltammetry.* Journal of Chemical Education, 1983. **60**: p. 702-706.
43. *Electrochemistry fundamentals*. [cited 2011 September 23, 2011]; Available from: http://www.cheng.cam.ac.uk/research/groups/electrochem/teaching.html.
44. Higuchi, E., H. Uchida, and M. Watanabe, *Effect of loading level in platinum-dispersed carbon black electrocatalysts on oxygen reduction activity evaluated by rotating disk electrode.* Journal of Electroanalytical Chemistry, 2005. **583**: p. 69-76.
45. Hou, J., *Nb-doped TiO_2 supported Pt catalyst preparation*. 2012: Blacksburg.
46. Cooper, K.R., et al., *Experimental methods and data analyses for polymer electrolyte fuel cells*. 2005: Scribner Associates, Inc.
47. *PEM fuel cell durability*. [cited 2012; Available from: http://www.me.sc.edu/fs/chao/pem_fuel_cell.htm.

48. Gloaguen, F., J.-M. Leger, and C. Lamy, *Electrocatalytic oxidation of methanol on platinum nanoparticles electrodeposited onto porous carbon substrates.* Journal of Applied Electrochemistry, 1997. **27**: p. 1052-1060.
49. Kinoshita, K. and P. Stonehart, *Preparation and characterization of highly dispersed electrocatalytic materials*, in *Modern Aspects of Electrochemistry*, J.O.M. Bockris and B.E. Conway, Editors. 1977, Plenum Press: New York, NY. p. 183-266.
50. Lai, S.C.S., et al., *Effects of electrolyte pH and composition on the ethanol electro-oxidation reaction.* Catalysis Today, 2010. **154**: p. 92-104.
51. Wang, H., Z. Jusys, and R.J. Behm, *Ethanol electro-oxidation on carbon-supported Pt, PtRu and Pt3Sn catalysts: A quantitative DEMS study.* Journal of Power Sources, 2006. **154**(2): p. 351-359.
52. Bard, A.J. and L.R. Faulkner, *Electrochemical methods: fundamentals and applications*. 2nd ed. 2001: Wiley & Sons, Inc.
53. Harris, K.R., P.J. Newitt, and Z.J. Derlacki, *Alcohol tracer diffusion, density, NMR and FTIR studies of aqueous ethanol and 2,2,2-trifluoroethanol solutions at 25°C.* Journal of the Chemical Society, Faraday Transactions, 1998. **94**(14): p. 1963-1970.
54. Dizechi, M. and E. Marschall, *Viscosity of some binary and ternary liquid mixtures.* Journal of Chemical and Engineering Data, 1982. **27**(3): p. 358-363.
55. Siegel, N.P., *Development and validation of a computational model for a proton exchange membrane fuel cell*. 2003, Virginia Tech: Blacksburg.

7. APPENDIX A

7.1. Stationary Disc Cyclic Voltammetry Results

PtSn/C

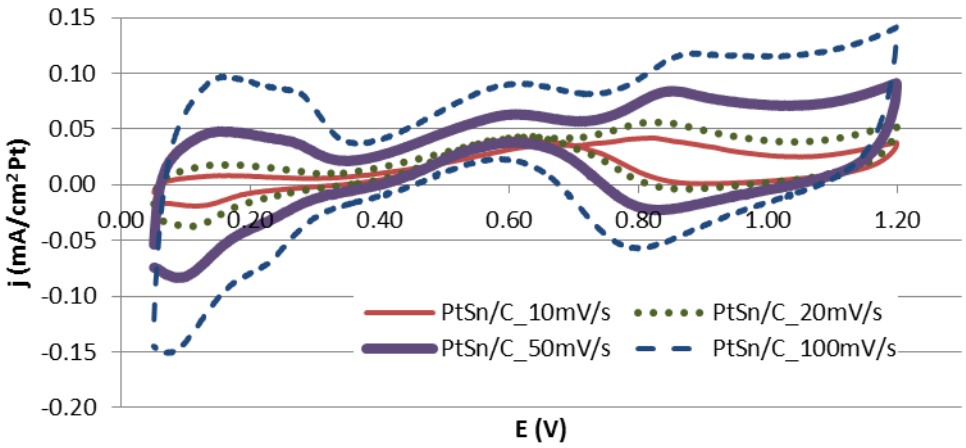

Figure 7-1. SDCV sweeps on a PtSn/C electrode in 0.01 M ethanol solution.

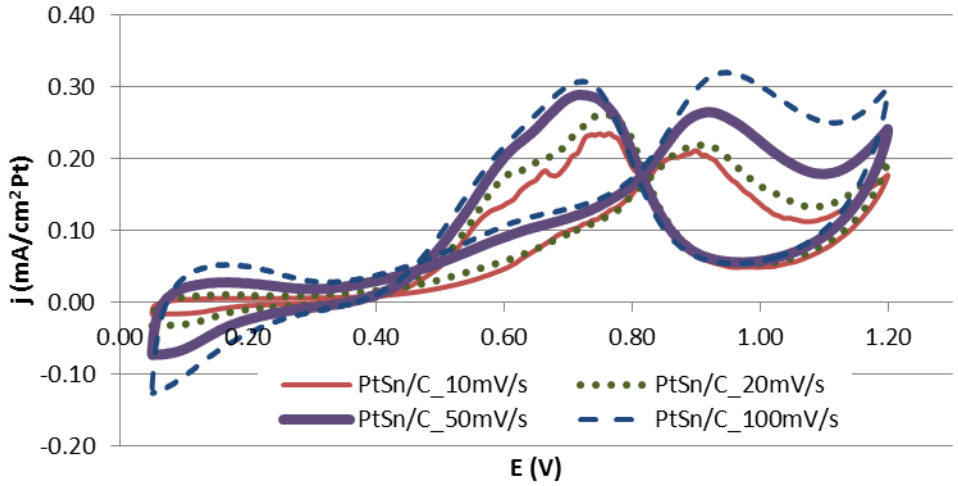

Figure 7-2. SDCV sweeps on a PtSn/C electrode in 0.1 M ethanol solution.

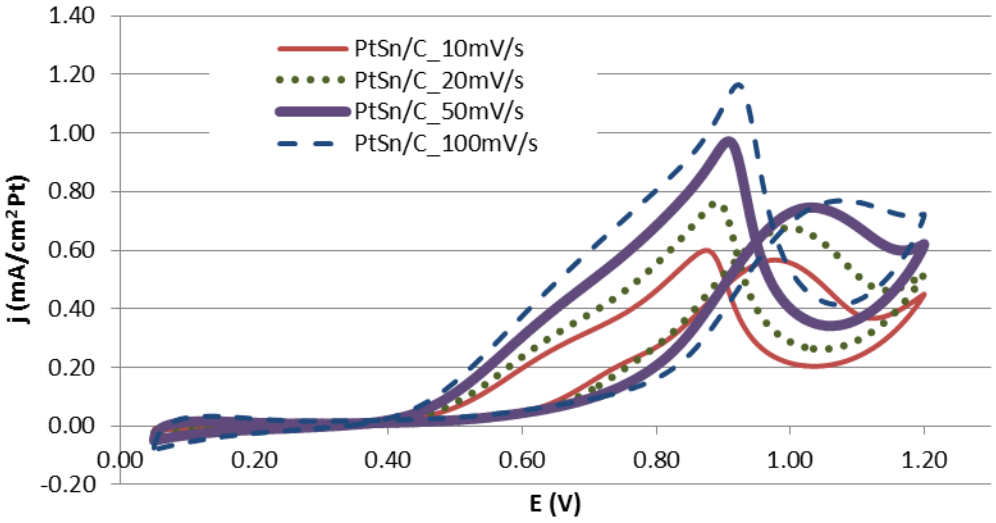

Figure 7-3. SDCV sweeps on a PtSn/C electrode in 1.0 M ethanol solution.

Pt/Nb-TiO_2-C

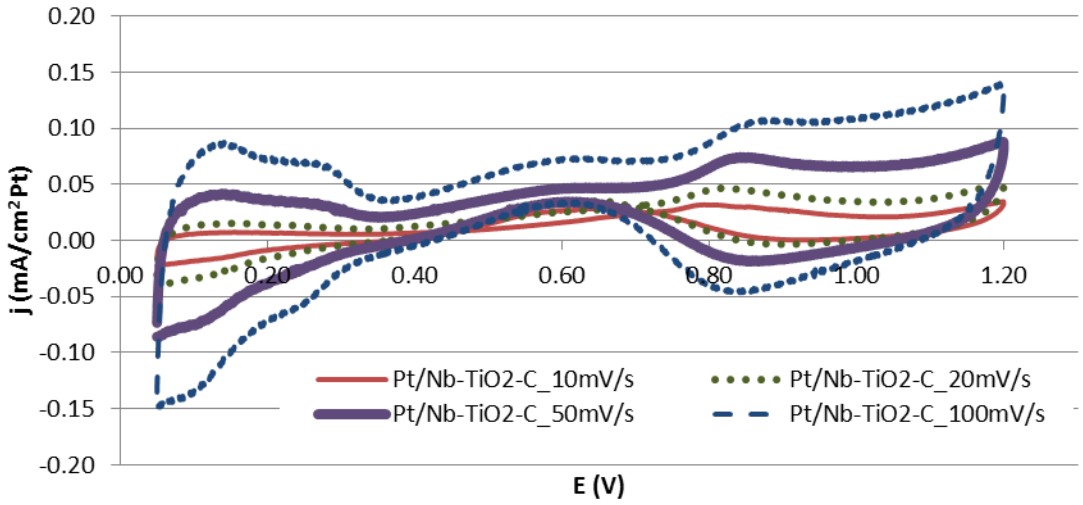

Figure 7-4. SDCV sweeps on a Pt/Nb-TiO_2-C electrode in 0.01 M ethanol solution.

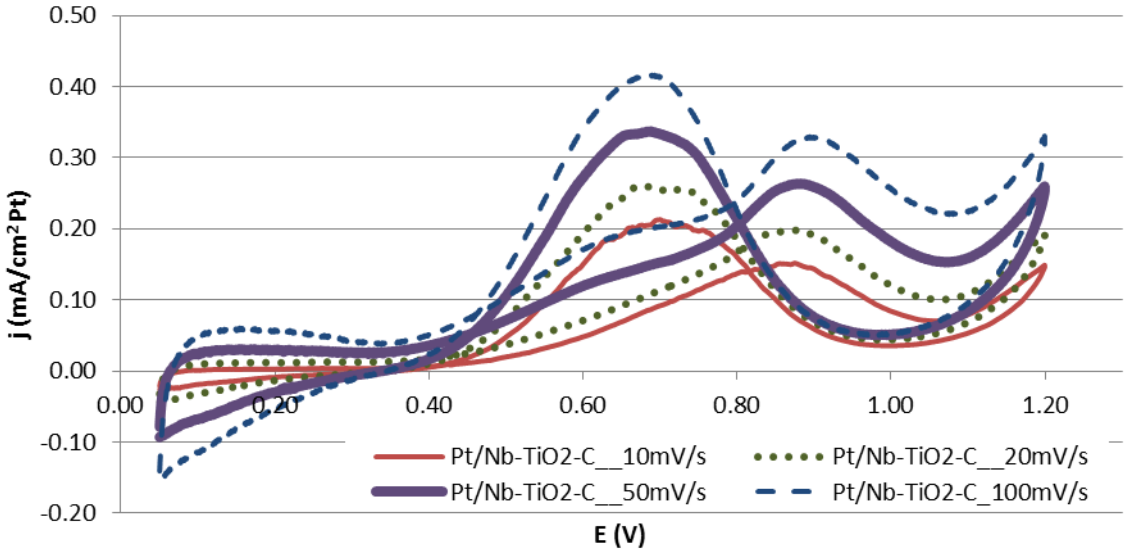

Figure 7-5. SDCV sweeps on a Pt/Nb-TiO2-C electrode in 0.1 M ethanol solution.

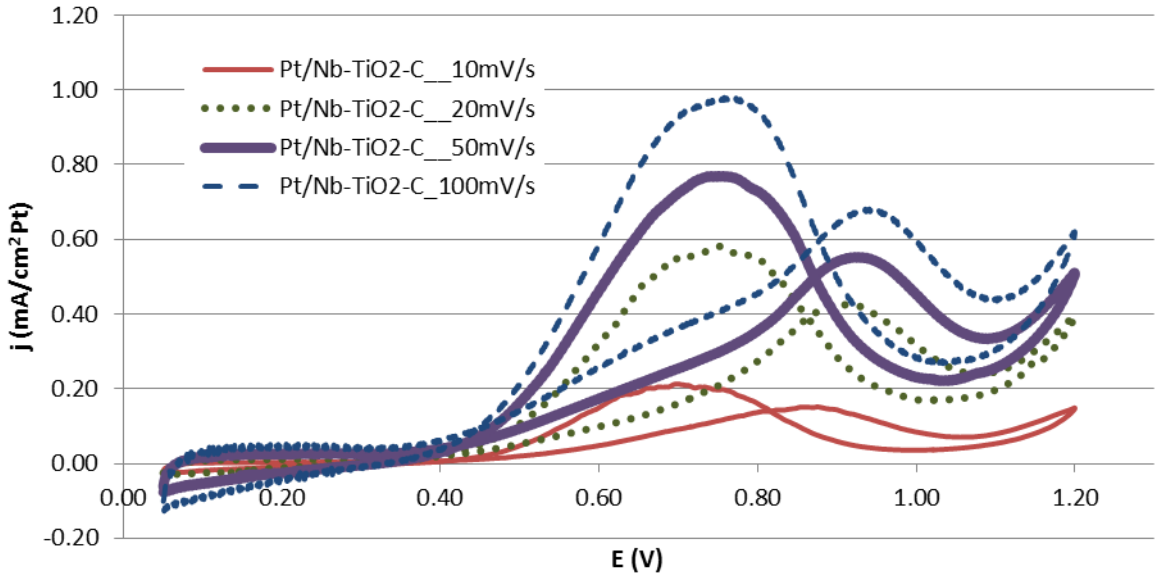

Figure 7-6. SDCV sweeps on a Pt/Nb-TiO2-C electrode in 1.0 M ethanol solution.

7.2. Stationary Disc Potentiostatic Results

Pt/C

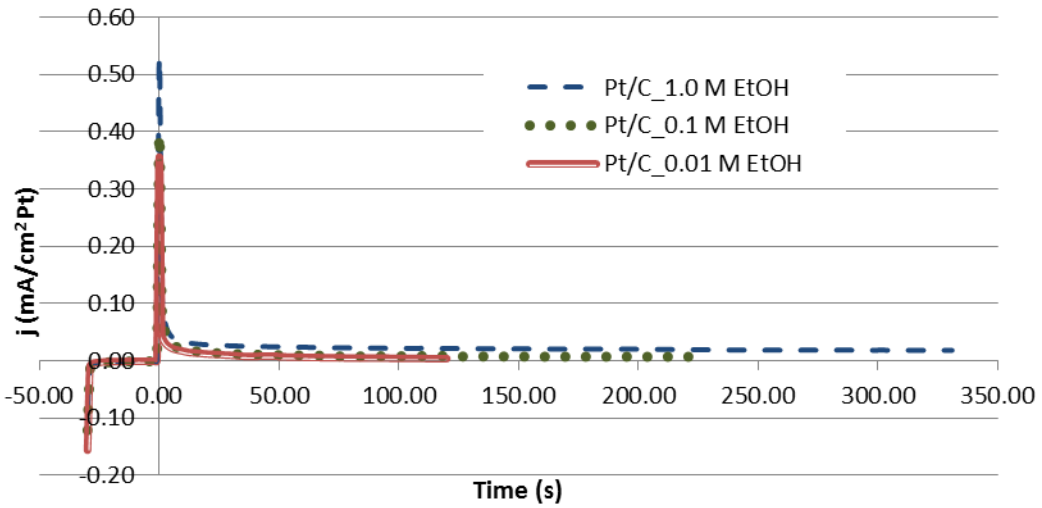

Figure 7-7. Complete SDPS data (0.05 V to 0.5 V hold) on a Pt/C electrode.

PtSn/C

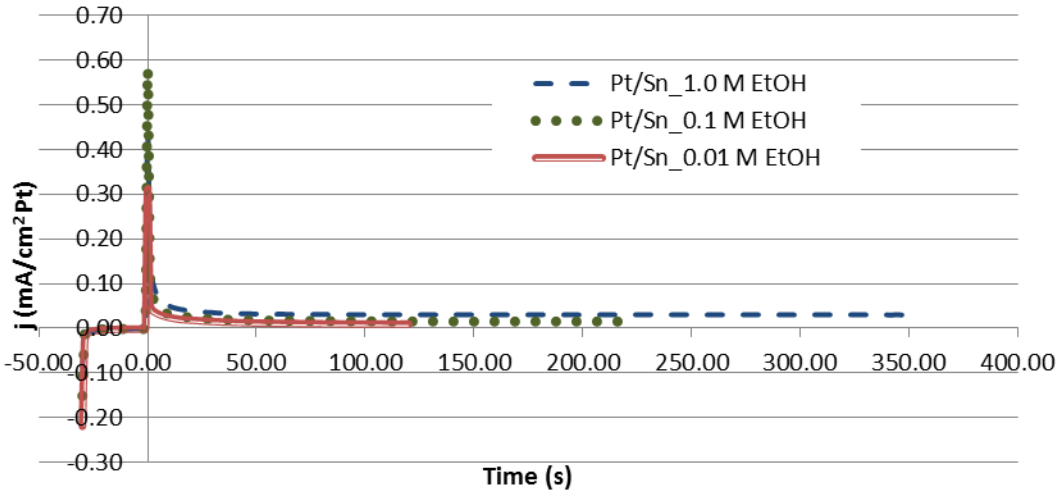

Figure 7-8. Complete SDPS data (0.05 V to 0.5 V hold) on a PtSn/C electrode.

Pt/Nb-TiO_2-C

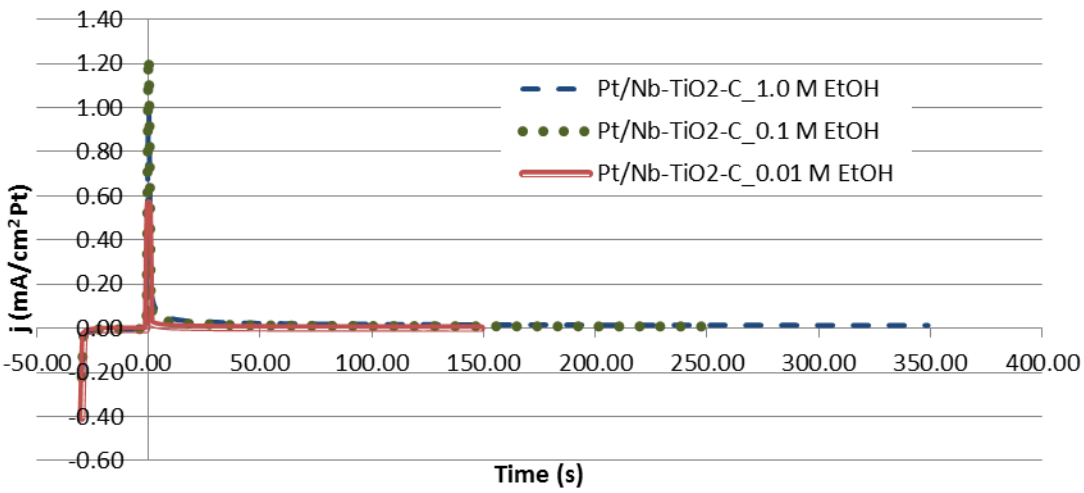

Figure 7-9. Complete SDPS data (0.05 V to 0.5 V hold) on a Pt/Nb-TiO_2-C electrode.

7.3. Rotating Disc Cyclic Voltammetry Results

Pt/C

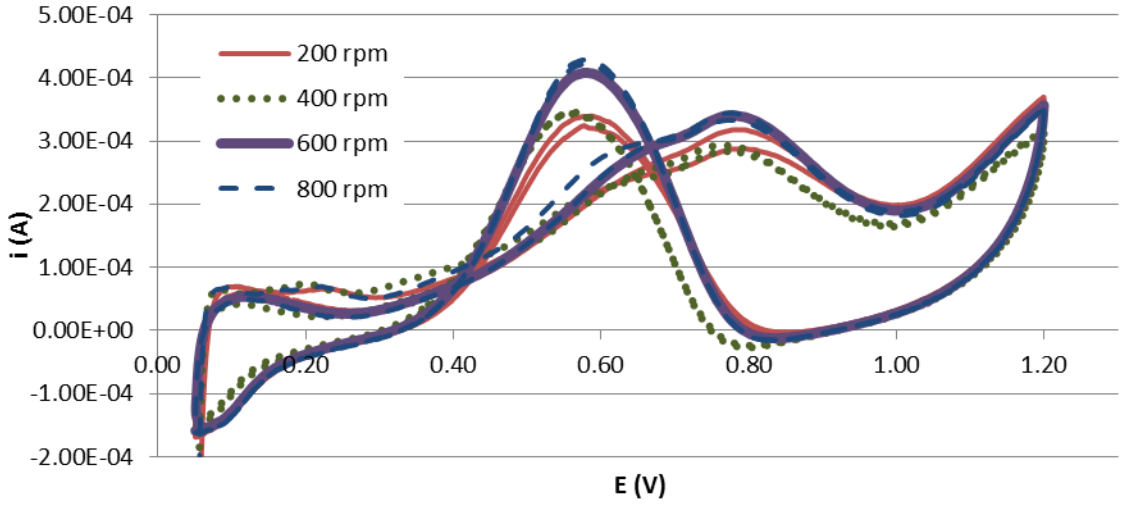

Figure 7-10. RDCV results for lower rotation rates on a Pt/C thin film electrode in 0.1 M ethanol solution.

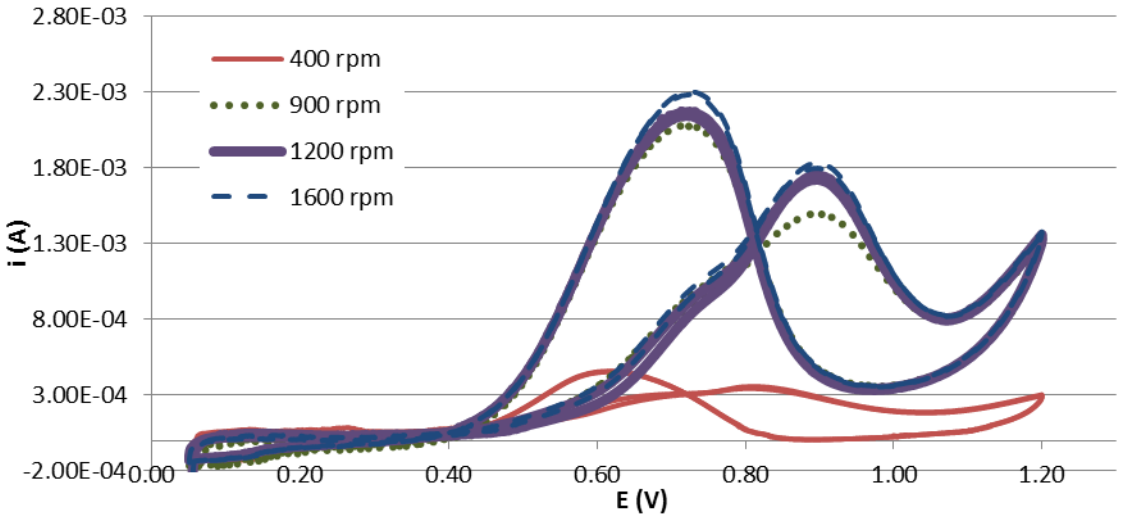

Figure 7-11. RDCV results for higher rotation rates on a Pt/C thin film electrode in 0.1 M ethanol solution.

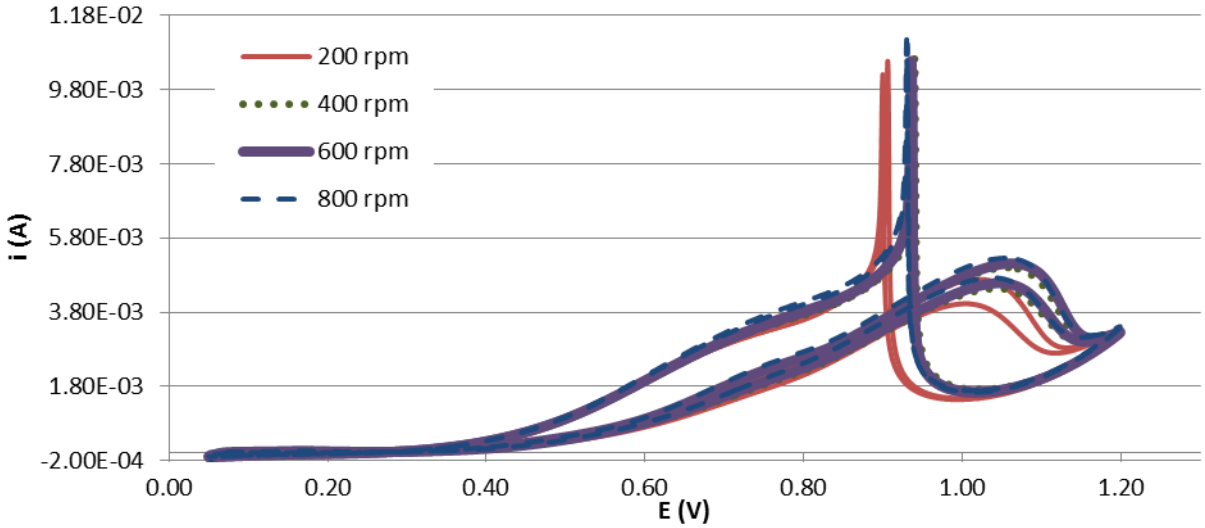

Figure 7-12. RDCV results for lower rotation rates on a Pt/C thin film electrode in 1.0 M ethanol solution.

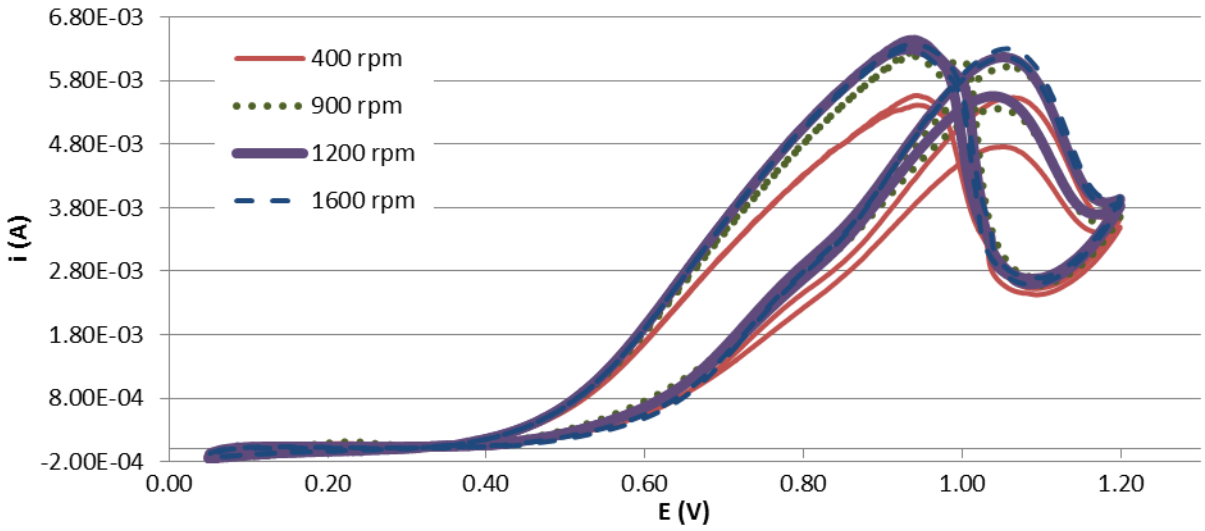

Figure 7-13. RDCV results for higher rotation rates on a Pt/C thin film electrode in 1.0 M ethanol solution.

PtSn/C

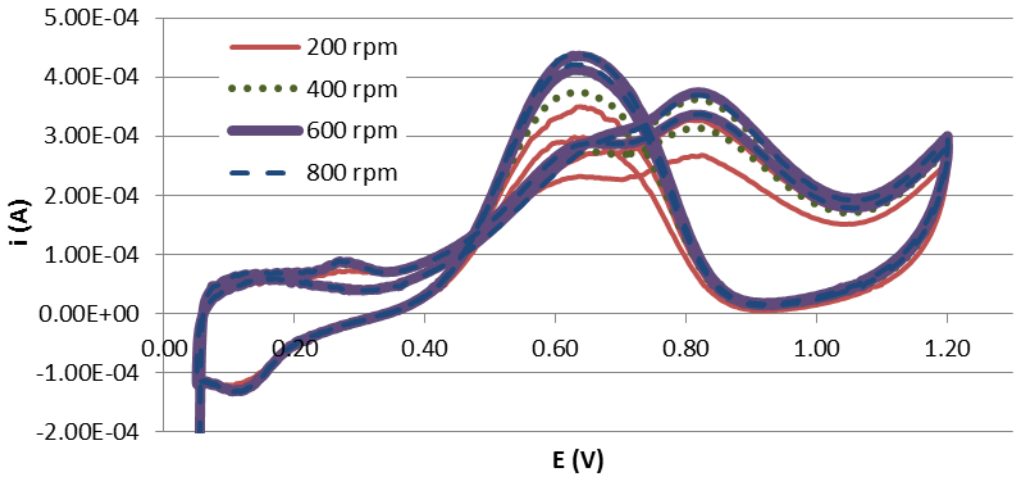

Figure 7-14. RDCV results for lower rotation rates on a PtSn/C thin film electrode in 0.01 M ethanol solution.

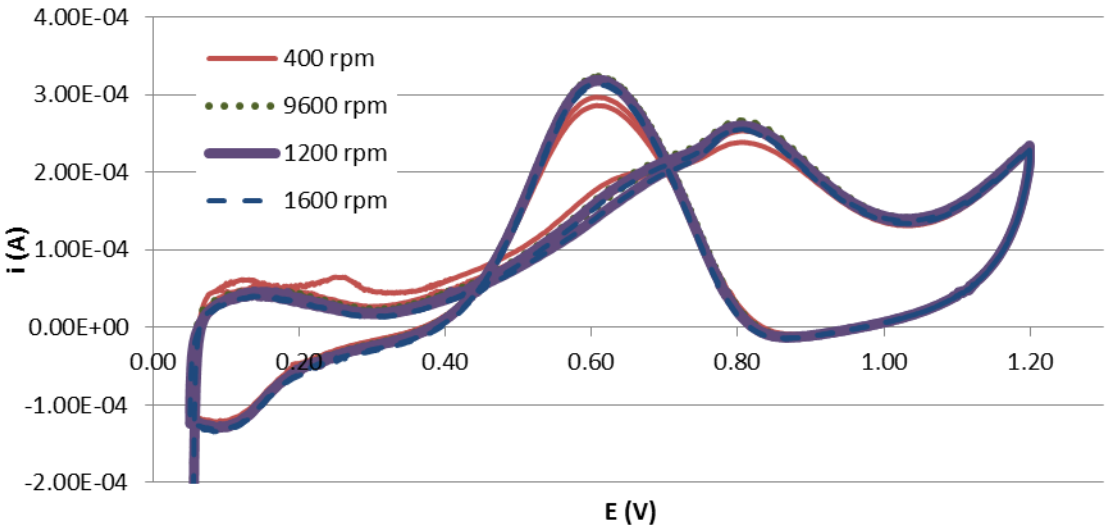

Figure 7-15. RDCV results for higher rotation rates on a PtSn/C thin film electrode in 0.01 M ethanol solution.

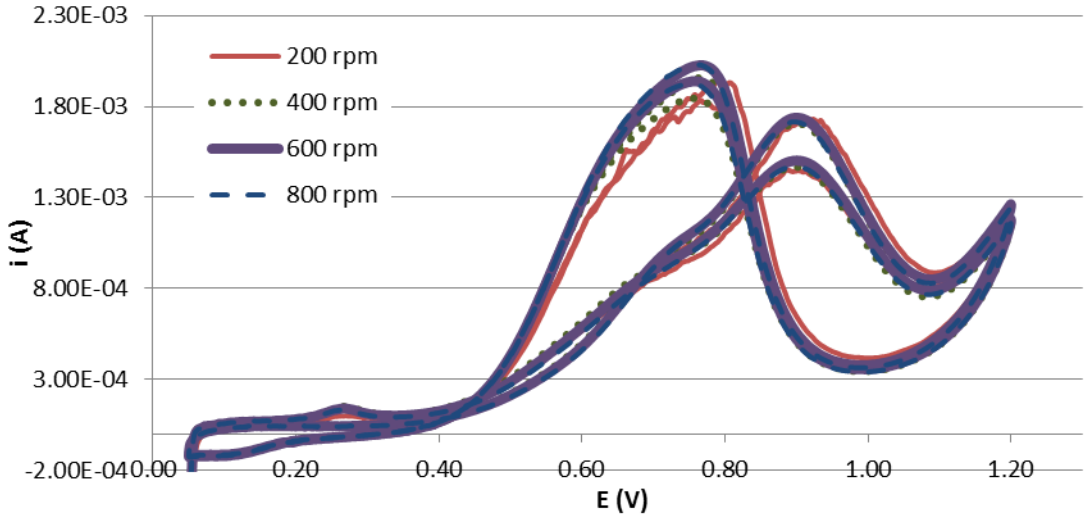

Figure 7-16. RDCV results for lower rotation rates on a PtSn/C thin film electrode in 0.1 M ethanol solution.

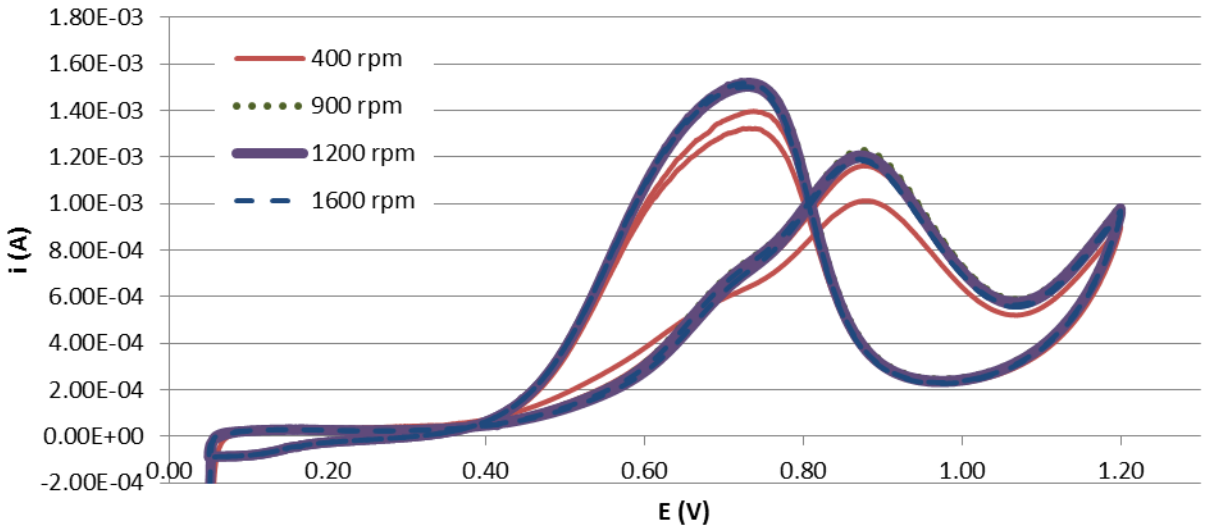

Figure 7-17. RDCV results for higher rotation rates on a PtSn/C thin film electrode in 0.1 M ethanol solution.

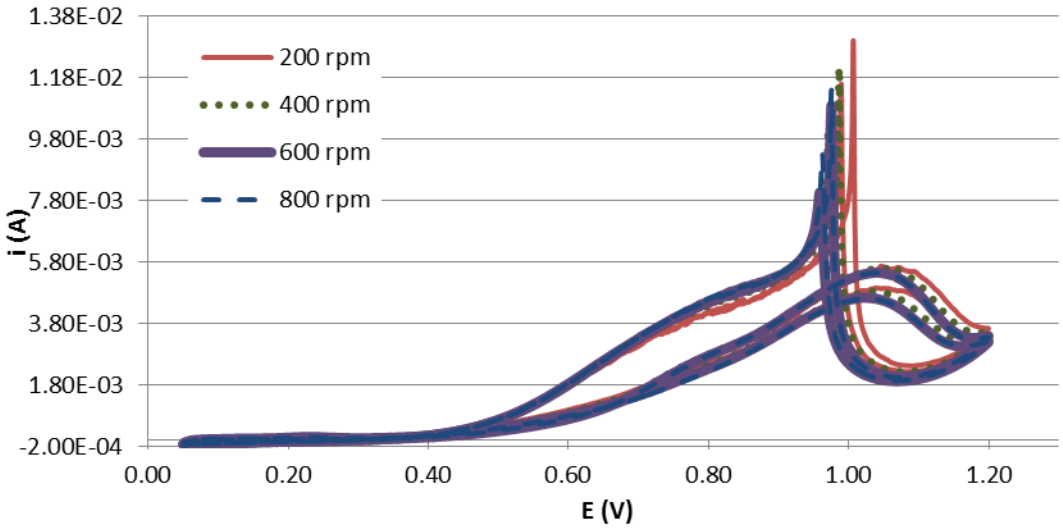

Figure 7-18. RDCV results for lower rotation rates on a PtSn/C thin film electrode in 1.0 M ethanol solution.

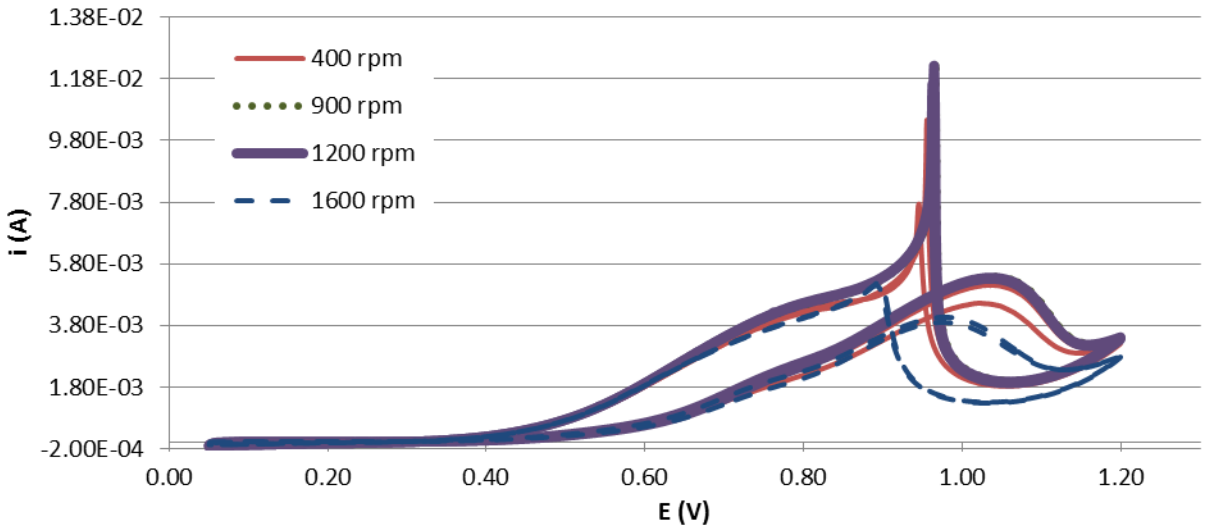

Figure 7-19. RDCV results for higher rotation rates on a PtSn/C thin film electrode in 1.0 M ethanol solution.

Pt/Nb-TiO_2-C

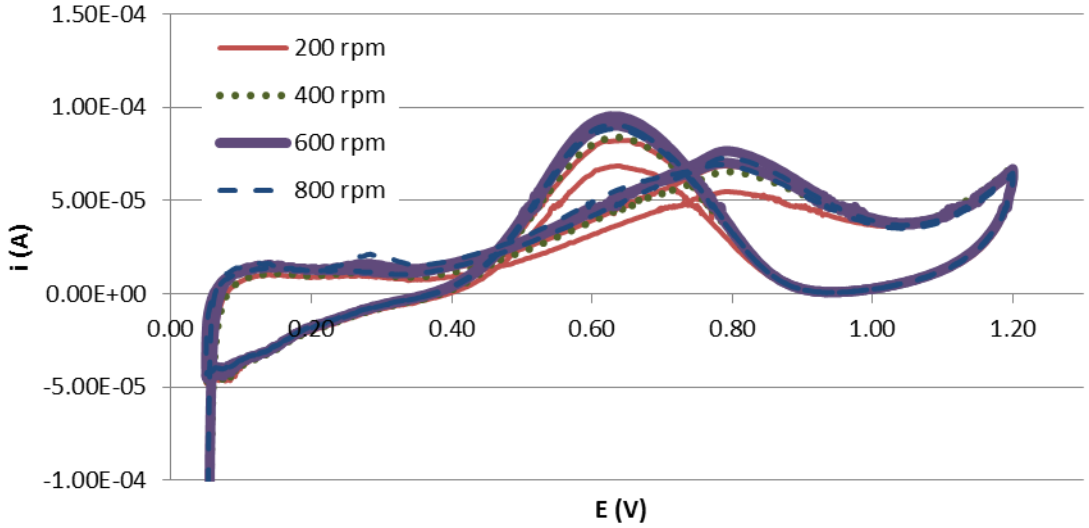

Figure 7-20. RDCV results for lower rotation rates on a Pt/Nb-TiO_2-C thin film electrode in 0.01 M ethanol solution.

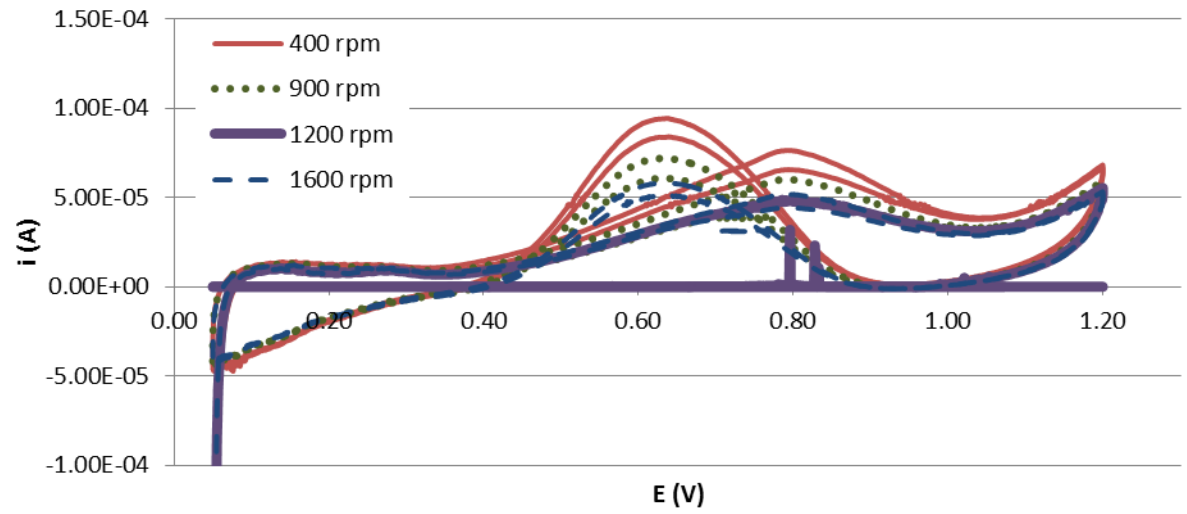

Figure 7-21. RDCV results for higher rotation rates on a Pt/Nb-TiO_2-C thin film electrode in 0.01 M ethanol solution.

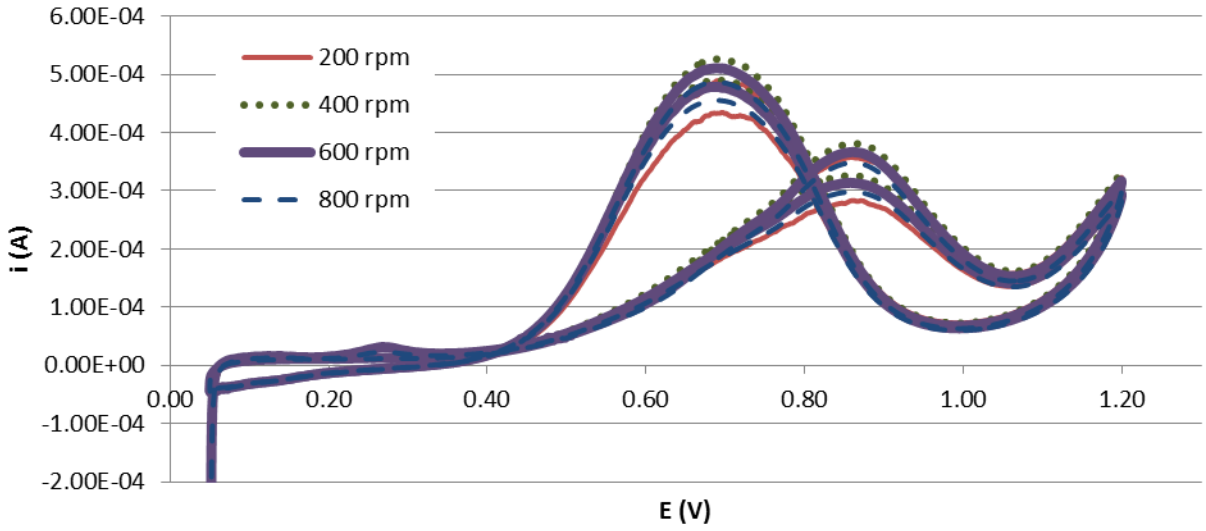

Figure 7-22. RDCV results for lower rotation rates on a Pt/Nb-TiO2-C thin film electrode in 0.1 M ethanol solution.

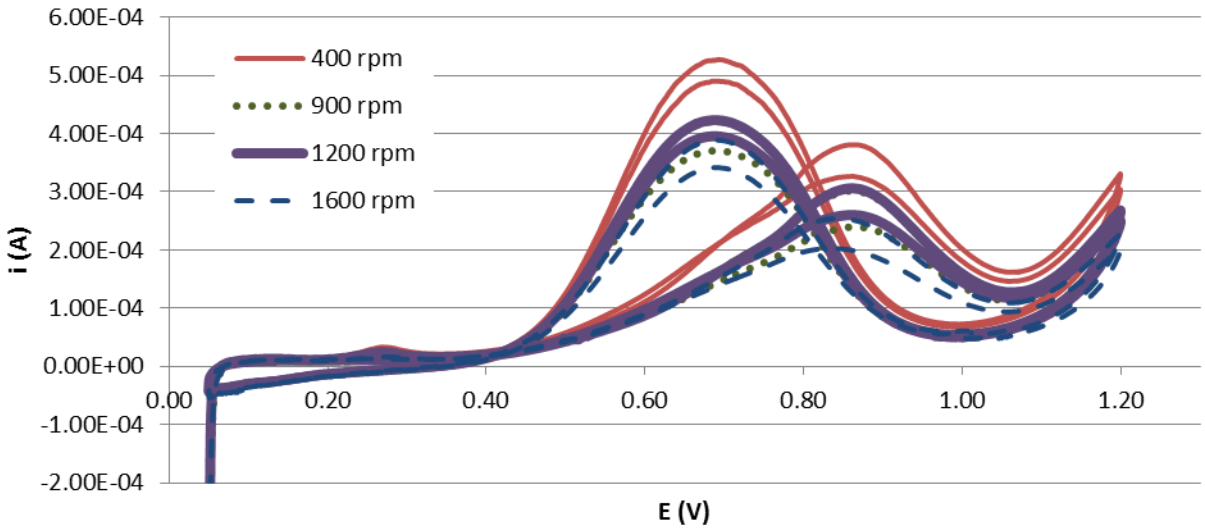

Figure 7-23. RDCV results for higher rotation rates on a Pt/Nb-TiO2-C thin film electrode in 0.1 M ethanol solution.

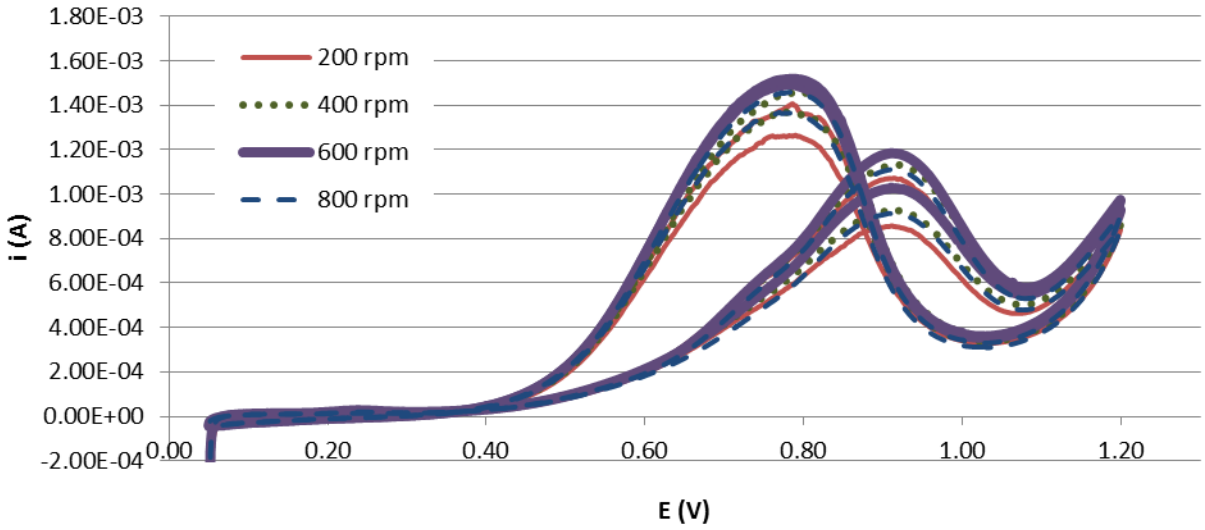

Figure 7-24. RDCV results for lower rotation rates on a Pt/Nb-TiO2-C thin film electrode in 1.0 M ethanol solution.

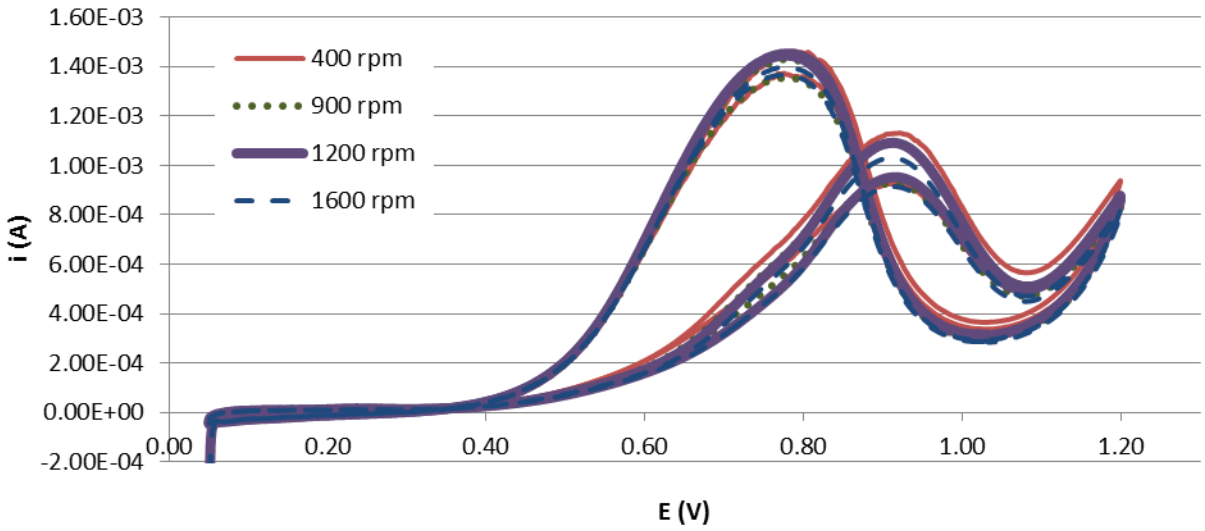

Figure 7-25. RDCV results for higher rotation rates on a Pt/Nb-TiO2-C thin film electrode in 1.0 M ethanol solution.

1. K-L Plots

Pt/C

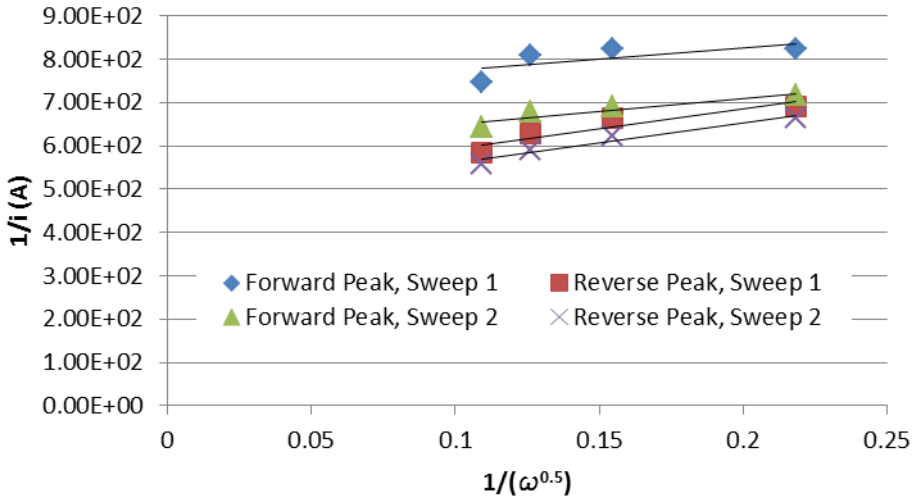

Figure 7-26. K-L plot using RDCV data from four rotational rates (200, 400, 600, and 800 rpm) in 0.1 M ethanol solution on a Pt/C thin film electrode.

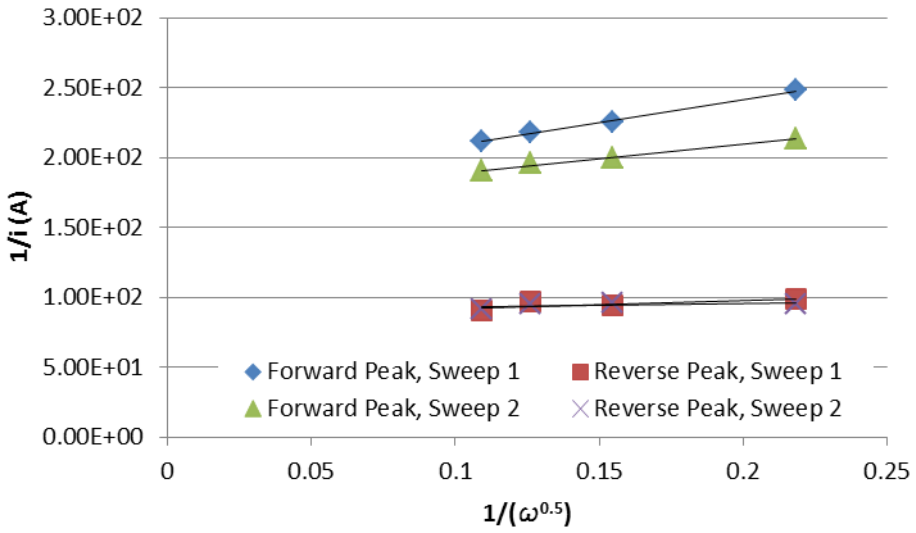

Figure 7-27. K-L plot using RDCV data from four rotational rates (200, 400, 600, and 800 rpm) in 1.0 M ethanol solution on a Pt/C thin film electrode.

PtSn/C

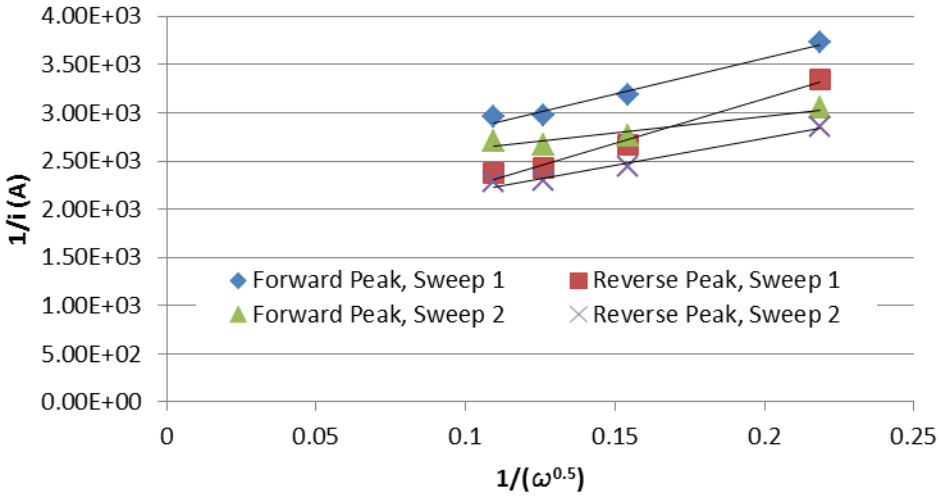

Figure 7-28. K-L plot using RDCV data from four rotational rates (200, 400, 600, and 800 rpm) in 0.01 M ethanol solution on a PtSn/C thin film electrode.

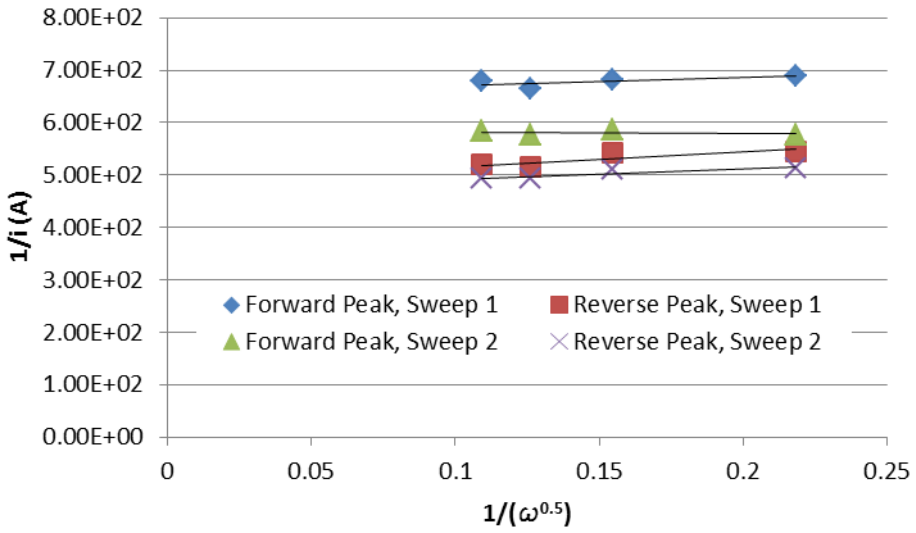

Figure 7-29. K-L plot using RDCV data from four rotational rates (200, 400, 600, and 800 rpm) in 0.1 M ethanol solution on a PtSn/C thin film electrode.

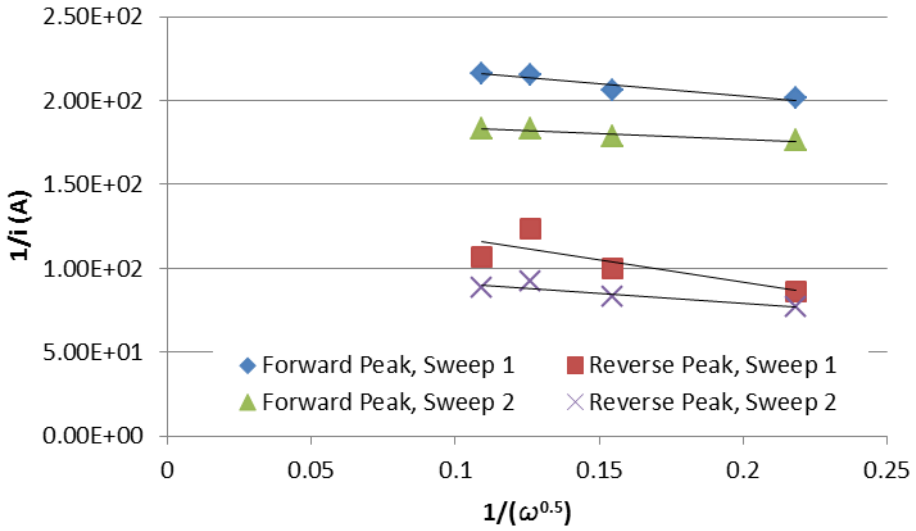

Figure 7-30. K-L plot using RDCV data from four rotational rates (200, 400, 600, and 800 rpm) in 1.0 M ethanol solution on a PtSn/C thin film electrode.

Pt/Nb-TiO_2-C

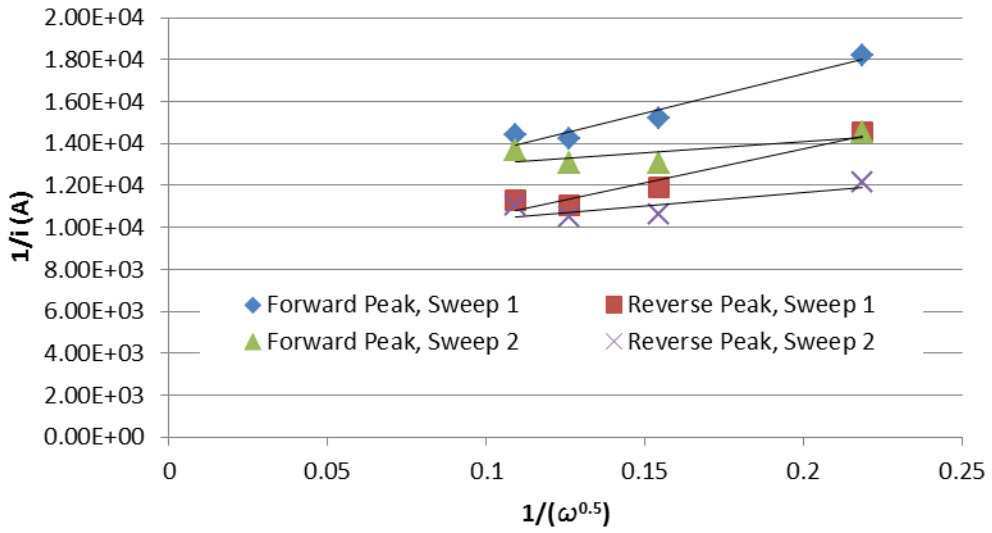

Figure 7-31. K-L plot using RDCV data from four rotational rates (200, 400, 600, and 800 rpm) in 0.01 M ethanol solution on a Pt/Nb-TiO_2-C thin film electrode.

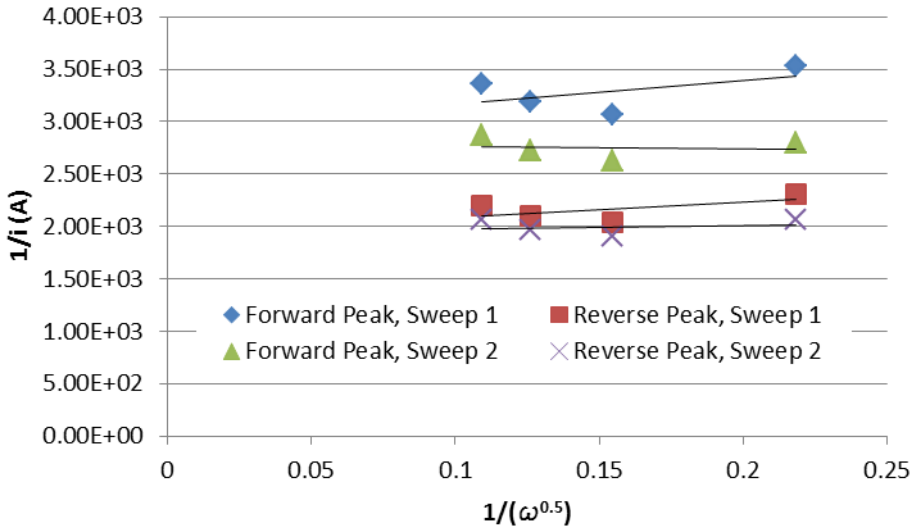

Figure 7-32. K-L plot using RDCV data from four rotational rates (200, 400, 600, and 800 rpm) in 0.1 M ethanol solution on a Pt/Nb-TiO2-C thin film electrode.

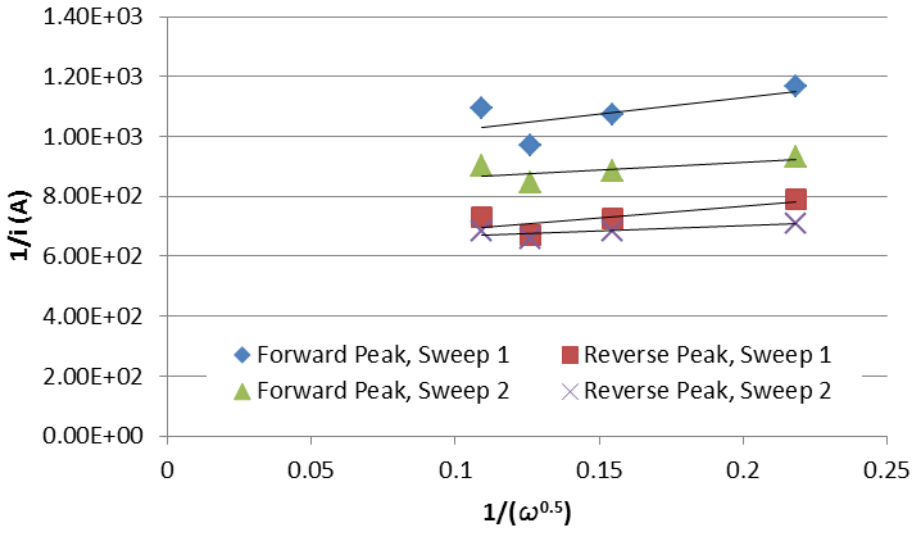

Figure 7-33. K-L plot using RDCV data from four rotational rates (200, 400, 600, and 800 rpm) in 1.0 M ethanol solution on a Pt/Nb-TiO2-C thin film electrode.